

AD-A067 969

IOWA STATE UNIV AMES ENGINEERING RESEARCH INST
THE INFLUENCE OF COMPRESSOR INLET GUIDE VANE / STATOR RELATIVE --ETC(U)
SEP 78

F/G 13/7

AFOSR-76-2916

UNCLASSIFIED

ISU-ERI-AMES-79037

AFOSR-TR-79-0509

NL

1 of 2

AD
A067969



ADA067969

APOSR-TR. 79-0509

4
B.S.
LEVEL *TL*

DDC FILE COPY

G. J. HOLBROOK
T. H. OKIISHI
SEPTEMBER 1978

TECHNICAL REPORT

**THE INFLUENCE OF COMPRESSOR INLET GUIDE VANE /
STATOR RELATIVE CIRCUMFERENTIAL POSITIONING
ON BLADE WAKE TRANSPORT AND INTERACTION**

TURBOMACHINERY
COMPONENTS RESEARCH PROGRAM

APPROVED FOR PUBLIC RELEASE; DISTRIBUTION UNLIMITED

Ch
DDC
APR 27 1979
A

ISU-ERI-AMES-78037
TCRL-13
ERI Project 1204

ENGINEERING RESEARCH INSTITUTE
IOWA STATE UNIVERSITY
AMES, IOWA 50010 USA

79 04 26 390

Qualified requestors may obtain additional copies from the
Defense Documentation Center, all others should apply
to the National Technical Information Service.

CONDITIONS OF REPRODUCTION

Reproduction, translation, publication, use and disposal in whole
or in part by or for the United States Government is permitted.

AIR FORCE OFFICE OF SCIENTIFIC RESEARCH (AFSO)
NOTICE OF TRANSMITTAL TO DDC
This technical report has been reviewed and is
approved for public release IAW AFR 190-12 (7b).
Distribution is unlimited.
A. D. BLOSE
Technical Information Officer

REPORT DOCUMENTATION PAGE		READ INSTRUCTIONS BEFORE COMPLETING FORM
1. REPORT NUMBER 18 AFOSR	2. GOVT ACCESSION NO. 19 TR-79-05091	3. RECIPIENT'S CATALOG NUMBER 9
4. TITLE (and Subtitle) 6 THE INFLUENCE OF COMPRESSOR INLET GUIDE VANE / STATOR RELATIVE CIRCUMFERENTIAL POSITIONING ON BLADE WAKE TRANSPORT AND INTERACTION.		5. TYPE OF REPORT & PERIOD COVERED INTERIM rept. 30 Sep 77 - 31 Aug 78
7. AUTHOR(s) 10 G. J. HOLBROOK T. H. OKIISHI		8. CONTRACT OR GRANT NUMBER(s) 15 AFOSR-76-2916
9. PERFORMING ORGANIZATION NAME AND ADDRESS IOWA STATE UNIVERSITY ENGINEERING RESEARCH INSTITUTE AMES, IOWA 50010		10. PROGRAM ELEMENT, PROJECT, TASK AREA & WORK UNIT NUMBERS 16 2307A4 17 A4 61102F
11. CONTROLLING OFFICE NAME AND ADDRESS AIR FORCE OFFICE OF SCIENTIFIC RESEARCH/NA BLDG 410 BOLLING AIR FORCE BASE, D C 20332		12. REPORT DATE 11 Sep 78
14. MONITORING AGENCY NAME & ADDRESS (if different from Controlling Office) 14 ISU-ERI-AMES-79037, TCRL-13		13. NUMBER OF PAGES 23
16. DISTRIBUTION STATEMENT (of this Report) Approved for public release; distribution unlimited.		15. SECURITY CLASS. (of this report) UNCLASSIFIED
17. DISTRIBUTION STATEMENT (of the abstract entered in Block 20, if different from Report)		15a. DECLASSIFICATION/DOWNGRADING SCHEDULE
18. SUPPLEMENTARY NOTES		12 / 125p.
19. KEY WORDS (Continue on reverse side if necessary and identify by block number) AXIAL-FLOW COMPRESSOR TURBOMACHINE WAKE INTERACTION AXIAL-FLOW TURBOMACHINE TURBOMACHINE FLUID FLOW AXIAL-FLOW FAN MULTISTAGE AXIAL-FLOW TURBOMACHINE AXIAL-FLOW BLOWER AXIAL-FLOW PUMP		
20. ABSTRACT (Continue on reverse side if necessary and identify by block number) A periodically sampling hot-wire measurement system was used to obtain numerous periodic-average (electronically and arithmetically averaged values of periodically sampled data) three-dimensional velocity vector data for flow through the first stage (inlet guide vane, rotor, and stator rows) of a low-speed, multistage, axial-flow research compressor. New data are presented for the maximum noise circumferential position of the first stator blade row. Comparisons are made between these data and similar data previously acquired and reported for the minimum noise configuration of the compressor. The inlet guide		

DD FORM 1 JAN 73 1473

404 418

EM

UNCLASSIFIED

79 04 26 390

20. (Continued)

vane (IGV) wake avenue was found to intersect first stator row blades at two span locations, one near the hub and the other near the tip, for maximum noise and at only one span location, near mid-span, for minimum noise. This difference in IGV wake / stator leading edge intersection patterns resulted in variations of the first stator exit flow deviation angle near the hub and tip portions of the compressor annulus. These variations were explained in terms of the larger fluctuations of stator inlet flow associated with the inlet guide vane wake avenues. The difference in IGV wake / stator leading edge interaction patterns was also judged to be consistent with the related level of compressor inlet noise. Blade-to-blade plane and hub-to-tip cross-section drawings showing blade wake locations and interaction patterns are included to aid data interpretation and comparison. In addition, examples of three-dimensional hub-to-tip velocity vector sheet drawings of blade row exit flow are shown.

ADMISSION NO.	
HTW	Write Section <input checked="" type="checkbox"/>
DUC	Dist Section <input type="checkbox"/>
UNANNOUNCED	<input type="checkbox"/>
JUSTIFICATION	
BY	
DISTRIBUTION/AVAILABILITY CODES	
Dist.	AVAIL. NO. OF SPECIAL
A	

**ENGINEERING
RESEARCH**
**ENGINEERING
RESEARCH**
**ENGINEERING
RESEARCH**
**ENGINEERING
RESEARCH**
**ENGINEERING
RESEARCH**

TECHNICAL REPORT

**THE INFLUENCE OF COMPRESSOR
INLET GUIDE VANE / STATOR RELATIVE
CIRCUMFERENTIAL POSITIONING ON BLADE
WAKE TRANSPORT AND INTERACTION**

G. J. Holbrook

T. H. Okiishi

September 1978

ISU-ERI-AMES-79037
TCRL-13
ERI Project 1204

DEPARTMENT OF MECHANICAL ENGINEERING
ENGINEERING RESEARCH INSTITUTE
IOWA STATE UNIVERSITY AMES

ACKNOWLEDGMENTS

This research was supported by the Engineering Research Institute of Iowa State University through funds provided by the Air Force Office of Scientific Research, Grant AFOSR 76-2916. The work was done in the Mechanical Engineering Department Turbomachinery Components Research Laboratory. The enthusiastic monitoring of Lieutenant Colonel Robert C. Smith, AFOSR Program Manager, is gratefully acknowledged. The cost sharing and other encouragement and help provided by the ISU Engineering Research Institute and Mechanical Engineering Department are sincerely appreciated. The authors are especially indebted to their research colleagues, Mr. Joel H. Wagner and Mr. Douglas P. Schmidt.

SUMMARY

A periodically sampling hot-wire measurement system was used to obtain numerous periodic-average (electronically and arithmetically averaged values of periodically sampled data) three-dimensional velocity vector data for flow through the first stage (inlet guide vane, rotor, and stator rows) of a low-speed, multistage, axial-flow research compressor. New data are presented for the maximum noise circumferential position of the first stator blade row. Comparisons are made between these data and similar data previously acquired and reported for the minimum noise configuration of the compressor. The inlet guide vane (IGV) wake avenue was found to intersect first stator row blades at two span locations, one near the hub and the other near the tip, for maximum noise and at only one span location, near mid-span, for minimum noise. This difference in IGV wake / stator leading edge intersection patterns resulted in variations of the first stator exit flow deviation angle near the hub and tip portions of the compressor annulus. These variations were explained in terms of the larger fluctuations of stator inlet flow associated with the inlet guide vane wake avenues. The difference in IGV wake / stator leading edge interaction patterns was also judged to be consistent with the related level of compressor inlet noise. Blade-to-blade plane and hub-to-tip cross-section drawings showing blade wake locations and interaction patterns are included to aid data interpretation and comparison. In addition, examples of three-dimensional hub-to-tip velocity vector sheet drawings of blade row exit flow are shown.

LIST OF FIGURES

<u>Figure</u>		<u>Page</u>
2.1.	Research compressor apparatus side view.	6
2.2.	Research compressor with probe measurement stations.	7
2.3.	Blade nomenclature.	9
2.4.	Schematic diagram showing axial location of probe measurement stations.	10
2.5.	Blade cascade showing relative positions of blades for several rotor sampling positions.	11
2.6.	Schematic set-up diagram of periodic-average flow measurement system.	14
3.1.	Research compressor performance curve and operating point.	18
3.2.	Hot-wire configuration relating velocity vector, \vec{V} , to hot-wire sensor and probe coordinates x, y, z.	20
3.3.	Hot-wire measurement positions and nomenclature, viewed from above along probe axis.	23
3.4.	Compressor coordinate system showing nomenclature and sign convention for three-dimensional periodic-average velocity and angle parameters.	29
4.1.	First stator blade section positions for minimum and maximum noise at 50% span.	32
4.2.	Blade-to-blade distribution of periodic-average flow field parameters. First rotor exit flow, minimum and maximum noise.	34
4.3.	First rotor exit flow velocity variations.	39
4.4.	Blade-to-blade distribution of periodic-average flow-field parameters. First stator exit flow, maximum noise (grouped by common span location for different rotor sampling positions).	42
4.5.	Blade-to-blade distribution of periodic-average flow field parameters. First stator exit flow, maximum noise (grouped by common rotor sampling position for different span locations).	47

<u>Figure</u>		<u>Page</u>
4.6.	Periodic-average cascade wake interaction drawings for first stage, maximum noise.	50
4.7.	Cross-section plane view of IGV wake avenue location in IGV row exit plane, measurement station 2.	62
4.8.	Cross-section plane view of rotor wake and IGV wake avenue locations in first rotor exit flow, measurement station 3.	64
4.9.	Cross-section plane view of rotor wake and IGV wake avenue locations at first stator blade leading edge plane.	65
4.10.	Cross-section plane view of stator wake and rotor wake locations for first stator exit flow, measurement station 4.	68
4.11.	Comparison of hub-to-tip variations of first stator deviation angle with stator circumferential placement.	71
4.12.	Three-dimensional velocity vector viewing angles.	73
4.13.	Three-dimensional velocity vector sheets, viewing angle variation.	74
4.14.	Three-dimensional velocity vector sheets, scale ratio variation.	77
4.15.	Hub-to-tip variation of first rotor relative exit flow. Rotor sampling position $Y_{OR}/S_R = 0.00$, minimum noise.	78
4.16.	Hub-to-tip distribution of radial velocity profiles.	80
4.17.	Hub-to-tip variation of first stator exit flow, maximum noise.	81

LIST OF TABLES

<u>Table</u>	<u>Page</u>
1.1. Stationary blade-row circumferential placement schedules for minimum and maximum noise.	2
1.2. Overall and octave band levels of compressor inlet noise for minimum and maximum noise blade-row schedules.	2
2.1. Blade geometry for IGV, rotor, and stator blade sections at several radial locations.	9
8.1. Hot-wire circumferential survey data obtained with the periodic-average measurement method for maximum noise.	94

SYMBOLS AND NOTATION

\vec{A}	unit vector along hot-wire sensor (Figure 3.2)
$b_0, b_1, b_2 \dots b_9$	effective cooling velocity/actual velocity ratio correlation coefficients
c	blade chord length (Figure 2.3), m
E_ℓ	linearized anemometer bridge voltage, volts
g	local acceleration of gravity, 9.8026 m/s^2
g_c	gravitational constant, 1.0 kgm/Ns^2
P_{atm}	barometric pressure (Equation 7.1), N/m^2
PHH	percent passage height from hub (Equation 7.4)
r	radius from compressor axis, m
R	gas constant, $\text{Nm/kg}^\circ\text{K}$
RPM	rotor rotational speed, rpm
R, Y, Z	compressor coordinate system (Figure 3.4)
S	circumferential space between blades, blade pitch (Figure 2.3), m or degrees
t	temperature, $^\circ\text{K}$
t_{baro}	barometer ambient temperature, $^\circ\text{K}$
t_{max}	blade section maximum thickness (Figure 2.3), m
U	rotor blade velocity (Equation 7.6), m/s
\vec{V}	absolute velocity (Figure 3.4), m/s
\vec{V}'	relative velocity (Equation 7.18), m/s
V_e	hot-wire effective cooling velocity (Equation 3.5), m/s
V_z	axial component of fluid velocity (Figure 3.4; Equation 7.16), m/s
V_θ	tangential component of absolute fluid velocity (Figure 3.4; Equation 7.17), m/s

PREVIOUS PAGE NOT FILMED
BLANK

V_{θ}	tangential component of relative fluid velocity (Equation 7.19), m/s
x, y, z	hot-wire probe coordinates fixed to probe (Figure 3.2)
Y	circumferential traversing position (Figure 2.5), degrees
Y_0	blade row circumferential setting position when Y is equal to zero, circumferential distance from the probe traversing measurement stations to reference blade stacking axis, positive in the direction of rotation (Figure 2.5), degrees
α	sensor yaw angle, angle between the velocity vector and hot-wire sensor (Figure 3.2; Equation 3.4), degrees
β_{mv}	approximate tangential flow angle (Figure 3.3), degrees
β_r	radial flow angle (Figure 3.4; Equation 7.14), degrees
β_{θ}	absolute tangential flow angle with respect to axial direction (Figure 3.3; Equation 7.13), degrees
β'_{θ}	relative tangential flow angle with respect to axial direction (Equation 7.20), degrees
γ	blade stagger angle (Figure 2.3), degrees
γ_{H_2O}	specific weight of water (Equation 7.3), N/m^3
γ_{hg}	specific weight of mercury, N/m^3
ΔH	total head-rise across the compressor, m of air
ΔP_n	differential pressure between calibration nozzle plenum pressure and atmospheric pressure, m of water
ΔP_{vent}	differential pressure across venturi, m of water
ϵ	vector sheet viewing angle (Figure 4.12), degrees
η	vector sheet viewing angle (Figure 4.12), degrees
θ_0	hot-wire sensor angle with respect to a plane normal to the probe axis (Figure 3.2), degrees
θ_{off}	measurement off-set angle (Figure 3.3), degrees
θ_p	probe pitch angle (Figure 3.2), degrees
θ_y	probe yaw angle (Figure 3.2), degrees

TABLE OF CONTENTS

	<u>Page</u>
ACKNOWLEDGMENTS	i
SUMMARY	iii
LIST OF FIGURES	v
LIST OF TABLES	vii
SYMBOLS AND NOTATION	ix
1. INTRODUCTION	1
2. RESEARCH COMPRESSOR FACILITY	5
2.1. Axial-Flow Research Compressor	5
2.2. Stationary Blade Row and Probe Actuators	12
2.3. Periodic-Average Measurement System	12
2.4. Miscellaneous	16
3. EXPERIMENTAL PROCEDURE	17
3.1. Periodic Sampling and Averaging Technique	17
3.2. Hot-Wire Velocity Measurement Technique	19
3.2.1. Probe Geometry	19
3.2.2. Effective Cooling Velocity	21
3.2.3. Measurement Technique	22
3.3. Calibration Procedures	24
3.3.1. Linearizer Coefficient Calibration	25
3.3.2. Effective Cooling Velocity Calibration	26
3.3.3. Second Order Velocity Calibration	26
3.4. Data Acquisition	27
3.5. Data Reduction	28

THIS PAGE NOT FILMED
BLANK

	<u>Page</u>
4. PRESENTATION AND DISCUSSION OF DATA	31
4.1. First Rotor Exit Flow Data	31
4.2. First Stator Exit Flow Data	41
4.3. Cross-Section Drawings	61
4.4. Three-Dimensional Velocity Vector Sheet Drawings	72
5. CONCLUSIONS	85
6. REFERENCES	87
7. APPENDIX A: PARAMETER EQUATIONS	89
7.1. General Parameters	89
7.1.1. Basic Fluid Properties	89
7.1.2. Blade-Element Quantity	89
7.1.3. Miscellaneous	90
7.2. Three-Dimensional Periodic-Average Hot-Wire Parameters	90
8. APPENDIX B: TABULATION OF PERIODIC-AVERAGE DATA	93

1. INTRODUCTION

An important facet of turbomachine design requiring further improvement involves the intelligent resolution of unsteady flow related problems (see, for example, Reference 1). How to properly manage the influences of the unsteadiness of turbomachine fluid flows on the aerodynamic and aeroelastic performance of such machines is not yet well known.

The periodic flow unsteadiness due to blade wake transport and interaction is of particular interest in considering discrete frequency noise generation, forced blade vibration, and energy transfer in turbomachines. For example, Schmidt and Okiishi [2]* observed that large variations in compressor inlet noise level resulted from changing only the relative circumferential positions of the stationary blade rows of a low-speed, three-stage, axial-flow research compressor. Unique (see Table 1.1) stator blade row circumferential positions were discovered to exist for the minimum and for the maximum inlet noise levels (see Table 1.2). A narrow band noise spectrum comparison [2] indicated that noise variations occurred mainly in the large peaks appearing at the blade passing frequency (887 Hz) and second harmonic frequency. As noted by Walker and Oliver [3], similar compressor inlet noise variations with changes in stationary blade row relative circumferential positioning were observed by some Australian researchers working with a single-stage compressor (inlet guide vane, rotor and

*Numbers in brackets indicate references, which are listed in section 6.

Table 1.1. Stationary blade-row circumferential placement schedules for minimum and maximum noise.

Noise Level	Blade-row Schedule			
	IGV YO_{IGV}/S_S	First Stator YO_{1S}/S_S	Second Stator YO_{2S}/S_S	Third Stator YO_{3S}/S_S
Minimum sound	0.000	0.17	0.56	0.77
Maximum sound	0.000	0.59	0.14	0.15

Table 1.2. Overall and octave band levels of compressor inlet noise for minimum and maximum noise blade-row schedules.

	Minimum Noise Blade-row Schedule	Maximum Noise Blade-row Schedule
Overall SPL (flat)	101.0 dB	112.5 dB
500 Hz octave band SPL	92.5 dB	98.5 dB
1000 Hz octave band SPL	96.5 dB	112.8 dB
Other octave band SPL	Insignificant difference	

stator rows). The variations in noise level obtained with changes in stator row circumferential positioning in both studies could be attributed to a combination of sound wave pattern interference and stator blade surface pressure fluctuation differences with the latter cause being related to the blade wake transport and interaction involved.

Other researchers have also dealt with interesting results of turbomachine blade wake transport and interaction. Smith [4] demonstrated with some low-speed, multistage, axial-flow compressor data how hot-wire sensed first rotor periodic exit flow patterns varied considerably with wire circumferential position relative to an inlet guide vane wake avenue. He further noted that the hot-wire sensed flow patterns behind the third rotor could also be altered significantly by moving the inlet guide vanes circumferentially relative to the hot-wire sensor. These data were used by Smith [4] to serve as evidence of his wake-chopping, -transport, and -modification model. Kerrebrock and Mikolajczak [5] proposed a wake transport theory to explain observed stator exit flow stagnation temperature nonuniformities in the circumferential direction. Gallus et al. [6] presented data illustrating large periodic variations in compressor blade and casing surface pressures with sequential changes in rotor blade sampling position. Schmidt and Okiishi [2] and Wagner and Okiishi [7] reported data showing appreciable periodic variations of velocity vectors in the exit flows of a rotor preceded upstream by an inlet guide vane row and of a stator row downstream of a rotor. These observations could be explained in terms of transport models like the ones proposed by Smith [4] and Kerrebrock and Mikolajczak [5].

The primary intent of the research reported here was to develop further knowledge about turbomachine blade wake transport and interaction. In order to accomplish this objective, new periodic-average velocity data were obtained for the maximum noise configuration of the first stage of the Iowa State research compressor. These data were compared with similar

data obtained earlier with the minimum noise set-up of the research compressor. Some interesting results were observed. Details are included in the following sections.

2. RESEARCH COMPRESSOR FACILITY

The research compressor facility of the Iowa State University Engineering Research Institute / Mechanical Engineering Department Turbomachinery Components Research Laboratory was used in this research program. Since this facility has been described in detail previously [2,7], only a summary of pertinent information will be repeated here.

2.1. Axial-Flow Research Compressor

A sketch of the low-speed, three-stage, axial-flow research compressor test rig appears in Figure 2.1. The rig consisted of a driving motor, compressor section, air straightening section, Venturi flow-meter, diffuser section and adjustable throttle plate. The driving motor was an 11 kW (15 hp) variable speed (300-3000 RPM) DC motor. Motor speed was electronically adjusted and maintained to within ± 1 RPM with a feedback-type control circuit. The speed was measured with a magnetic pickup / frequency counter arrangement.

The compressor section, illustrated in more detail in Figure 2.2, consisted of a smooth, gradually contracting inlet passage followed by a constant cross-sectional area annulus containing an inlet guide vane (IGV) row and three identical rotor/stator stages. The compressor flow path involved constant hub and tip diameters of 0.285 m (11.2 in.) and 0.406 m (16.0 in.), respectively, resulting in a hub/tip radius ratio of 0.7. The blades were composed of British C4 sections reflecting a free vortex design and were made of Monsanto ABS plastic. General blade characteristics are given below:

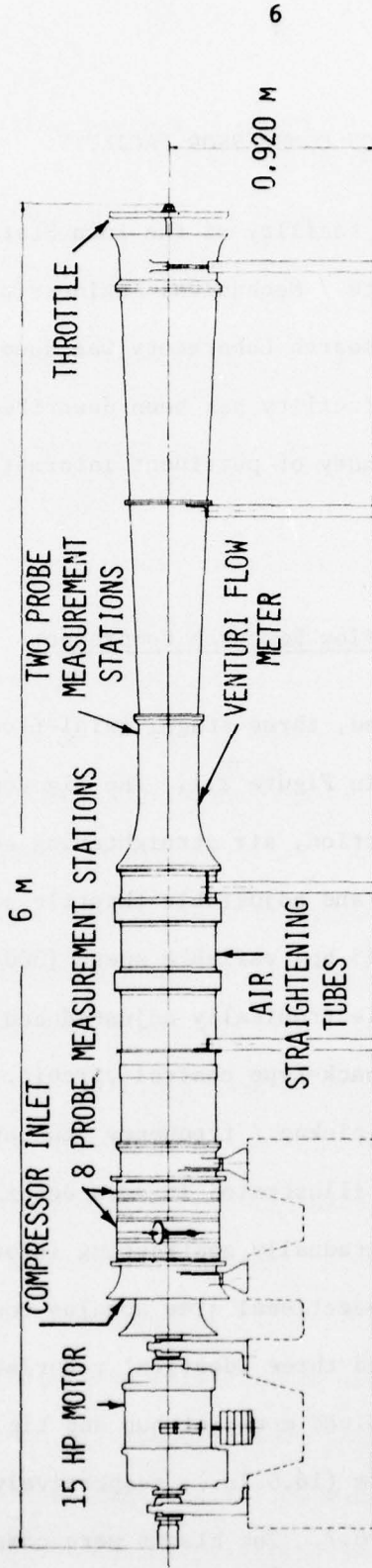


Figure 2.1. Research compressor apparatus side view.

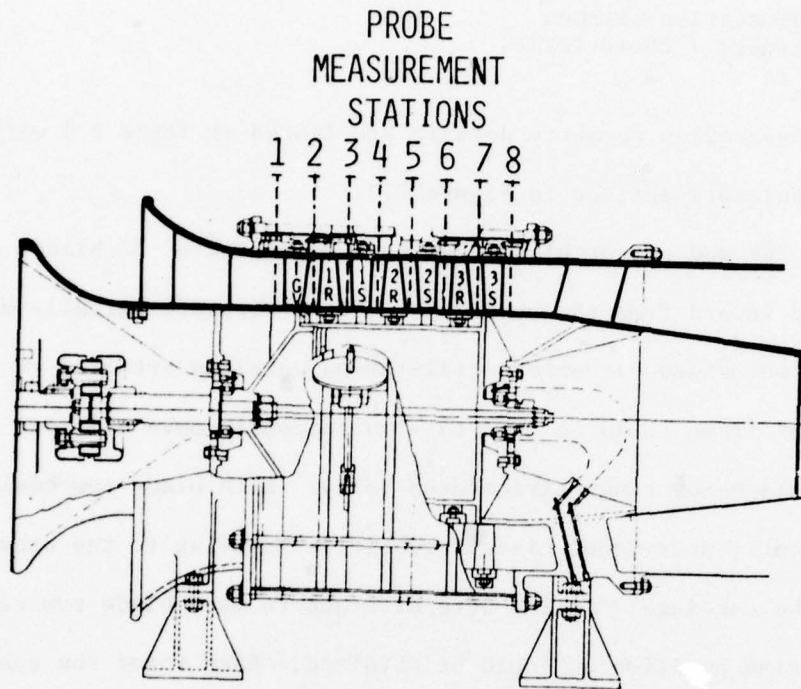


Figure 2.2. Research compressor with probe measurement stations.

Number of blades per row	IGV and stator rows - 37 rotor rows - 38
Blade span (constant)	6.10 cm (2.4 in.)
Blade chord (constant), c	3.05 cm (1.2 in.)
Blade section maximum thickness / chord ratio, t_{\max}/c	10%

Blade section geometry details are listed in Table 2.1 with the nomenclature defined in Figure 2.3.

The IGV and stator blade rows each consisted of 37 blades cantilevered inward from the outer casing on a circumferentially movable ring. A motorized circumferential-motion carriage attached to the compressor frame could be used to simultaneously move all four stationary blade row rings circumferentially. Each blade row could be independently positioned circumferentially relative to the others within the carriage. Scales were attached to each blade row ring so that precise positioning could be obtained. Each rotor row consisted of 38 blades cantilevered outward from hub rings that were aligned and fixed so that the stacking axes of the corresponding rotor blades in each row were in line when viewed along the compressor axis.

The axial location of each probe measurement station is shown in Figure 2.4. The measurement stations were approximately midway between blade rows. As shown in Figure 2.5 for the first stage only, these measurement stations were aligned axially in the compressor. Measurements at each station were made through one access hole only. Circumferential traversing of the flow was accomplished by moving all blades in the circumferential direction past the stationary probe.

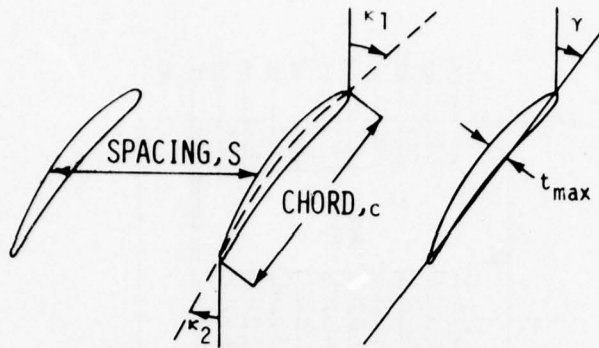


Figure 2.3. Blade nomenclature.

Table 2.1. Blade geometry for IGV, rotor and stator blade sections at several radial locations.

Blade Row	Percent Passage Ht. From Hub PHH	Solidity c/S	Stagger γ degrees	Blade Angles		Camber $\kappa_1 - \kappa_2$ degrees
				Inlet κ_1 degrees	Outlet κ_2 degrees	
IGV	0	1.263	20.35	0.00	42.10	-42.10
	10	1.211	20.05	0.00	40.77	-40.77
	20	1.164	19.69	0.00	39.47	-39.47
	30	1.121	19.25	0.00	38.23	-38.23
	40	1.080	18.65	0.00	37.08	-37.08
	50	1.041	18.15	0.00	36.05	-36.05
	60	1.004	17.63	0.00	35.02	-35.02
	70	0.971	17.05	0.00	33.93	-33.93
	80	0.940	16.45	0.00	32.92	-32.92
	90	0.913	15.65	0.00	32.10	-32.10
100	0.887	14.15	0.00	31.40	-31.40	
Rotor	0	1.299	-20.54	-42.40	3.90	-46.30
	10	1.250	-24.39	-44.76	-2.84	-41.92
	20	1.205	-28.11	-46.85	-9.51	-37.34
	30	1.164	-31.70	-48.53	-15.96	-32.57
	40	1.123	-35.15	-49.82	-21.88	-27.94
	50	1.078	-38.47	-50.81	-27.06	-23.75
	60	1.035	-41.66	-51.77	-31.64	-20.13
	70	0.999	-44.71	-52.90	-35.78	-17.12
	80	0.968	-47.63	-53.98	-39.26	-14.72
	90	0.939	-50.41	-54.82	-41.91	-12.91
100	0.909	-53.07	-55.50	-44.10	-11.40	
Stator	0	1.263	40.24	54.80	26.70	28.10
	10	1.211	39.32	53.48	25.67	27.81
	20	1.164	38.39	52.36	24.68	27.68
	30	1.121	37.46	51.43	23.74	27.69
	40	1.080	36.54	50.25	22.77	27.48
	50	1.041	35.61	48.56	21.72	27.84
	60	1.004	34.68	47.13	20.76	26.37
	70	0.971	33.75	46.65	20.01	26.64
	80	0.940	32.83	46.36	19.34	27.02
	90	0.913	31.90	45.59	18.62	26.97
100	0.887	30.97	44.50	17.85	26.65	

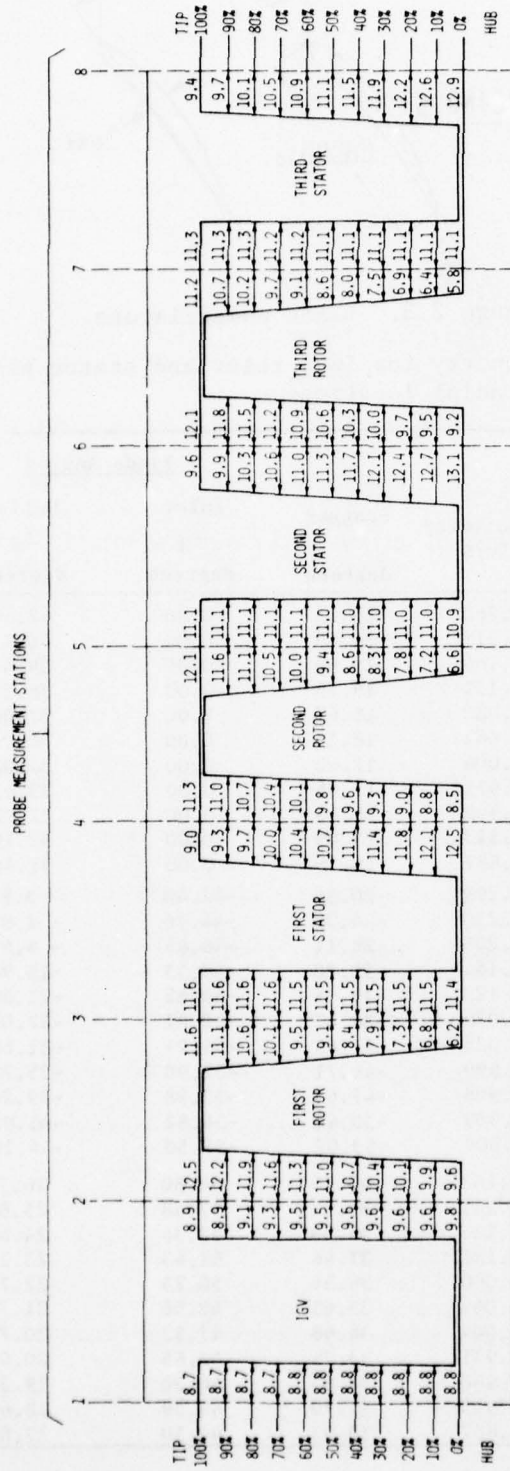


Figure 2.4. Schematic diagram showing axial location of probe measurement stations (dimensions in mm).

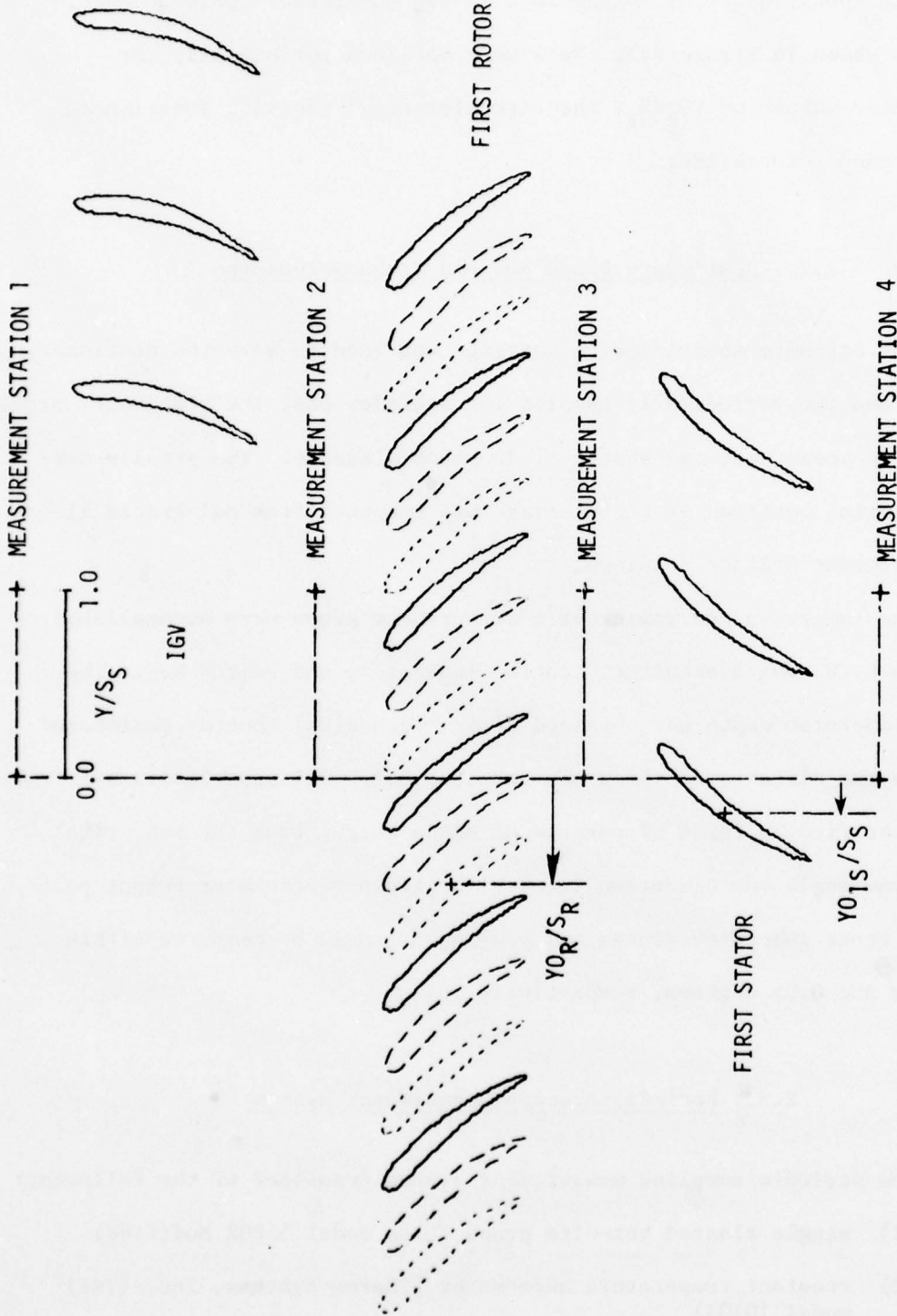


Figure 2.5. Blade cascade showing relative positions of blades for several rotor sampling positions. (S_R is rotor blade spacing; S_S is stator spacing; Y is measurement circumferential location; Y_{0R} is reference rotor blade circumferential location; Y_{0S} is reference first stator blade circumferential location.)

Data were obtained for values of Y/S_S from 0.0 to 1.0. The circumferential position of all blade rows in the compressor could be specified as shown in Figure 2.5. Data were obtained periodically for particular values of Y_{O_R}/S_R , the circumferential sampling position of a reference rotor blade.

2.2. Stationary Blade Row and Probe Actuators

The circumferential-motion carriage was used to move the stationary blades and the periodically sampled rotor blades past the stationary probe in thirty steps over one stator blade pitch distance. The precise circumferential position of the carriage was computed from calibrated linear potentiometer voltage readings.

The immersion and yawing of a measurement probe were accomplished with an L. C. Smith actuator, control indicator, and switch box. The probe immersion depth was obtained from a mechanical counter calibrated to give the distance of the probe from the hub. All span locations were specified in terms of percent of blade height from the hub. The probe yaw angle was discerned from calibrated potentiometer output voltages. Probe immersion depths and yaw angles could be measured within 0.15 mm and 0.05 degrees, respectively.

2.3. Periodic-Average Measurement System

The periodic sampling measurement system consisted of the following:

- (1) single slanted hot-wire probe (Disa model 55P02 Modified)
- (2) constant temperature anemometer (Thermo-Systems, Inc. (TSI) model 1010A)

- (3) linearizer (TSI model 1072)
- (4) photo-electric triggering circuit
- (5) periodic sample-and-hold circuit
- (6) signal averaging circuit
- (7) multi-channel scanning digital voltmeter (Hewlett-Packard model 3480 D)
- (8) desk-top programmable calculator (Hewlett-Packard model 9821 A)
- (9) monitoring oscilloscopes (Tektronic, Inc.)

A schematic diagram of this system is shown in Figure 2.6.

The hot-wire probe involved a single platinum-plated wire $5\ \mu\text{m}$ in diameter. The sensing portion of the wire was 1.25 mm long with copper and gold plating at the ends. The wire was slanted at an angle of 54.7° to the axis of the probe. This peculiar angle results in the sensor being in three orthogonal orientations when the probe is rotated in 120° increments around its axis. With the constant temperature anemometer, it was possible to obtain a direct relationship between the velocity of the flow as sensed by the wire and the voltage output from the anemometer. A linearizer made this relationship approximately linear and expanded the voltage output range.

The photo-electric triggering circuit and the periodic sample-and-hold circuit were specially built in-house for the system. With these components it was possible to synchronize data sampling with any particular periodic sampling position of the rotor blades. A 5 μsecond sample was acquired each revolution of the rotor. The photo-electric pickup was attached to the circumferential positioning carriage so that, as mentioned earlier, the periodic rotor sampling position

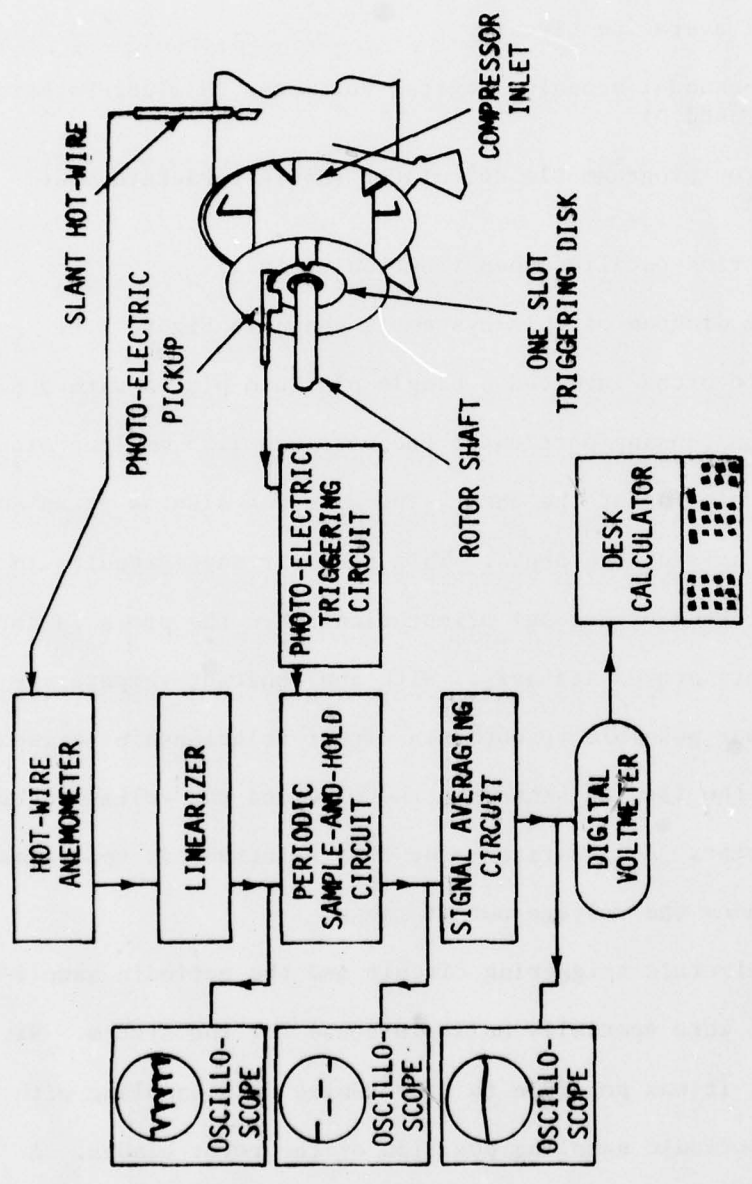


Figure 2.6. Schematic set-up diagram of periodic-average flow measurement system.

relative to the stationary blades did not change as the carriage was moved circumferentially past the probe. Any specific periodic rotor sampling position could be obtained by mechanically moving the photoelectric pickup sensor relative to the circumferential carriage. A long arm and scale were used to obtain precise positioning of the pickup. The rotor sampling position was measured from the reference line of the probe measurement stations as shown in Figure 2.5.

A low pass filter with a time constant of 1.0 second was used to obtain an electronic average of the periodic sample-and-hold signal. From this averaged signal a specified number of samples were taken and arithmetically averaged to produce a single electronically and arithmetically averaged value of periodically sampled data hereafter called periodic-average data.

A multi-channel scanning digital voltmeter (DVM) and a desk-top programmable calculator were used together to digitize, read, display, manipulate, and store data. The interfacing enabled the calculator to selectively read and store voltage values. The calculator had the capability to record data and programs on cassette tape. All raw data were stored on tape and reduced at a later time. Extensive use was made of existing programs for calibration, data acquisition, and reduction procedures (see Schmidt and Okiishi [2]).

Various oscilloscopes were used to continuously monitor the hot-wire signal, circumferential position, and the yaw angle orientation of the probe.

2.4. Miscellaneous

An air nozzle with a throat diameter of 0.25 inches and a contraction ratio of 144 to 1 was used to calibrate the hot-wire anemometer system. The nozzle used regulated compressed air with air temperature maintained at a desired level with a variable current heater, blower, and heat exchanger arrangement. The flow at the nozzle exit was uniform and could be varied between 0 and 50 m/s. A water-in-glass inclined manometer was used to precisely measure the total-static pressure differential across the nozzle.

All working fluid temperatures were obtained with copper-constantan thermocouples and a precision millivolt potentiometer. Venturi flow-meter pressures were measured with an inclined water-in-glass manometer. Ambient and room conditions were measured with mercury-in-glass thermometers and a mercury-in-glass barometer. Room air temperature was kept nearly constant (± 0.30 °C) with a thermostatically operated water chiller, blower, and heat exchanger system.

3. EXPERIMENTAL PROCEDURE

The experimental procedure used has been described in detail elsewhere [2,7]. Only salient information is summarized in this section. All of the data presented here were obtained with the periodic sampling measurement system previously described. The compressor was operated at 1400 RPM with a flow coefficient of 0.42 as shown in Figure 3.1. The rotor speed was maintained to within ± 1 RPM. The flow coefficient was calculated from the Venturi flowmeter data and ambient conditions once equilibrium was established. Adjustments of the flow to maintain the reference flow coefficient value were made by moving the throttle plate at the exit of the compressor diffuser section.

3.1. Periodic Sampling and Averaging Technique

The flow field within a turbomachine consists of at least two types of fluctuating flows: a periodically varying one occurring at the blade passing frequency and a randomly varying one related to turbulence. By periodically sampling the flow and averaging these values, it is possible to extract the periodically unsteady flow information from the total flow situation [8]. This idea is the basis of the periodic sampling technique used here. Initial testing of this measurement technique showed that the arithmetic averaging of 180 samples of an electronically averaged periodic signal was sufficient to obtain reasonably precise periodic-average flow data. Specific information on the precision of this measurement technique can be

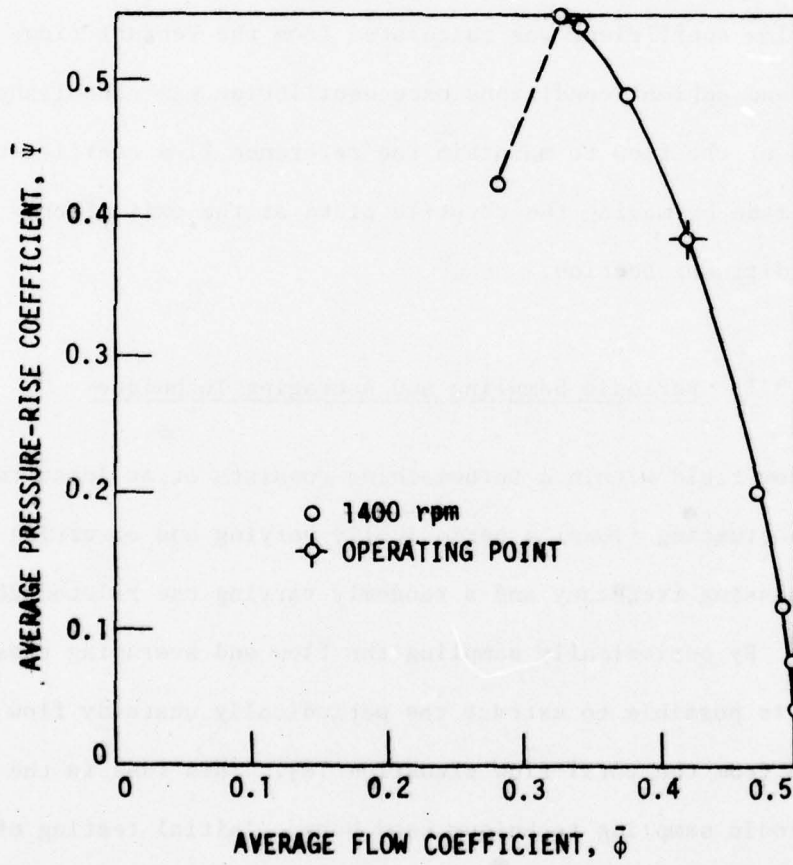


Figure 3.1. Research compressor performance curve and operating point.

found in Schmidt and Okiishi [2]. The calculator/DVM sampled the electronically averaged periodic signal 180 times, once every 0.17 second, and then arithmetically averaged these 180 values to obtain one periodic-average value. During the calculator/DVM sampling time (about 30 seconds) approximately 700 hot-wire periodic samples were taken to produce the electronically averaged signal.

3.2. Hot-Wire Velocity Measurement Technique

A single slanted hot wire was used to obtain three-dimensional velocity vector data. Some familiarity with the probe geometry and sign conventions is necessary to understand this measurement technique.

3.2.1. Probe Geometry

The hot-wire probe configuration sketched in Figure 3.2 shows the relationship between the probe coordinate system and a velocity vector \vec{V} . The z-axis corresponds to the probe axis. The sensing wire was in the x-z plane. θ_0 was the angle (35.3°) the sensing wire made with the x-axis. The probe yaw angle, θ_y , changed with the amount of turning about its axis when the probe was rotated, but the probe pitch angle, θ_p , remained the same. The sensor yaw angle, α , was the angle between the velocity vector \vec{V} and the sensor wire. The unit vector \vec{A} represents the sensor wire orientation. To obtain a relationship between the various angles, the dot product of the two vectors was taken:

$$\vec{A} = \cos \theta_0 \vec{i} + \sin \theta_0 \vec{k} \quad (3.1)$$

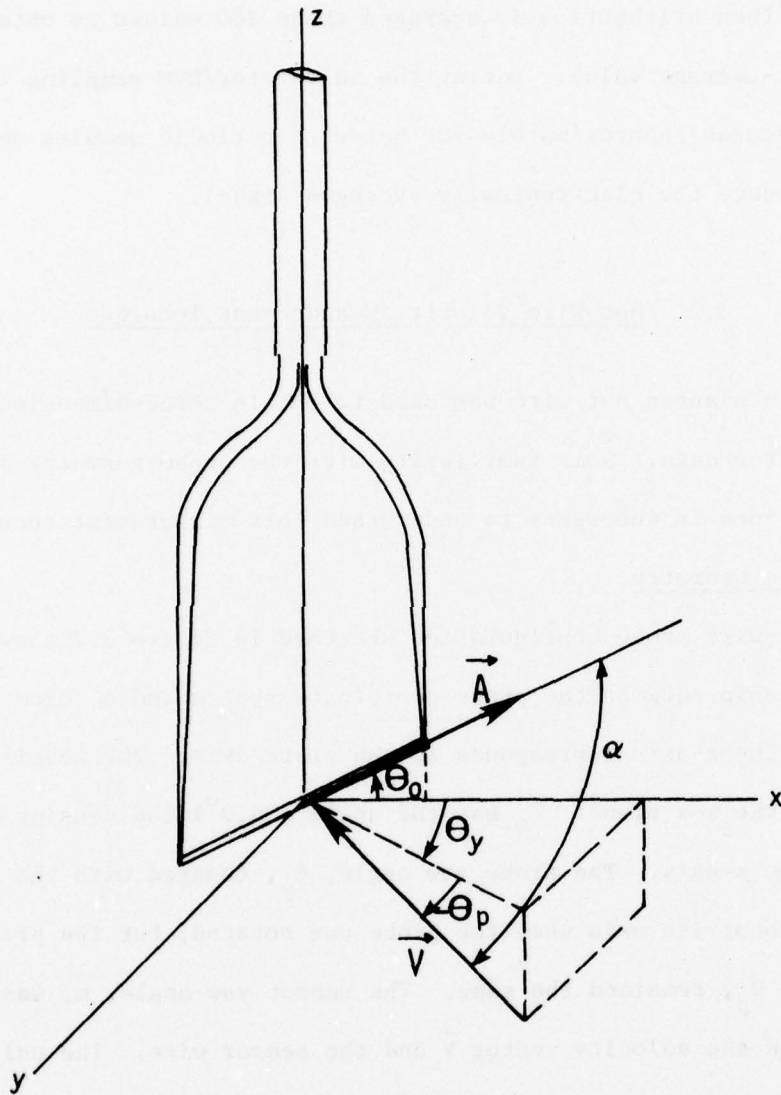


Figure 3.2. Hot-wire configuration relating velocity vector, \vec{V} , to hot-wire sensor and probe coordinates x , y , z .

$$\vec{V} = -V \cos \theta_p \cos \theta_y \vec{i} - V \cos \theta_p \sin \theta_y \vec{j} - V \sin \theta_p \vec{k} \quad (3.2)$$

$$\begin{aligned} \vec{A} \cdot \vec{V} &= |\vec{A}| |\vec{V}| \cos (180 - \alpha) = -|\vec{V}| \cos \theta_0 \cos \theta_p \cos \theta_y \\ &\quad - |\vec{V}| \sin \theta_0 \sin \theta_p \end{aligned} \quad (3.3)$$

$$\therefore \cos \alpha = \cos \theta_0 \cos \theta_p \cos \theta_y + \sin \theta_0 \sin \theta_p \quad (3.4)$$

3.2.2. Effective Cooling Velocity

If a hot-wire velocity calibration is done with the probe fixed at a sensor yaw angle of 90° to the flow and then this probe is used to measure velocities at sensor yaw angles other than 90° , the indicated velocity will not be the actual velocity but a so-called effective cooling velocity, V_e . This effective cooling velocity was related to the linearized anemometer output voltage, E_ℓ , by the second order equation

$$V_e = K_1 + K_2 E_\ell + K_3 E_\ell^2 \quad (3.5)$$

where K_1 , K_2 , and K_3 are coefficients determined from a second order calibration of the wire. The hot-wire measurement technique was based on knowing the exact relationship between the effective cooling velocity and the actual velocity. The relationship used by Schmidt and Okiishi [2] was

$$\begin{aligned} V_e/V &= b_0 + b_1 \alpha + b_2 \theta_p + b_3 V + b_4 \alpha^2 + b_5 \theta_p^2 + b_6 V^2 + b_7 \alpha \theta_p \\ &\quad + b_8 \alpha V + b_9 \theta_p V \end{aligned} \quad (3.6)$$

The coefficients (b_0 - b_9) in this equation were determined through extensive calibration of the sensor over a range of velocities, yaw angles, and pitch angles.

3.2.3. Measurement Technique

Hot-wire measurements leading to a single periodic-average velocity vector were made by taking data at each of three different sensor yaw angle orientations at a particular point in space.

The probe was first rotated about its axis while monitoring the hot-wire signal until the angular orientation that produced a minimum effective cooling velocity (a minimum hot-wire output voltage) was determined. This occurred when the sensor was approximately in the same yaw direction as the velocity vector. From this angular orientation (β_{mv} , see Figure 3.3), three values of probe yaw angle or offset were used for data sampling. The offset angles, $\theta_{a,off}$, $\theta_{b,off}$, and $\theta_{c,off}$, shown in Figure 3.3, were found to affect the precision of the measurement technique. As recommended by Schmidt and Okiishi [2], the following offset angles were used:

$$\begin{aligned}\theta_{a,off} &= 20^\circ \\ \theta_{b,off} &= 60^\circ \\ \theta_{c,off} &= -20^\circ\end{aligned}$$

For each of these wire orientations, two equations relating the velocity and angular orientation of the velocity vector relative to the probe were obtained. The resulting six equations are:

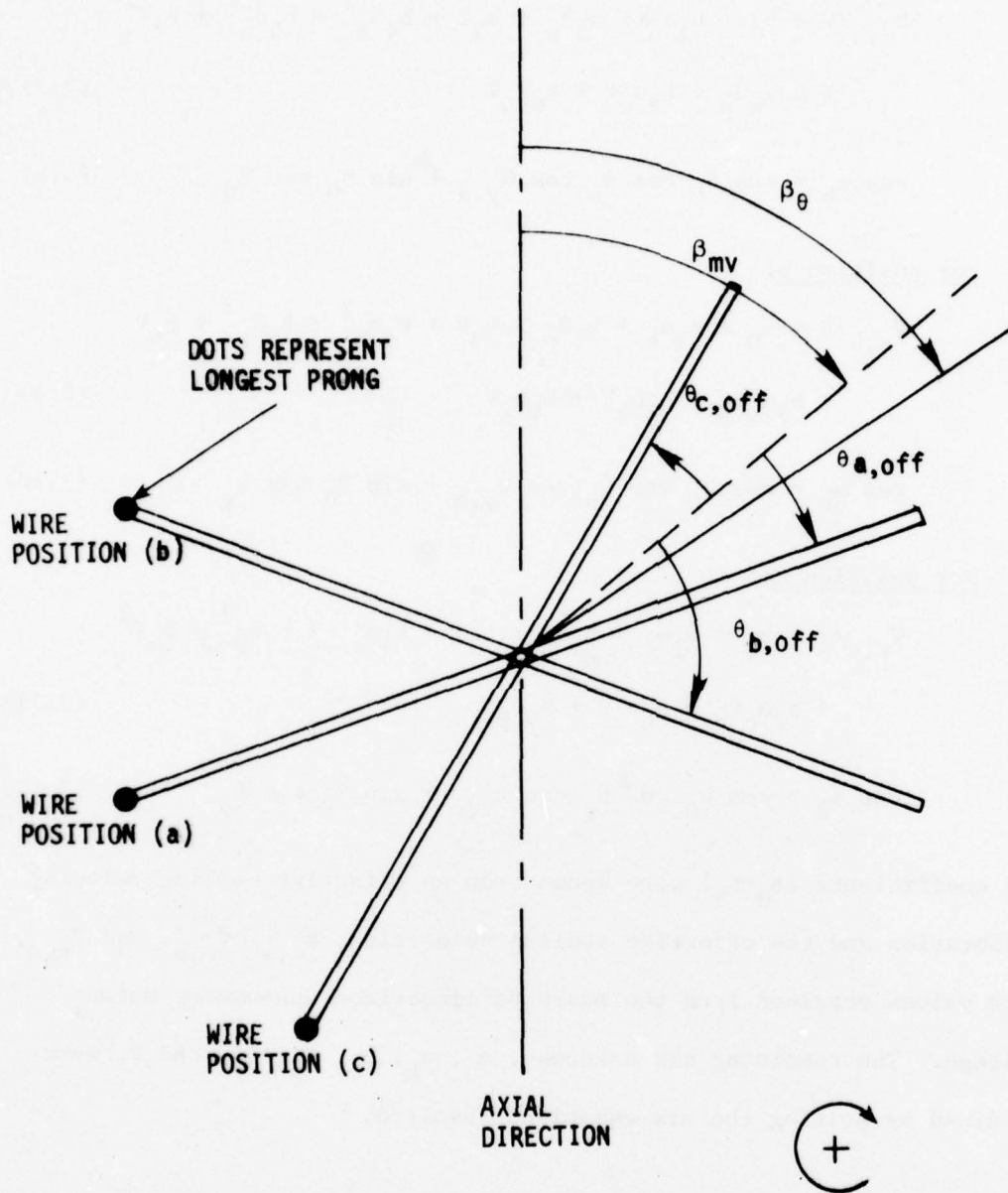


Figure 3.3. Hot-wire measurement positions and nomenclature, viewed from above along probe axis.

For position a:

$$V_{e,a}/V = b_0 + b_1\alpha_a + b_2\theta_p + b_3V + b_4\alpha_a^2 + b_5\theta_p^2 + b_6V^2 \\ + b_7\alpha_a\theta_p + b_8\alpha_a V + b_9\theta_p V \quad (3.7)$$

$$\cos \alpha_b = \cos \theta_0 \cos \theta_p \cos \theta_{y,a} + \sin \theta_0 \sin \theta_p \quad (3.8)$$

For position b:

$$V_{e,b}/V = b_0 + b_1\alpha_b + b_2\theta_p + b_3V + b_4\alpha_b^2 + b_5\theta_p^2 + b_6V^2 \\ + b_7\alpha_b\theta_p + b_8\alpha_b V + b_9\theta_p V \quad (3.9)$$

$$\cos \alpha_b = \cos \theta_0 \cos \theta_p \cos \theta_{y,b} + \sin \theta_0 \sin \theta_p \quad (3.10)$$

For position c:

$$V_{e,c}/V = b_0 + b_1\alpha_c + b_2\theta_p + b_3V + b_4\alpha_c^2 + b_5\theta_p^2 + b_6V^2 \\ + b_7\alpha_c\theta_p + b_8\alpha_c V + b_9\theta_p V \quad (3.11)$$

$$\cos \alpha_c = \cos \theta_0 \cos \theta_p \cos \theta_{y,c} + \sin \theta_0 \sin \theta_p \quad (3.12)$$

The coefficients (b_0 - b_9) were known from an effective cooling velocity calibration and the effective cooling velocities, $V_{e,a}$, $V_{e,b}$, and $V_{e,c}$, were values obtained from the measured linearized anemometer output voltage. The remaining six unknowns, α_a , α_b , α_c , θ_p , θ_y , and V , were obtained by solving the six equations involved.

3.3. Calibration Procedures

Complete velocity sensing calibration was done with the calibration nozzle. The probe was positioned one nozzle diameter above the

exit plane. Static pressure at this location was assumed to be atmospheric while plenum static wall pressure was assumed to be equal to the plenum total pressure. The nozzle velocity was calibrated using the following equation:

$$V = \sqrt{\frac{2g_c \gamma_{H_2O} \Delta P_n}{\rho}} \quad (3.13)$$

where

V = velocity, m/s

g_c = gravitational constant 1.0 kgm/Ns^2

γ_{H_2O} = specific weight of water, N/m^3

ΔP_n = differential pressure between plenum pressure and atmospheric pressure, m of water

ρ = density of air, kg/m^3

3.3.1. Linearizer Coefficient Calibration

Before the anemometer output voltage can be linearized, a fourth order fit of the known nozzle velocity versus anemometer output voltage must be accomplished to obtain values of the linearizer coefficients. This calibration was done with the wire at 90° to the nozzle flow. The nozzle velocity was varied from 0 to 23 m/s. From these data, the fourth order linearizer coefficients were computed along with percent error of each data point. Errors were normally less than 0.5% with none greater than 1.0%. The "zeroth" order term was assumed to be equal to zero. This calibration was done only once for each new sensor.

3.3.2. Effective Cooling Velocity Calibration

An extensive calibration of a new sensor was done to determine the ten coefficients (b_0 - b_9) of the effective cooling velocity/actual velocity relationship. The effective cooling velocity calibration was done for the following conditions:

Velocity	11.6, 15.2, 19.2, 22.3, m/s
Pitch angle	-9 to 6, degrees, in increments of 3 degrees
Probe yaw angle	0 to 90, degrees, in increments of 5 degrees
	0 to -90, degrees, in increments of 5 degrees

This is a representative range of conditions expected to be encountered in the compressor. The probe yaw angle was varied over each of six pitch angles at each velocity. Separate calibrations were accomplished for positive and for negative yaw angles due to slight asymmetry of the hot-wire sensor. The appropriate set of coefficients was then used in data reduction depending on the sign of the yaw angle. Errors between the actual velocity and the least squares fit of the data were generally less than 1.0% with only a few greater than 2.0%.

3.3.3. Second Order Velocity Calibration

A second order calibration was frequently repeated (each time the sensor was used for a day of data taking) with the hot wire positioned at 90° to the nozzle flow to obtain the coefficients for the effective cooling velocity equation

$$V_i = K_1 + K_2 E_\ell + K_3 E_\ell^2 \quad (3.5)$$

where

V_e = effective cooling velocity

E_{λ} = linearized anemometer output voltage

K_1, K_2, K_3 = second order coefficients

Once temperature equilibrium was reached, the linearized anemometer output voltage was recorded over a range of velocities from 4 to 23 m/s. The three coefficients and percent error of each data point were computed. Errors were always less than 2.0%, usually less than 1.0%.

3.4. Data Acquisition

Circumferential traverses of the compressor flow field were made behind the first rotor and the first stator for the maximum noise position of the first stator blade row.

Prior to taking data, temperature equilibrium was obtained, instruments were allowed to warm up, manometers were zeroed, linearizer coefficients were set, probe yaw angle and circumferential-position potentiometers were calibrated, flow coefficient was calculated and the flow adjusted until the reference value of flow coefficient was obtained, and a second order calibration of the sensor was performed. The probe was positioned in the compressor at the desired immersion depth. The zero of the periodic rotor sampling position was adjusted using the variable triggering delay capacitor with the photo-electric pickup positioned at zero. Once the zero was obtained, the photo-electric pickup was moved circumferentially to give the desired rotor sampling position. With the probe at 90° to the axial direction of the compressor, a complete circumferential survey was made with the sensor output signal displayed on an x-y storage oscilloscope to

obtain an approximate idea of axial velocity variation with circumferential position. From this trace, the location of the blade wake could be determined. Thirty data positions in space were established over a circumferential distance of 9.73° (one stator blade pitch) with 0.25° increments within the wake region and 0.50° increments elsewhere. The circumferential positioning carriage was then placed at the $Y/S_S = 0.0$ (see Figure 2.5) position for the first set of data. A periodic-average velocity vector at each of the thirty positions was obtained as described earlier.

3.5. Data Reduction

Data reduction was accomplished with the desk-top calculator. The six nonlinear simultaneous equations were solved using the Newton-Raphson numerical technique. Usually less than five iterations were required for each point.

The compressor coordinate system is shown in Figure 3.4. The probe axis corresponds to the radial direction, R , in the compressor. The Z -axis is aligned axially with the positive direction in the direction of flow. The Y -axis is positive in the direction of shaft rotation. Also shown are the sign conventions for β_θ , β_r , V_θ , V_z and V_r . The flow parameters calculated during the data reduction are:

- (1) absolute velocity, \vec{V} , m/s
- (2) axial velocity, V_z , m/s
- (3) absolute tangential velocity, V_θ , m/s
- (4) radial velocity, V_r , m/s

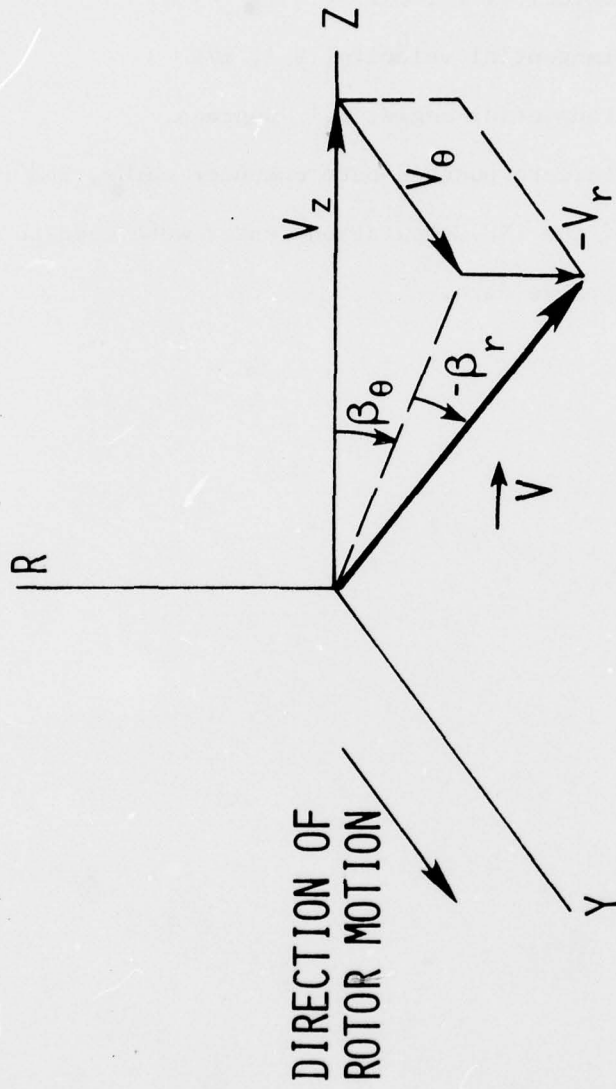


Figure 3.4. Compressor coordinate system showing nomenclature and sign convention for three-dimensional periodic-average velocity and angle parameters.

- (5) tangential flow angle, β_θ , degrees
- (6) radial angle, β_r , degrees
- (7) relative velocity, \vec{V}' , m/s
- (8) relative tangential velocity, V_θ' , m/s
- (9) relative tangential angle, β_θ' , degrees

Selected results were punched onto computer cards, and the computing facilities of the ISU Computation Center were used to generate various displays of these data.

4. PRESENTATION AND DISCUSSION OF DATA

In this section some new periodic-average hot-wire data for flow behind the first rotor and first stator blade rows (maximum noise configuration) of a low-speed, multistage, axial-flow research compressor are presented. These data are compared with similar data previously presented and discussed by Wagner and Okiishi [7] for the minimum noise configuration of the compressor. Various methods are used to examine and interpret these data. Scalar plots showing axial, tangential, and radial velocity component variations in the circumferential direction for different rotor sampling positions are presented and interpreted. Some radial, tangential, and relative tangential flow angles are also shown. Blade-to-blade plane and hub-to-tip cross-section drawings constructed from these data are used to aid information interpretation and understanding. In addition, drawings of three-dimensional velocity vector sheets are presented. Trends observed are pointed out and explanations are offered for some of the differences noted between maximum and minimum noise operation flow.

4.1. First Rotor Exit Flow Data

First rotor blade row exit flow data for the maximum and for the minimum noise compressor configurations are compared in detail in this section to determine the extent of first stator upstream influence. The first stator blade row positions for maximum and for minimum noise are sketched in Figure 4.1 for a radial span location of 50%. Data were

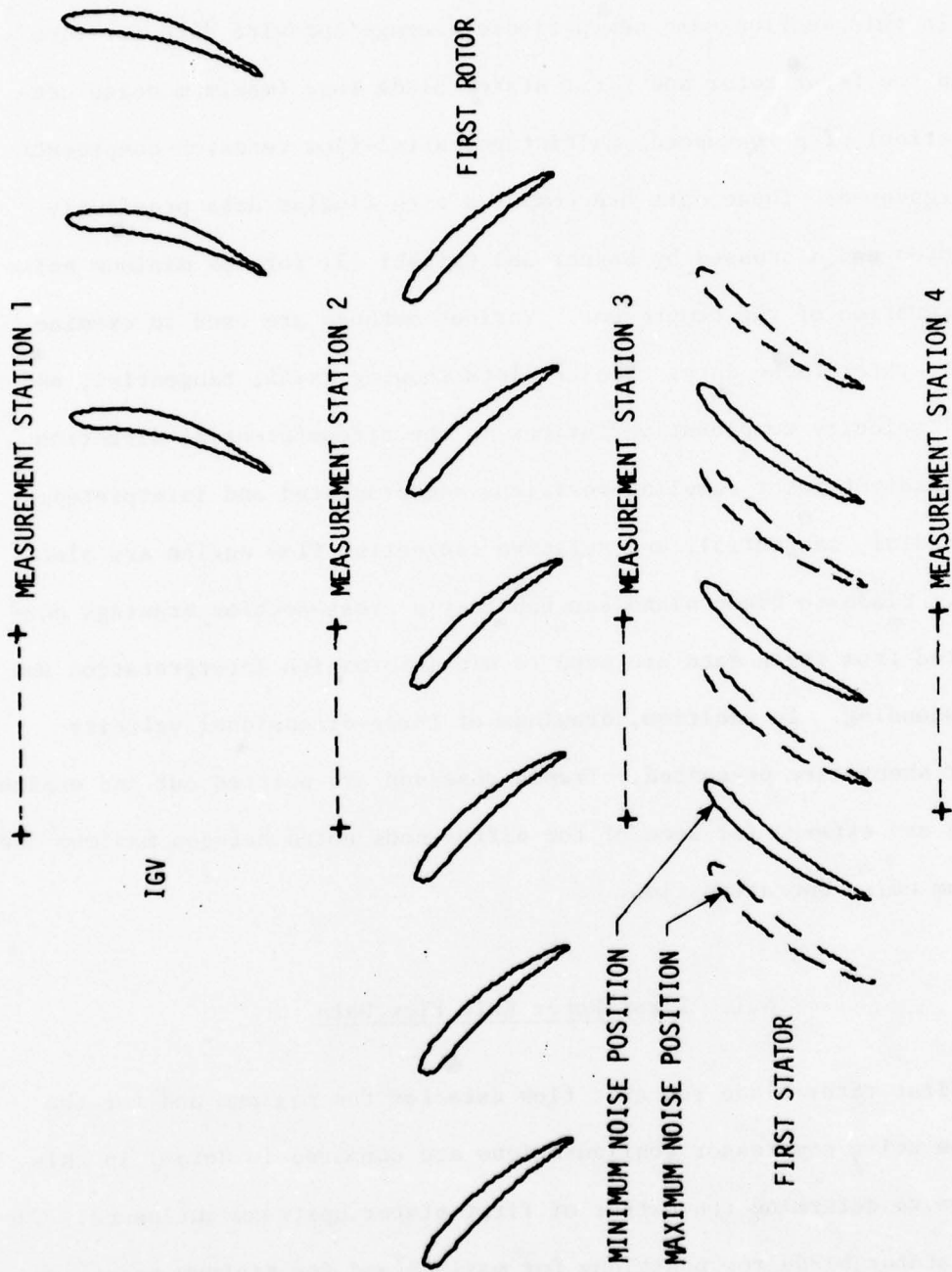
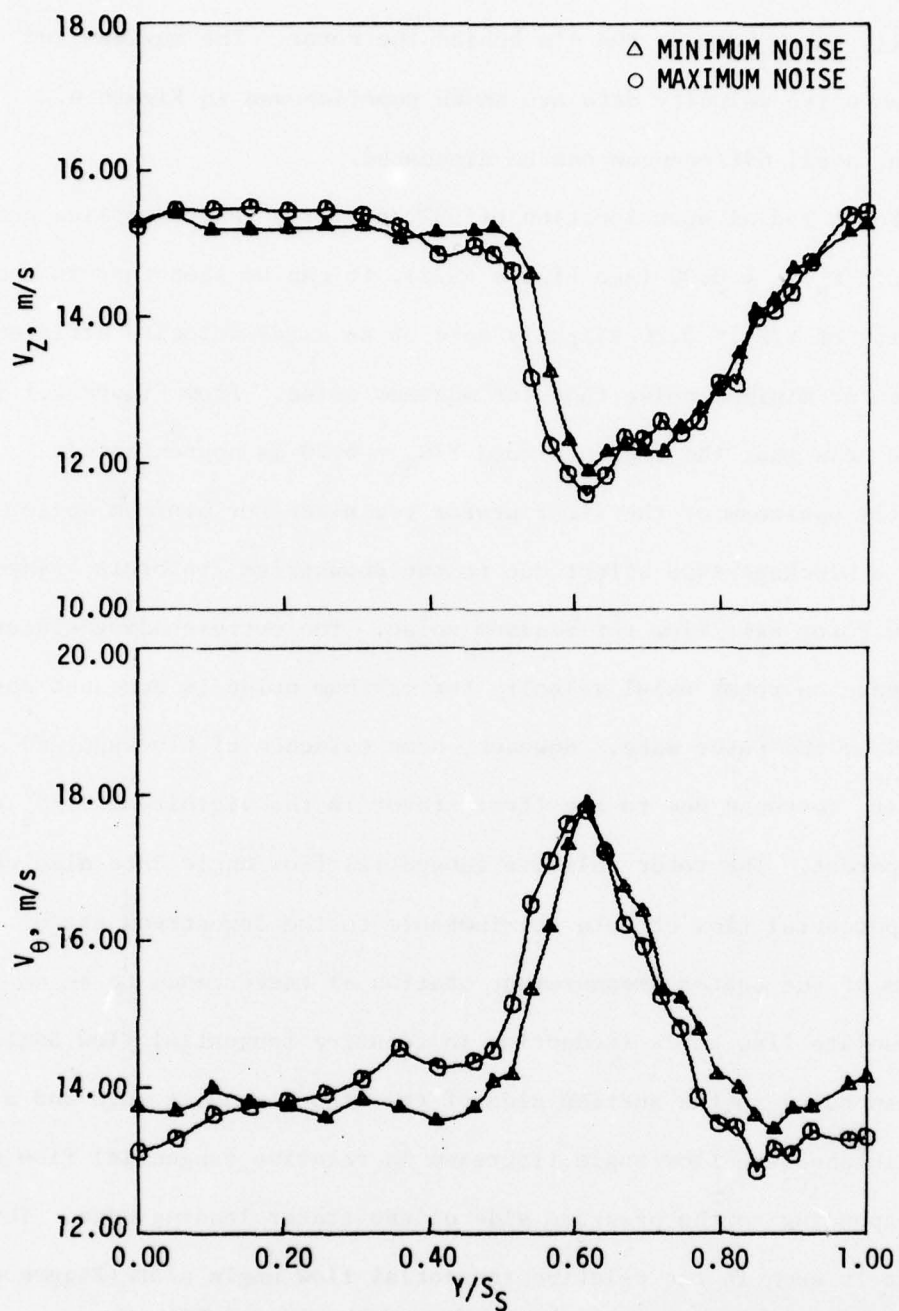


Figure 4.1.1. First stator blade section positions for minimum and maximum noise at 50% span.

actually taken between the +'s behind the rotor. The maximum and minimum noise velocity data are shown superimposed in Figure 4.2 so that small differences can be discussed.

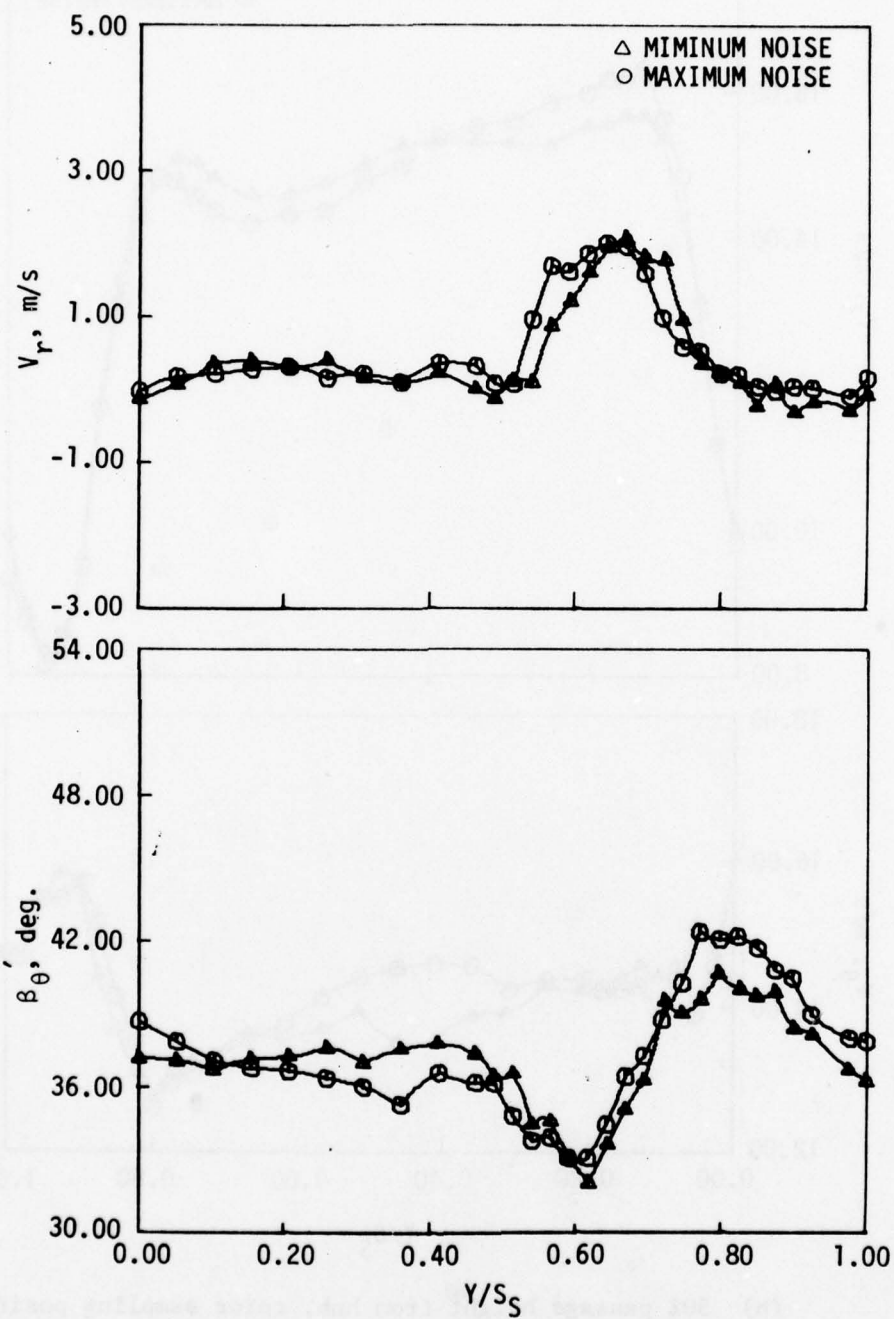
For a radial span location of 50% and for a rotor sampling position of $Y_{0R}/S_R = 0.00$ (see Figure 4.2a), it can be seen that in the vicinity of $Y/S_S = 0.20$ slightly more of an axial velocity deficiency exists for minimum noise than for maximum noise. From Figure 4.1 it can be seen that the region around $Y/S_S = 0.20$ is approximately directly upstream of the first stator row blade for minimum noise. Thus, a blockage-type effect due to the downstream stator is evident in the rotor exit flow for minimum noise. The corresponding stator influence on rotor axial velocity for maximum noise is somewhat obscured by the rotor wake. However, some evidence of blockage and axial velocity decrease due to the first stator in the vicinity of $Y/S_S = 0.70$ is apparent. The rotor relative tangential flow angle data also reflect some potential flow effects attributable to the downstream stator. Upstream of the stator (measurement station 3) there tends to be an increase in absolute flow angle (reduction in relative tangential flow angle) corresponding to the suction side of the stator leading edge and a reduction in absolute flow angle (increase in relative tangential flow angle) corresponding to the pressure side of the stator leading edge. This effect is seen in the relative tangential flow angle plot (Figure 4.2a) around $Y/S_S = 0.20$ for minimum noise and $Y/S_S = 0.80$ for maximum noise.

The axial velocity and relative tangential flow angle variation differences for maximum and minimum noise lead to tangential velocity variation differences that can be consistently explained in terms of



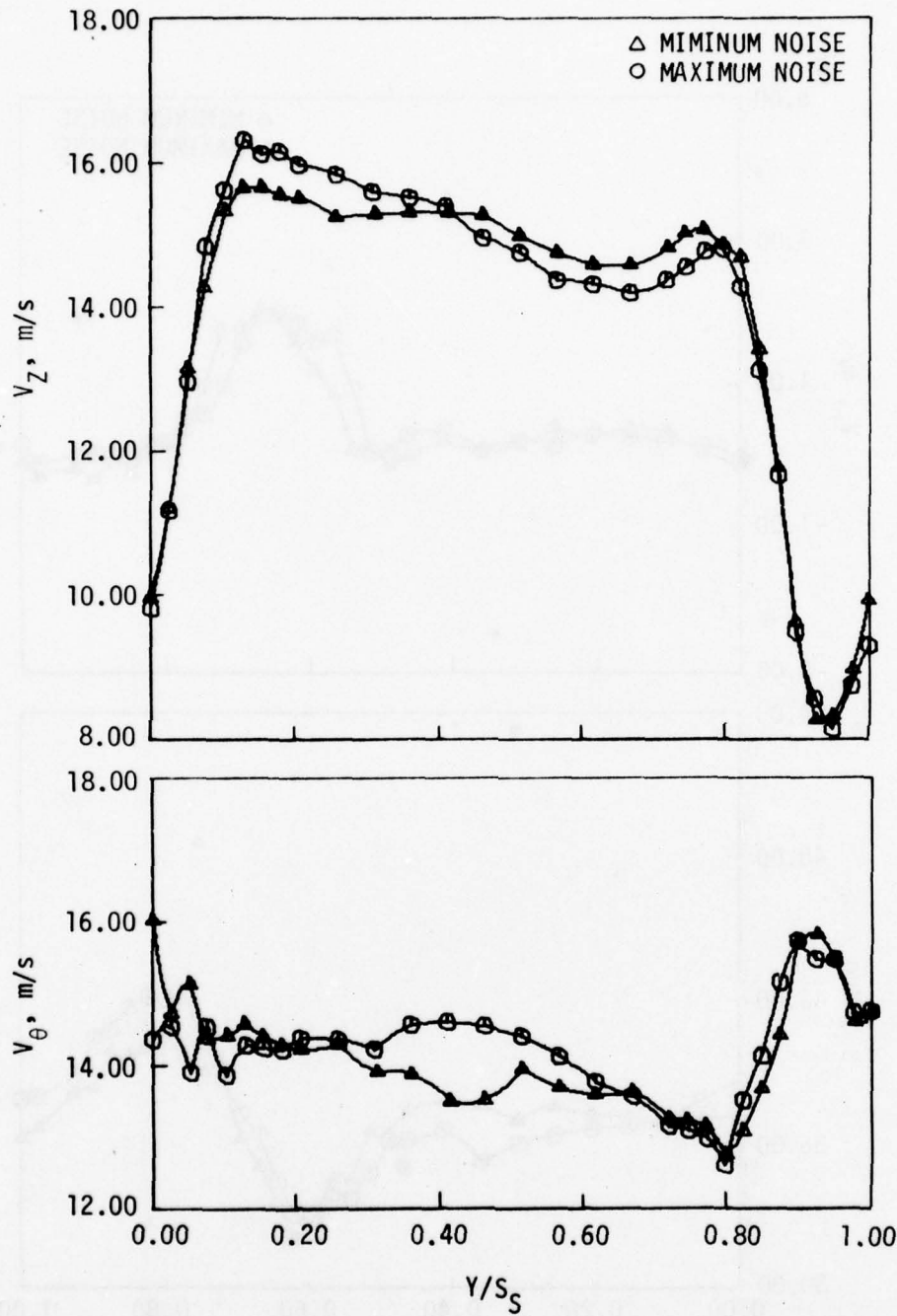
(a) 50% passage height from hub, rotor sampling position $Y_{0R}/S_R = 0.00$.

Figure 4.2. Blade-to-blade distribution of periodic-average flow-field parameters. First rotor exit flow, minimum and maximum noise.



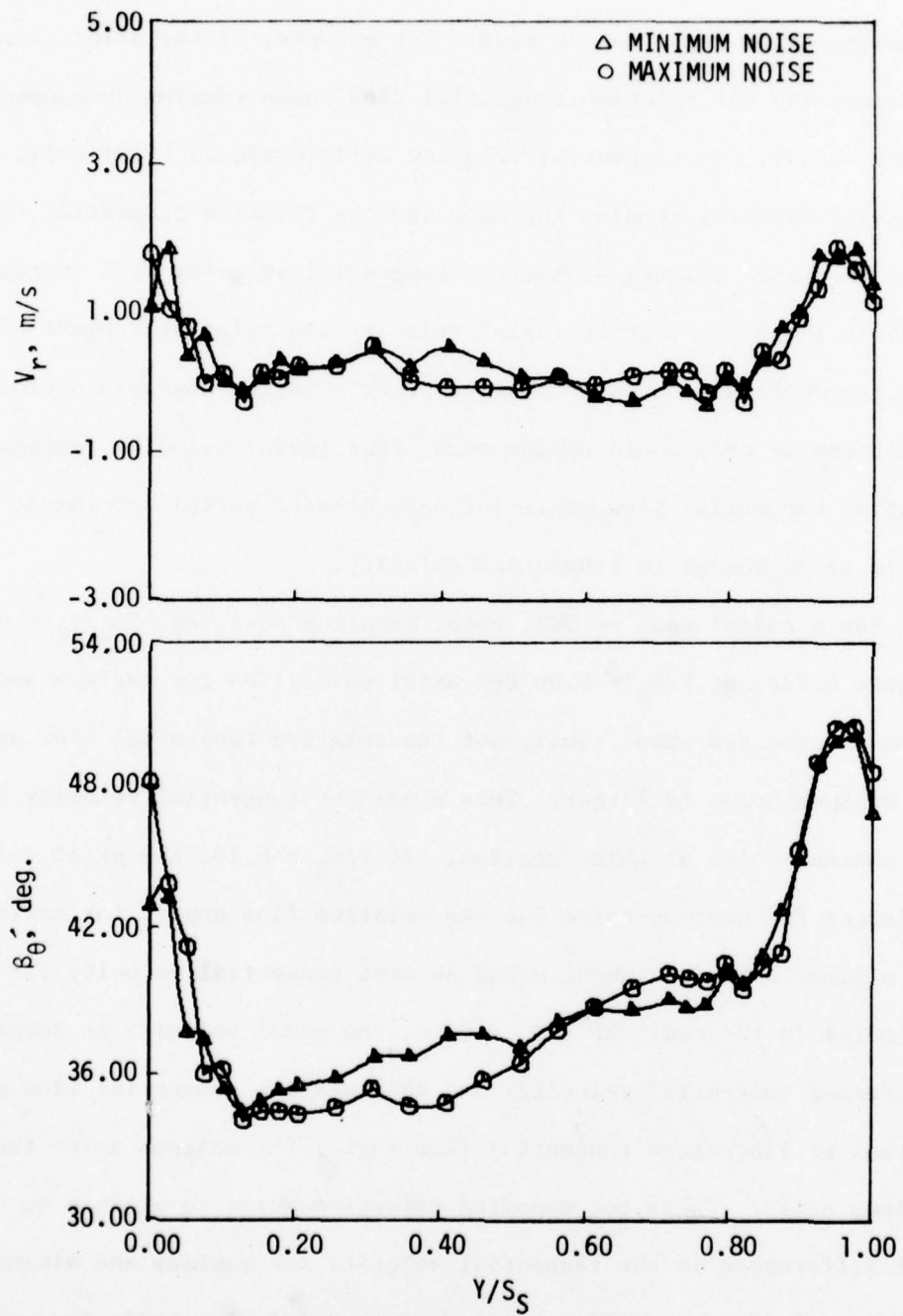
(a) Concluded.

Figure 4.2. Continued.



(b) 50% passage height from hub, rotor sampling position
 $Y_{O_R}/S_R = 0.69$.

Figure 4.2. Continued.

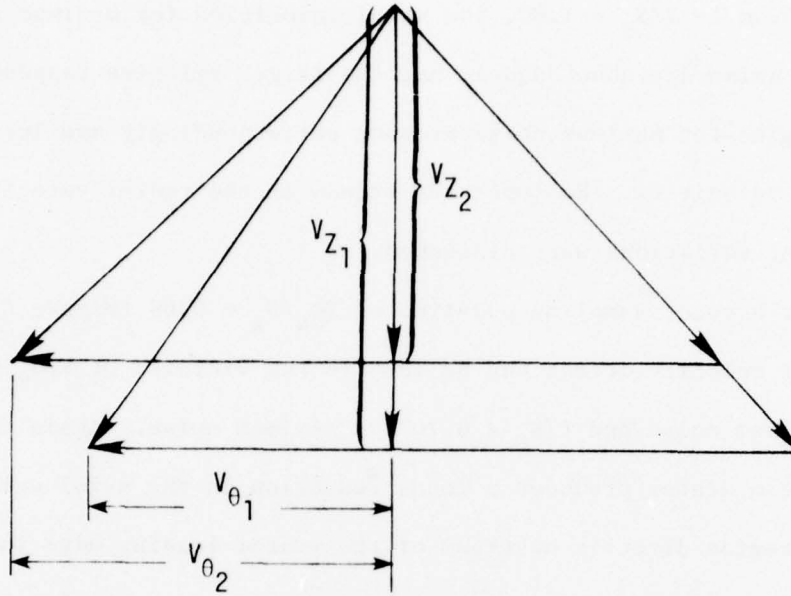


(b) Concluded.

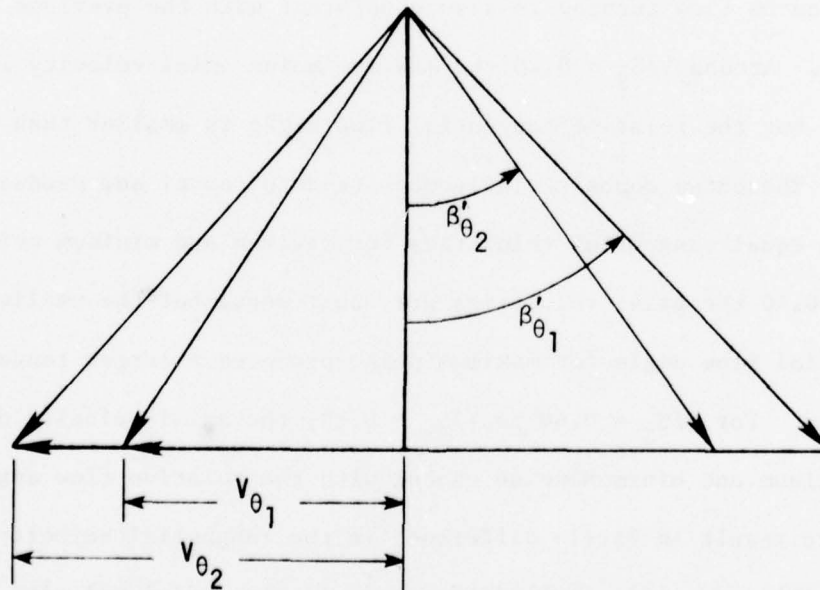
Figure 4.2. Concluded.

velocity triangles, like the ones of Figure 4.3. Here the relationship between the axial velocity, tangential velocity, and relative tangential flow angle can be seen. For example, if the axial velocity decreases and the relative tangential flow angle remains unchanged (Figure 4.3a), the tangential velocity will increase. Similarly, if the axial velocity remains the same and the relative tangential flow angle decreases (Figure 4.3b), the tangential velocity will increase. Possibly these two effects (axial velocity and relative tangential velocity decrease) could combine to produce large tangential velocity variations or they could oppose each other (axial velocity decrease, relative tangential flow angle increase or vice versa) and result in little or no change in tangential velocity.

For a radial span of 50%, rotor sampling position, $Y_{0R}/S_R = 0.00$ (Figure 4.2a), at $Y/S_S = 0.00$ the axial velocities for maximum and minimum noise are about equal, but the relative tangential flow angle for maximum noise is larger. Thus a smaller tangential velocity occurs for maximum noise at this location. At $Y/S_S = 0.10$, the axial velocity is larger for maximum noise but the relative flow angles for maximum and minimum noise are about equal so that tangential velocity for maximum noise is reduced. At $Y/S_S = 0.20$, the axial velocity is larger (decreased tangential velocity) and the relative tangential flow angle is smaller (increased tangential flow angle) for maximum noise than for minimum noise. These two opposing effects combine to produce no significant differences in the tangential velocity for maximum and minimum noise. At $Y/S_S = 0.40$, the smaller relative tangential flow angle for maximum noise with about equal axial velocities for maximum and minimum noise



(a) Axial velocity variation influence on tangential velocity.



(b) Relative tangential flow angle variation influence on tangential velocity.

Figure 4.3. First rotor exit flow velocity variations.

results in a larger tangential velocity for maximum noise. For $Y/S_S = 0.60$ to $Y/S_S = 1.00$, the axial velocities for maximum and minimum noise are about equal, but the larger relative tangential flow angles for maximum noise produce correspondingly smaller tangential velocities. No important trends in the radial velocity component variations were discerned.

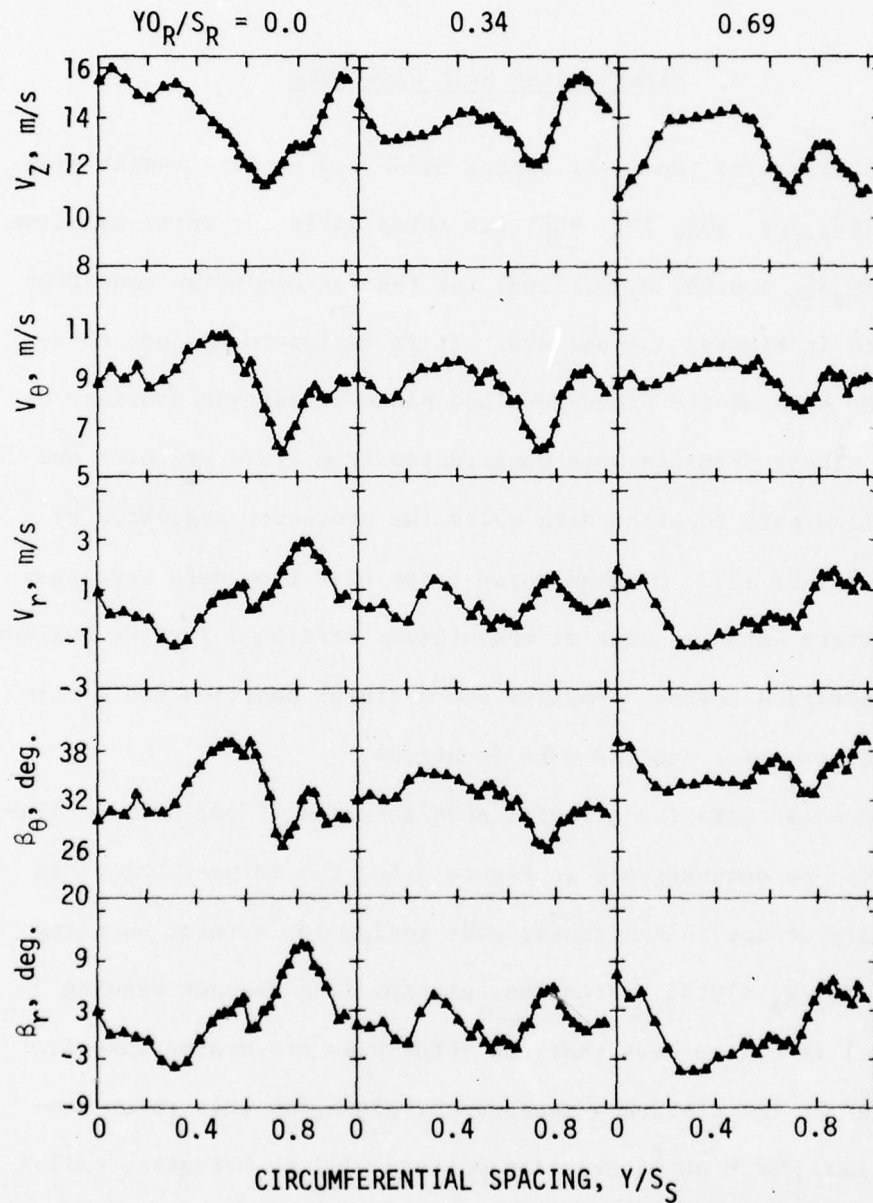
For a rotor sampling position of $Y_{O_R}/S_R = 0.69$ (Figure 4.2b), an axial velocity defect can be seen in the vicinity of $Y/S_S = 0.20$ for minimum noise and $Y/S_S = 0.70$ for maximum noise. Again the downstream stator produces a local reduction in the axial velocity in the region directly upstream of the stator leading edge location. The maximum noise stator upstream influence can now be clearly seen because it is not occurring within the rotor wake region. The stator influence on flow turning is also consistent with the previous observations. Around $Y/S_S = 0.20$ the maximum noise axial velocity is larger, but the relative tangential flow angle is smaller than minimum noise. These two opposing influences tend to cancel and produce approximately equal tangential velocities for maximum and minimum noise. Near $Y/S_S = 0.40$ the axial velocities are about equal but the smaller relative tangential flow angle for maximum noise produces a larger tangential velocity. For $Y/S_S = 0.60$ to $Y/S_S = 0.80$, the axial velocity differences for maximum and minimum noise cancel with the relative flow angle differences to result in little difference in the tangential velocity values. Again, there are only small differences in the radial velocity data for maximum and minimum noise operation and significant trends are not apparent.

It should be noted that changing the position of the first stator blade row did not appreciably affect the circumferential position of the rotor wake.

4.2. First Stator Exit Flow Data

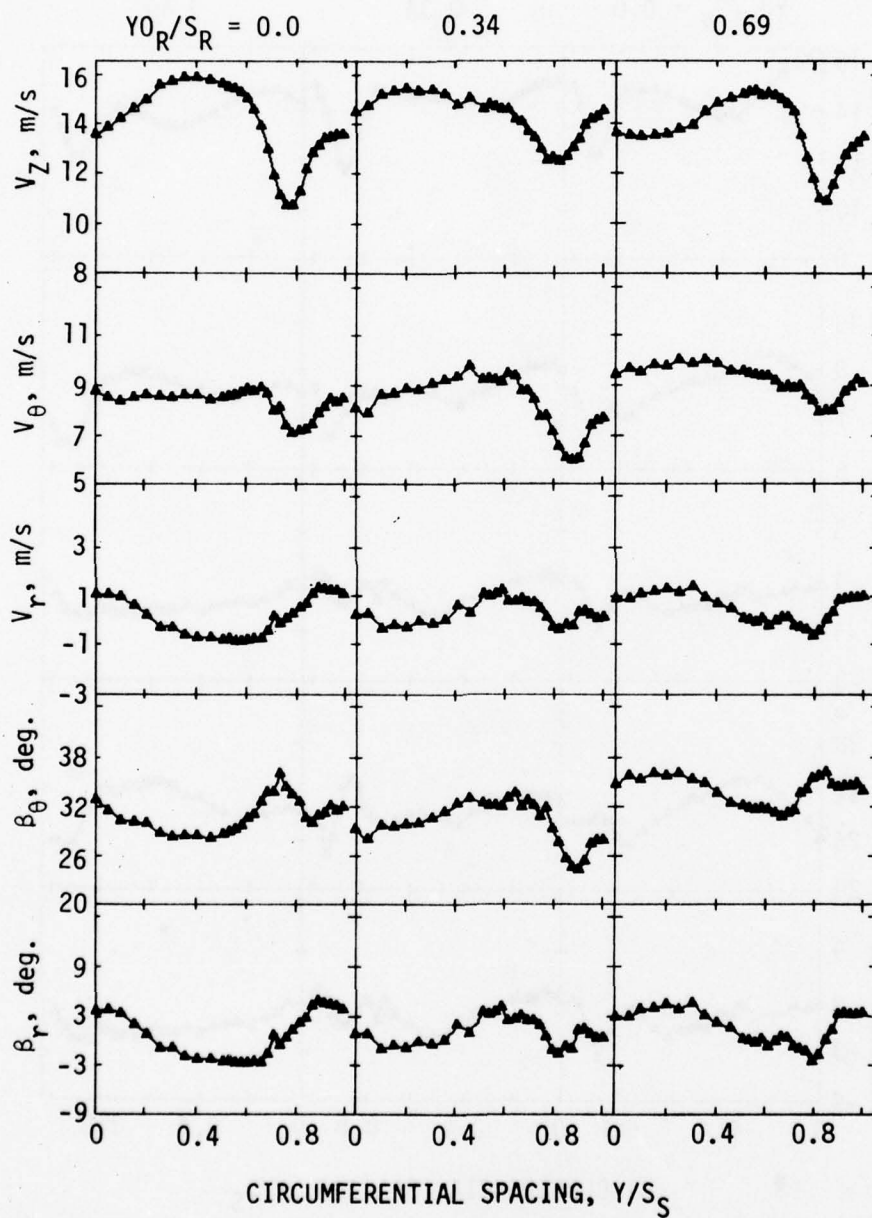
Data taken behind the first stator blade row at five radial span locations (10%, 30%, 50%, 70%, 90%) for three different rotor sampling positions ($Y_{O_R}/S_R = 0.00, 0.34, 0.69$) for the maximum noise condition are presented in Figures 4.4 and 4.5. It is easier to discuss these data with the help of the blade-to-blade plane or cascade drawings of Figure 4.6. These drawings were constructed from fluid velocity and heated air flow path location data using the procedure suggested by Wagner and Okiishi [7]. Minimum noise rotor exit flow data were used for wake pattern establishment at measurement station 3 for the maximum noise configuration cascade drawings since stator position had little if any effect on rotor and IGV wake locations.

Maximum noise data for a radial span location of 50% will be discussed first. As demonstrated in Figure 4.4c, the largest defect in axial velocity occurs in the stator wake region for a rotor sampling position of $Y_{O_R}/S_R = 0.34$. From the corresponding cascade drawing (Figure 4.6c) it can be seen that the rotor wake and stator wake are "interacting" at the station 4 measurement plane for this rotor sampling position. Such an interaction pattern will be hereafter called an interacted stator wake flow. As explained by Kerrebrock and Mikolajczak [5], a chopped rotor wake involves a "slip velocity" from



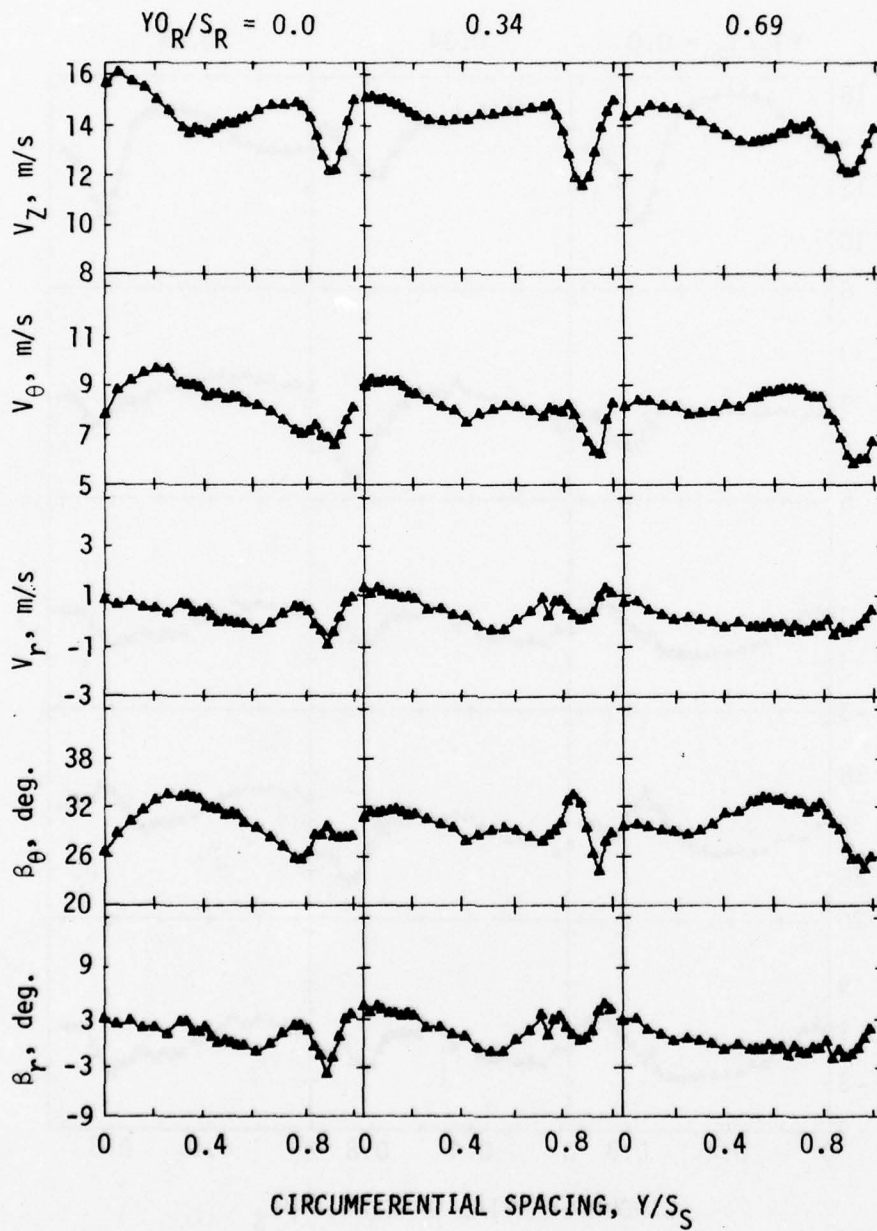
(a) 10% passage height from hub.

Figure 4.4. Blade-to-blade distribution of periodic-average flow-field parameters. First stator exit flow, maximum noise.



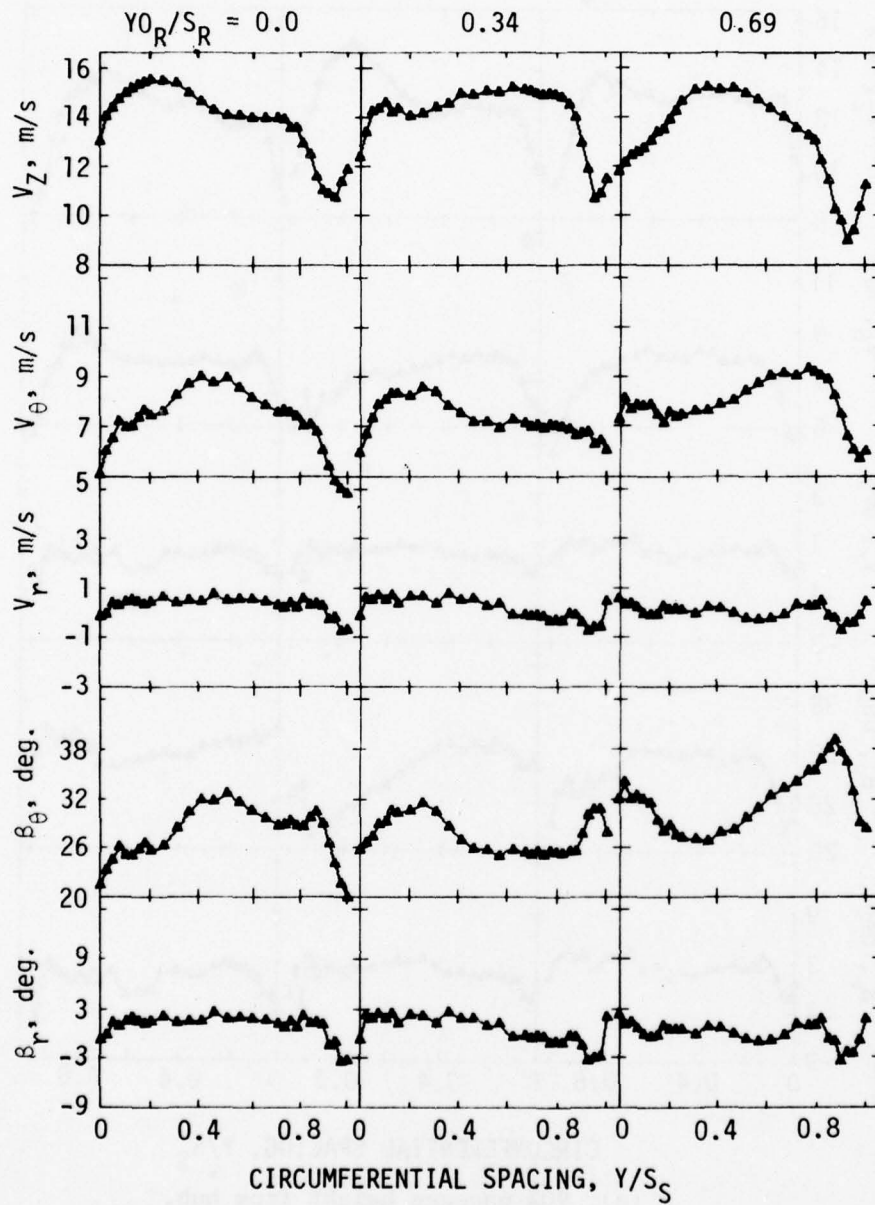
(b) 30% passage height from hub.

Figure 4.4. Continued.



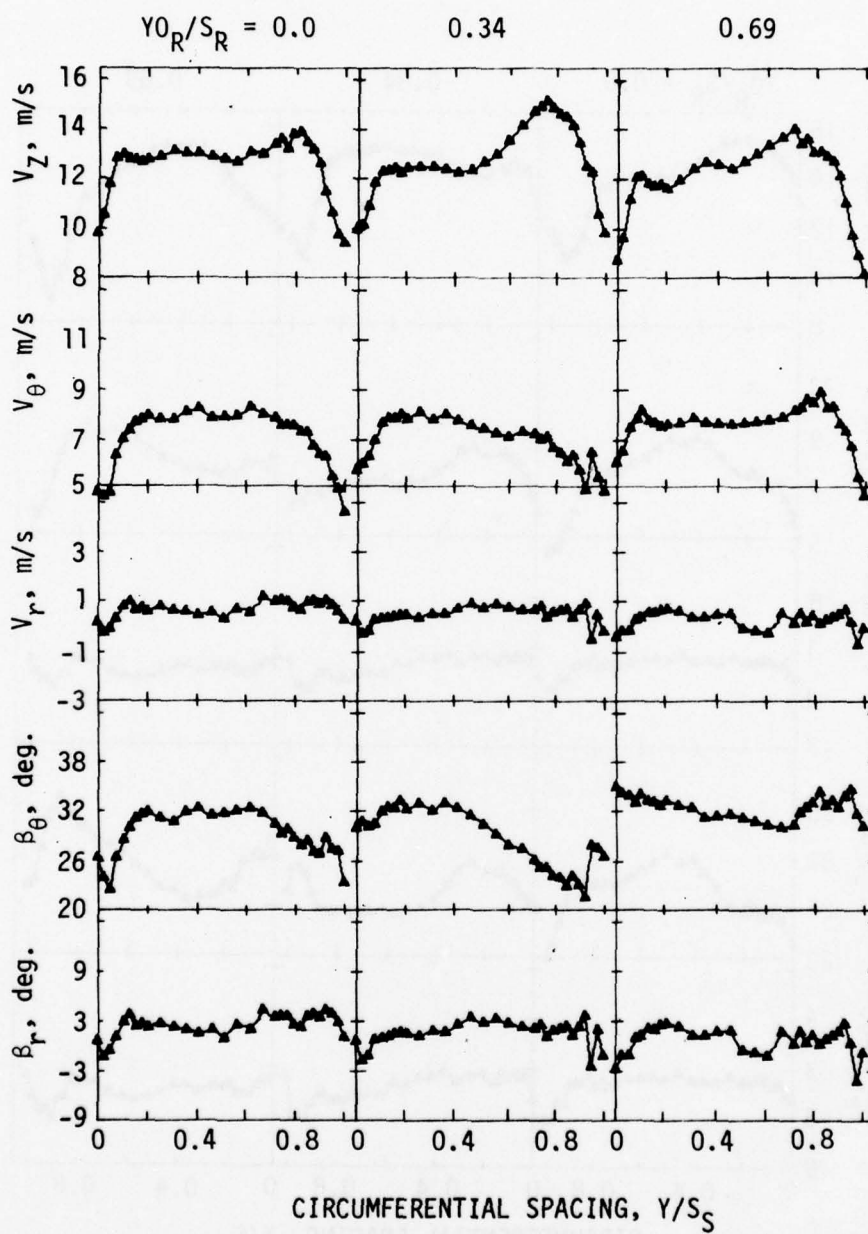
(c) 50% passage height from hub.

Figure 4.4. Continued.



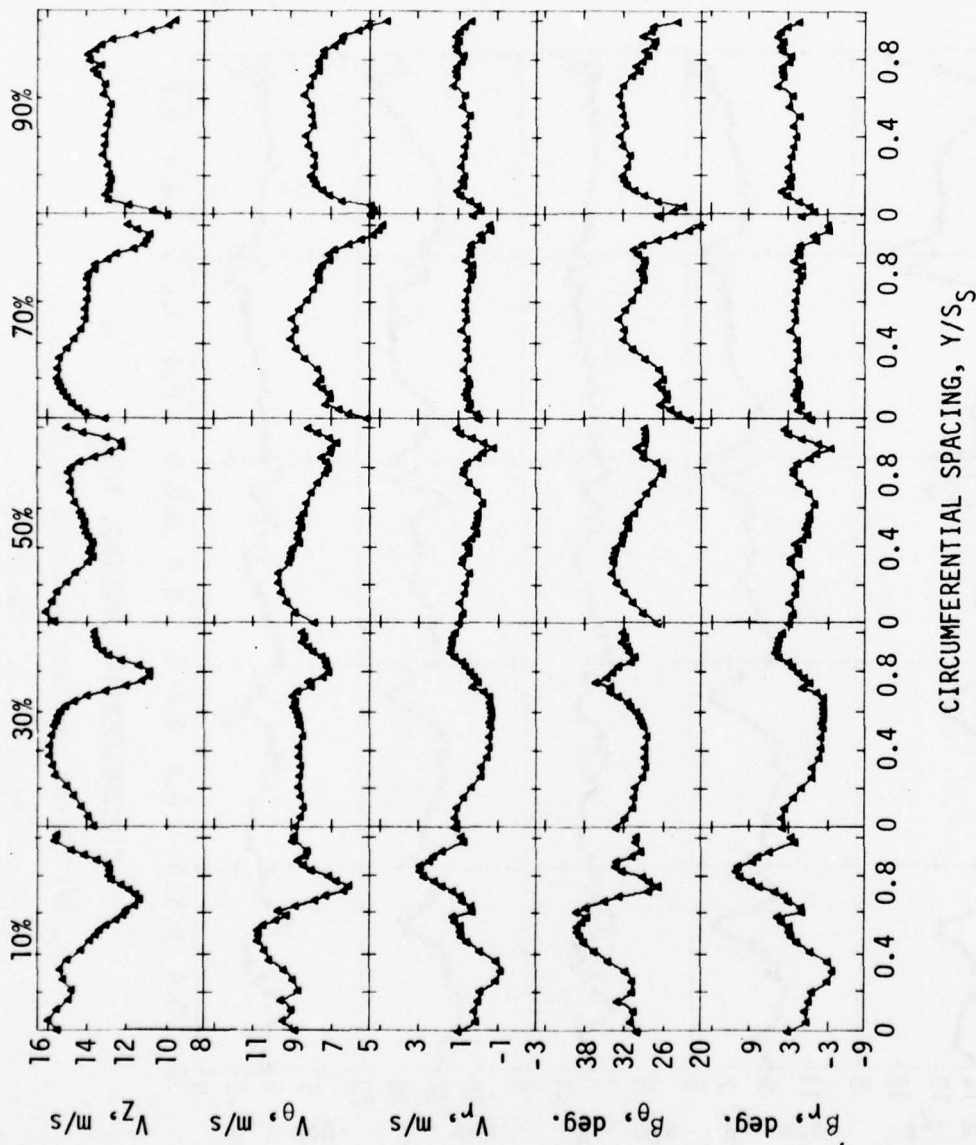
(d) 70% passage height from hub.

Figure 4.4. Continued.



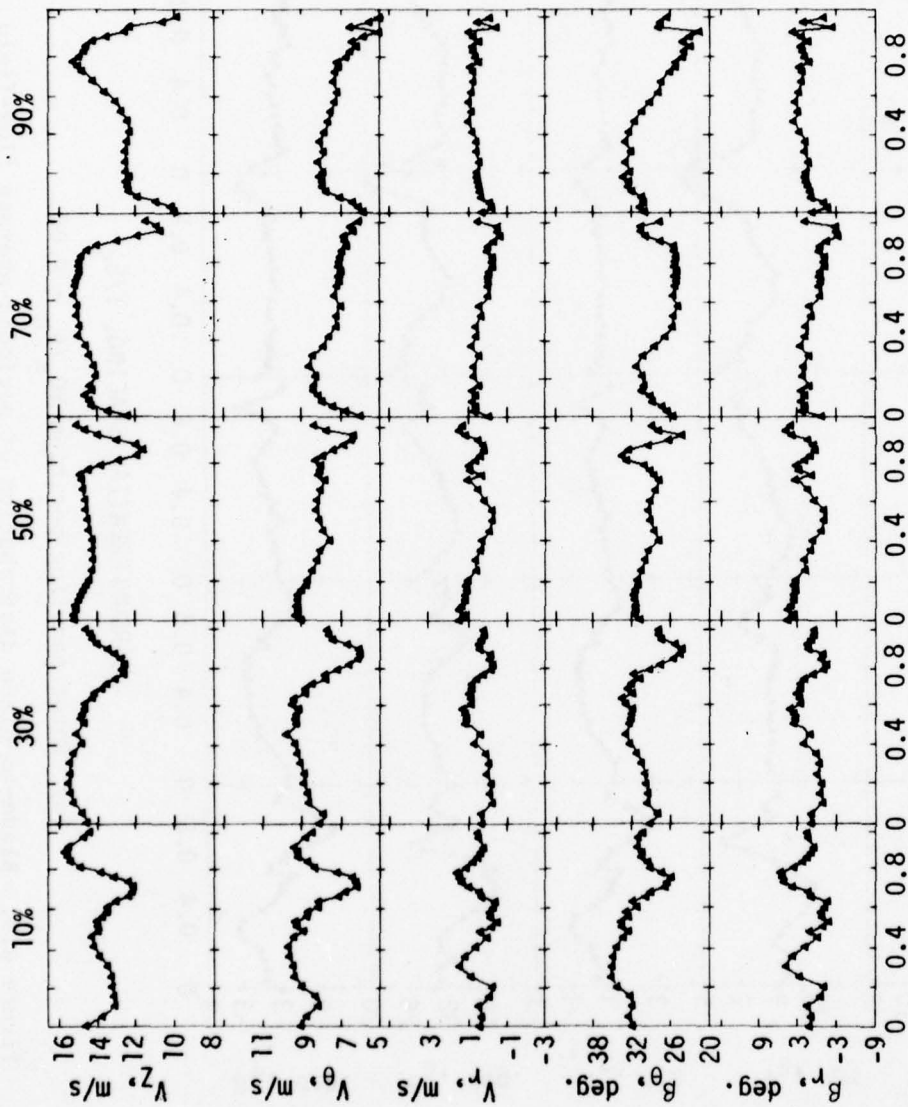
(e) 90% passage height from hub.

Figure 4.4. Concluded.



(a) Rotor sampling position $Y_{0R}/S_R = 0.00$.

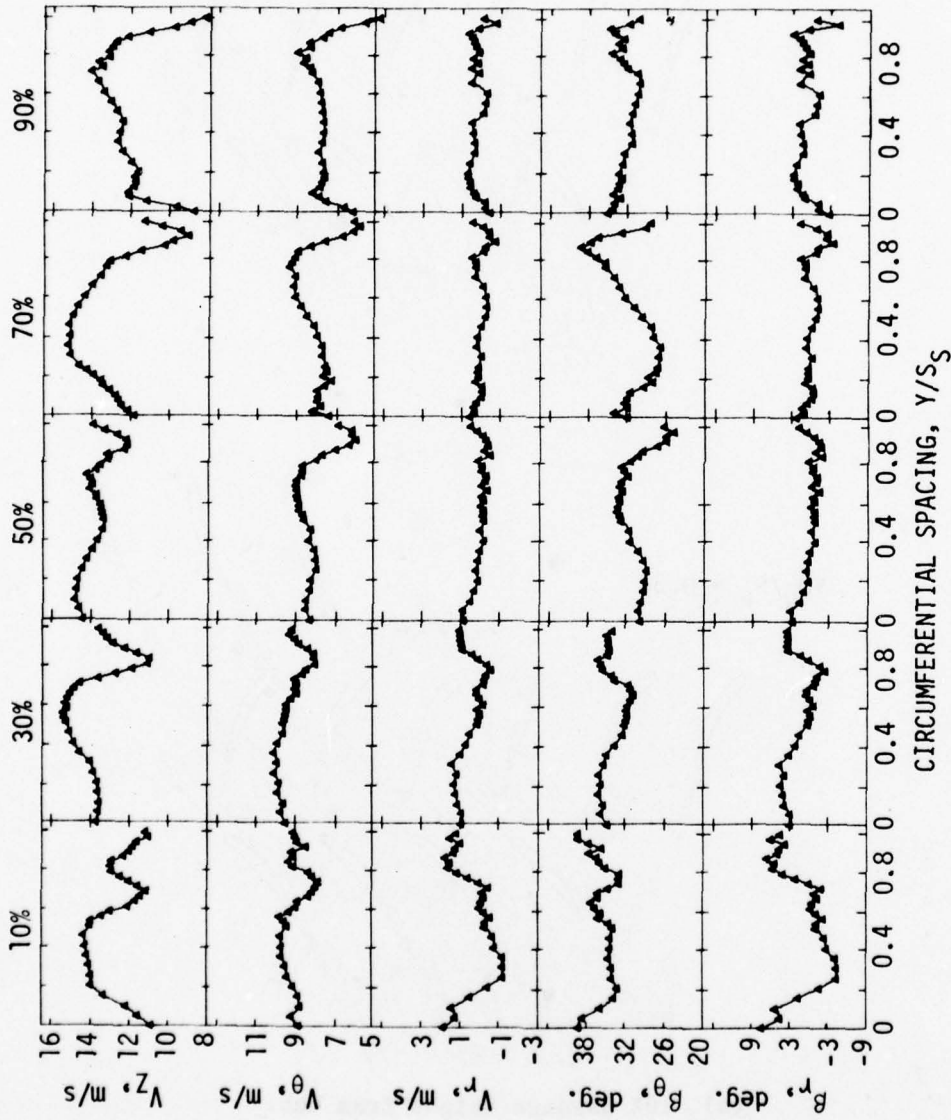
Figure 4.5. Blade-to-blade distribution of periodic-average flow-field parameters. First stator exit flow, maximum noise.



CIRCUMFERENTIAL SPACING, Y/S_s

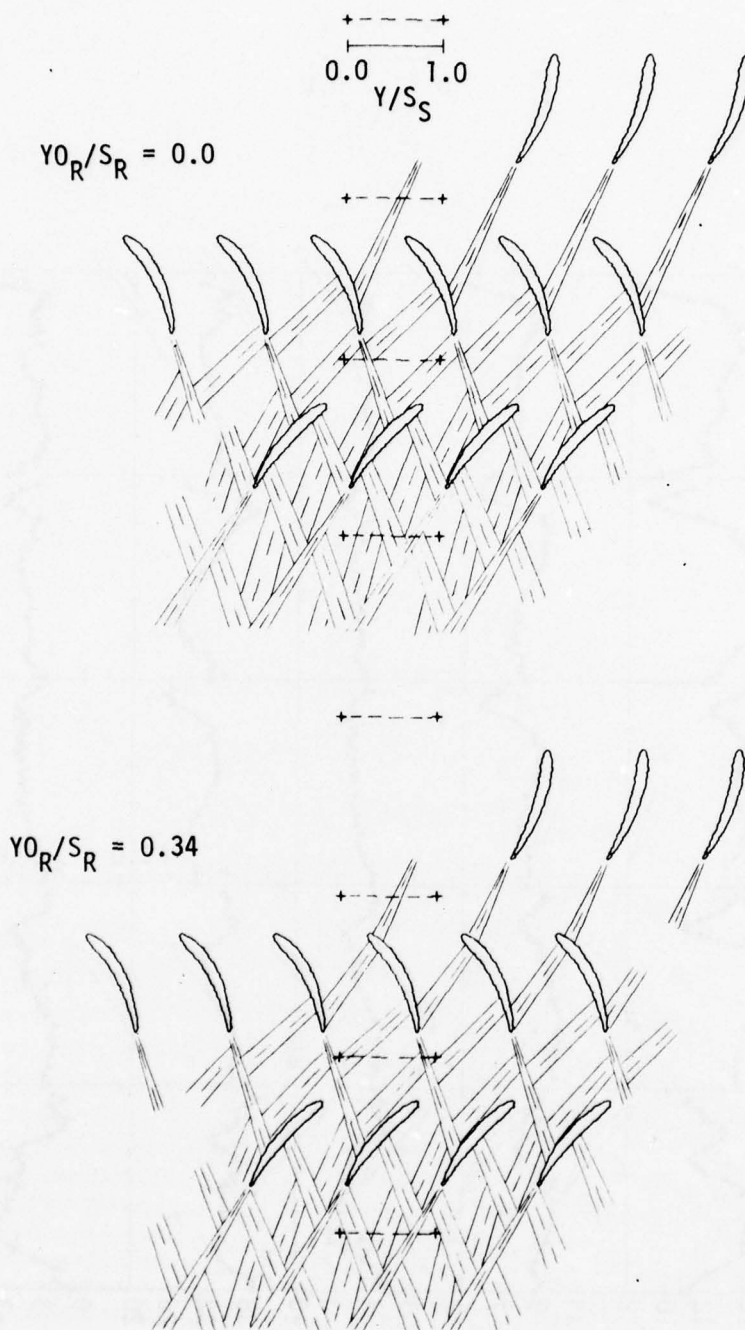
(b) Rotor sampling position $Y_{0R}/S_R = 0.34$.

Figure 4.5. Continued.



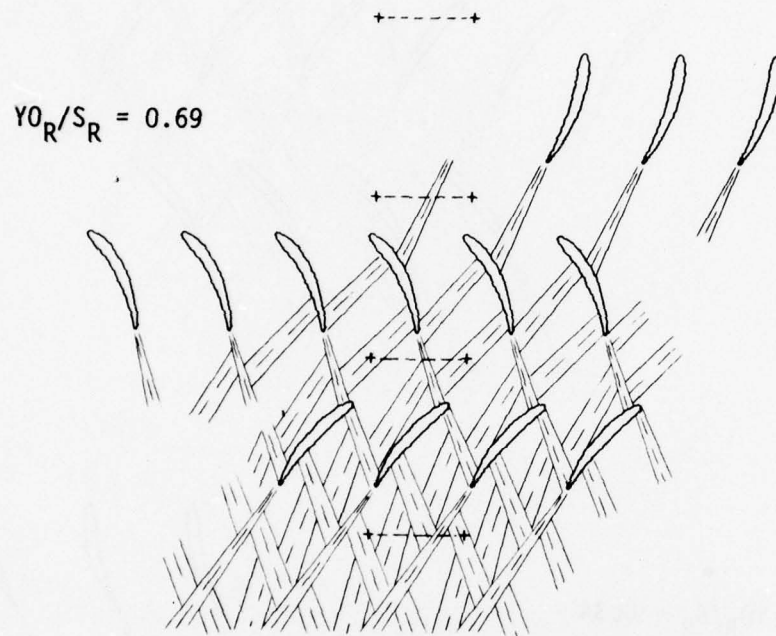
(c) Rotor sampling position $Y_{0R}/S_R = 0.69$.

Figure 4.5. Concluded.



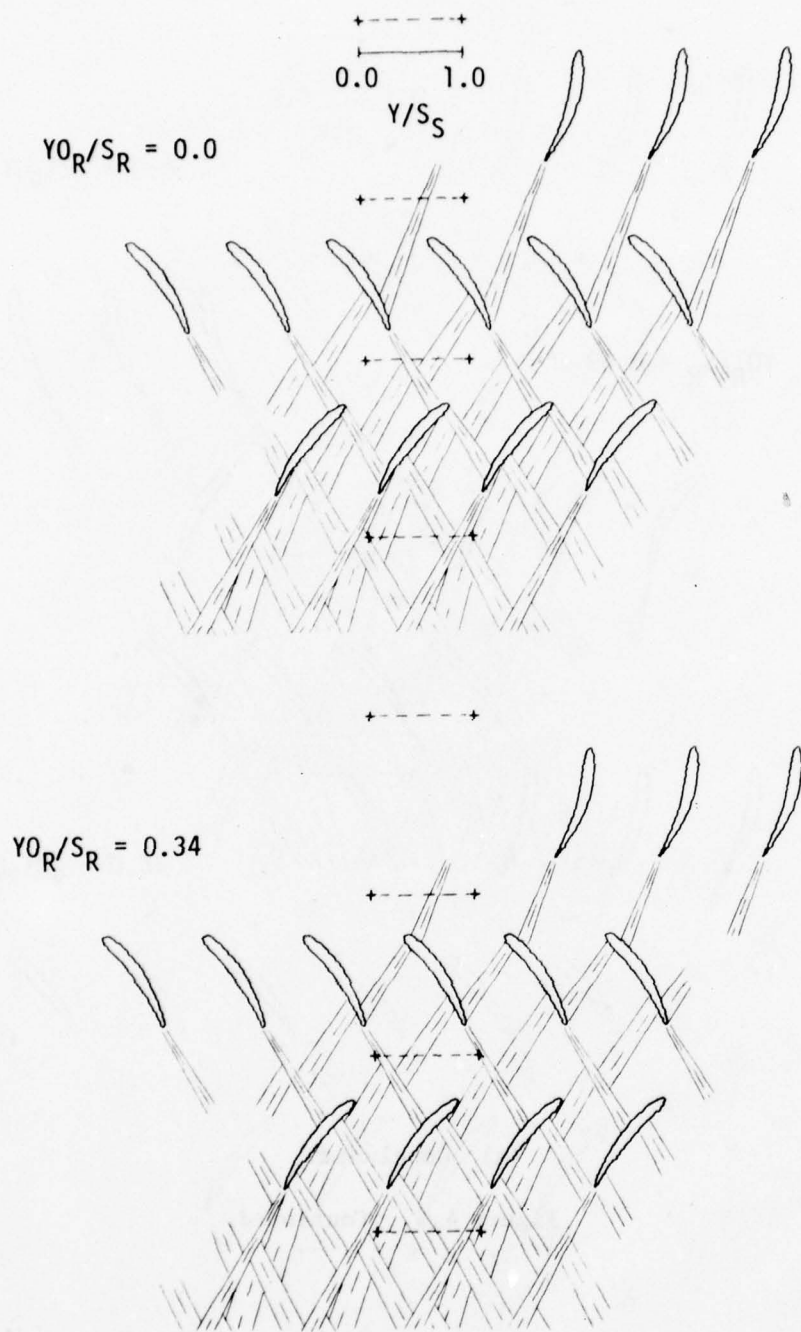
(a) 10% passage height from hub.

Figure 4.6. Periodic-average cascade wake interaction drawings for first stage, maximum noise.



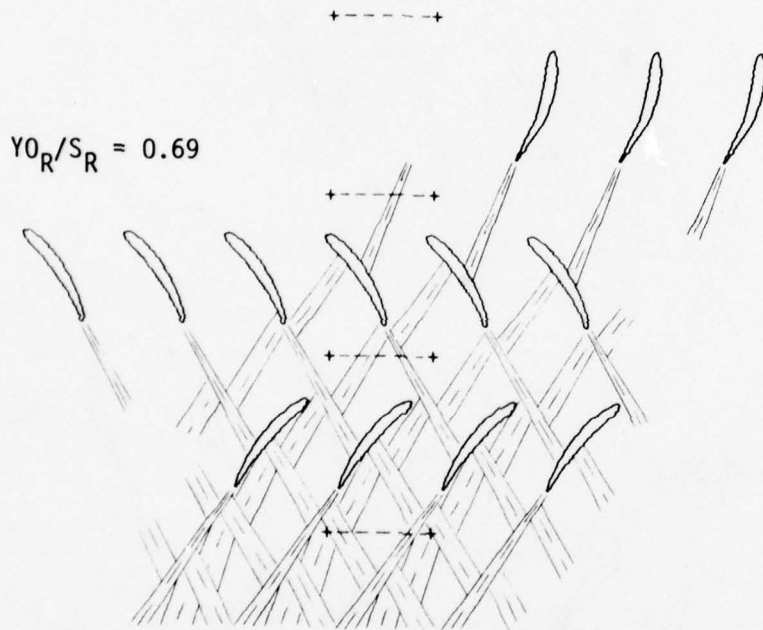
(a) Concluded.

Figure 4.6. Continued.



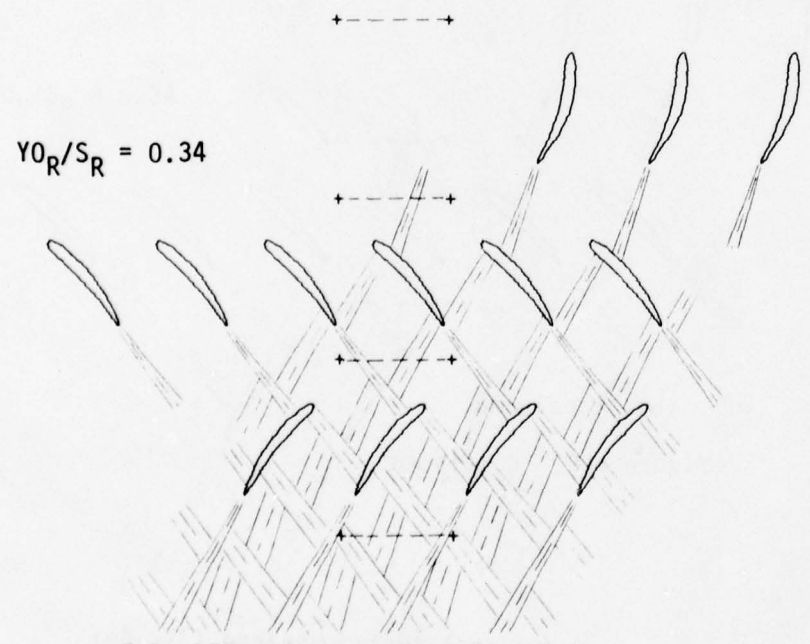
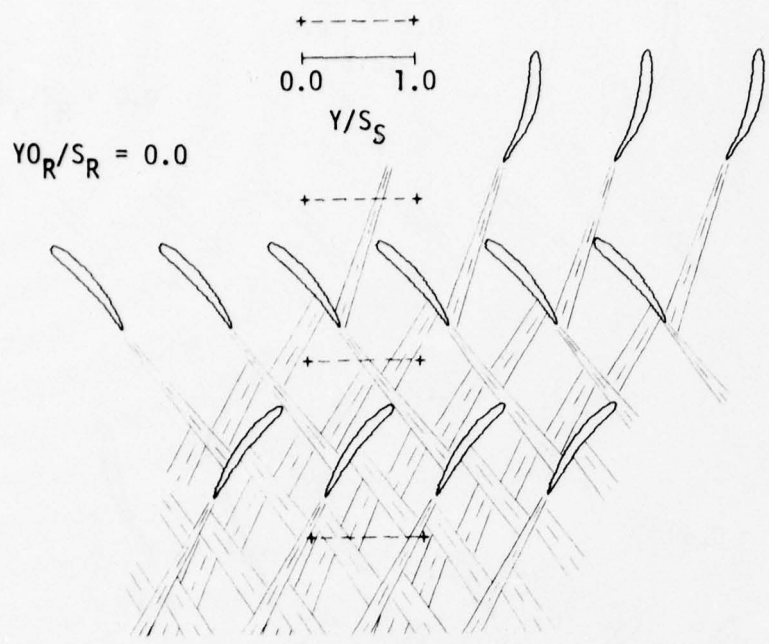
(b) 30% passage height from hub.

Figure 4.6. Continued.



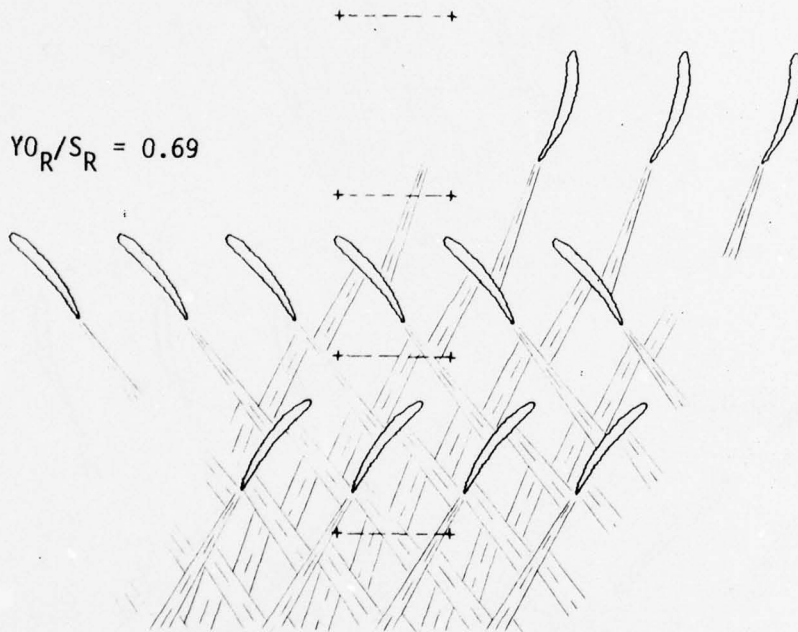
(b) Concluded.

Figure 4.6. Continued.



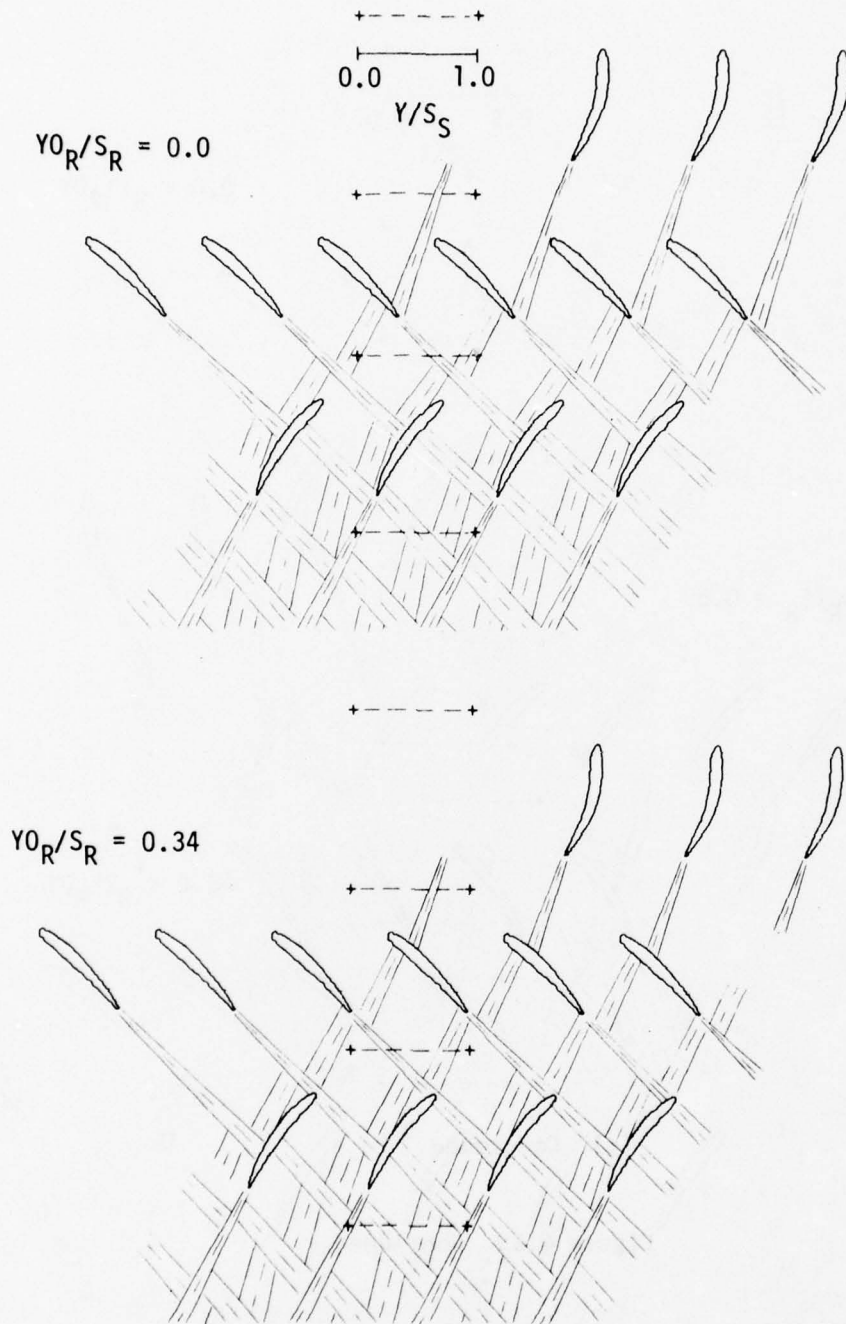
(c) 50% passage height from hub.

Figure 4.6. Continued.



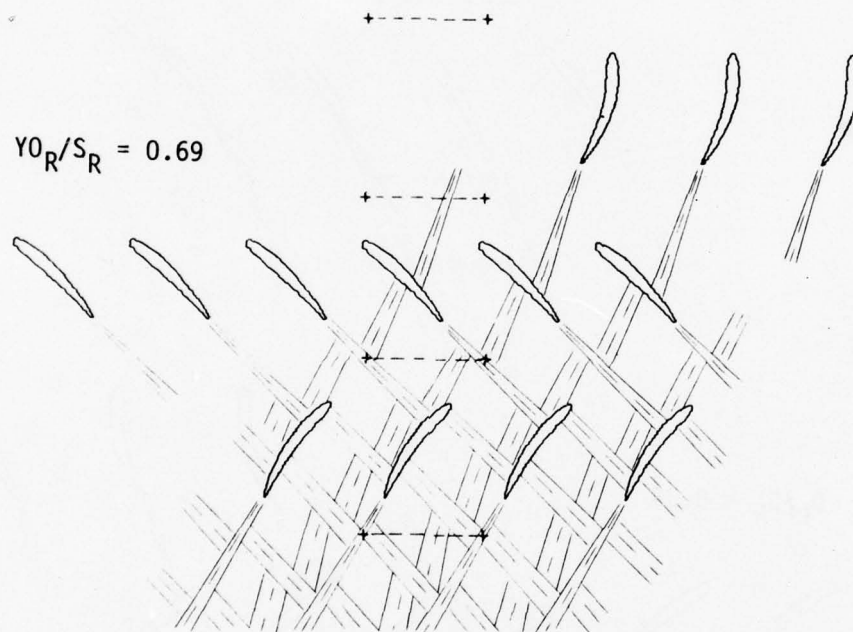
(c) Concluded.

Figure 4.6. Continued.



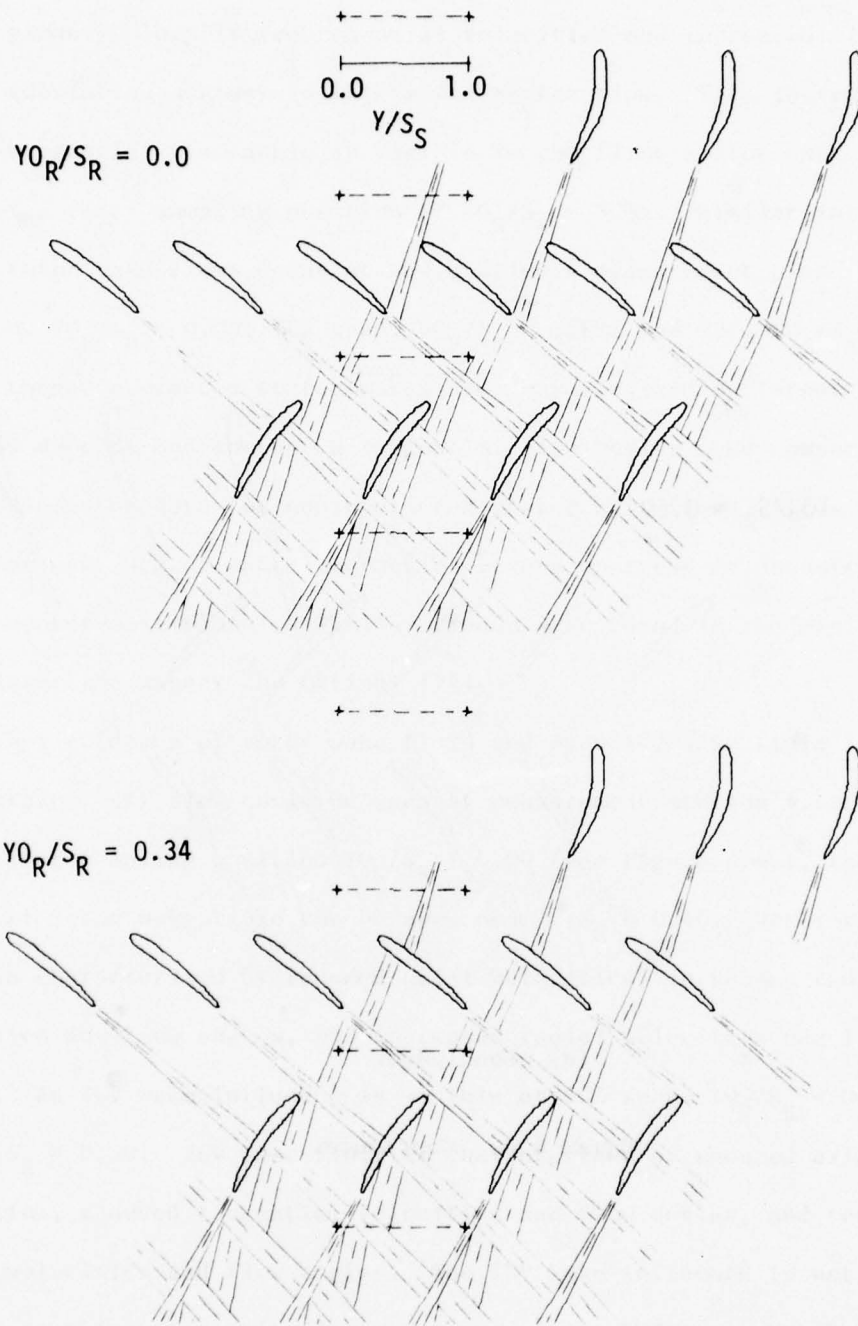
(d) 70% passage height from hub.

Figure 4.6. Continued.



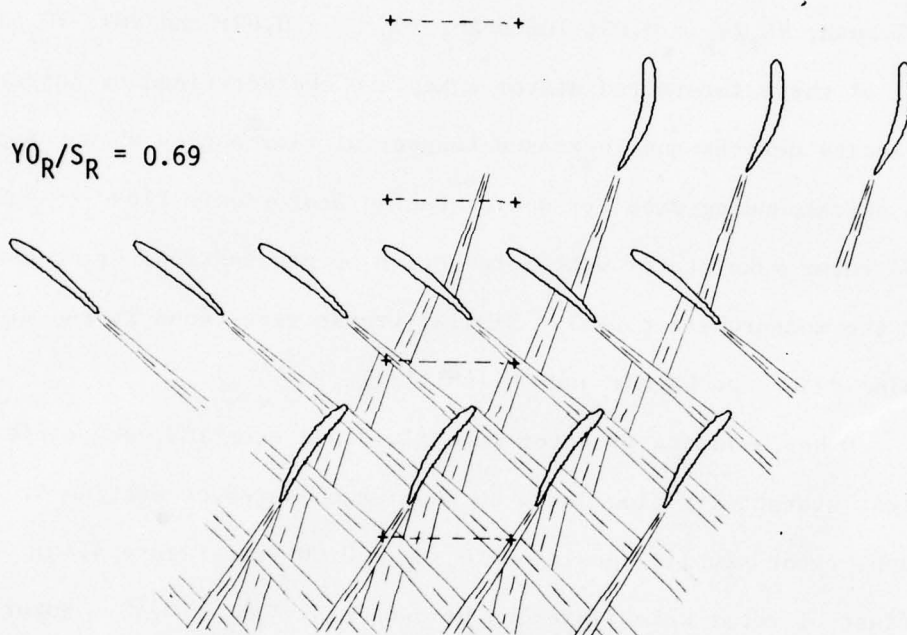
(d) Concluded.

Figure 4.6. Continued.



(e) 90% passage height from hub.

Figure 4.6. Continued.



(e) Concluded.

Figure 4.6. Concluded.

the stator blade suction surface to pressure surface. This slip motion produces locally reduced axial velocities and increased flow angles (deviation angles) in interacted stator flow. This increase in the tangential flow angle is visible in the first stator exit data for a rotor sampling position of $Y_{O_R}/S_R = 0.34$. Similar interacted stator wake flows occur at the station 4 measurement plane for 30% span, $Y_{O_R}/S_R = 0.00$; 70% span, $Y_{O_R}/S_R = 0.69$; and 90%, $Y_{O_R}/S_R = 0.69$. All of these interacted stator wakes are characterized by larger axial velocity defects and increased tangential flow angles when compared to corresponding data for noninteracted stator exit flows (flows where the rotor wake/stator wake interaction occurs upstream or downstream of the measurement plane). Similar trends were found in the minimum noise data (see Wagner and Okiishi [7]).

Other evidence of rotor wake fluid and even IGV wake fluid in the first stator exit flow could be seen at measurement station 4. For 50% span, rotor sampling position $Y_{O_R}/S_R = 0.00$ (see Figure 4.4c), the effect of rotor wake fluid can be seen near $Y/S_S = 0.40$. Rotor wake fluid is characterized by reduced axial velocities, increased tangential velocities and flow angles, and increased radial velocities and flow angles. An IGV wake influence is visible at 50% span, $Y_{O_R}/S_R = 0.34$ near $Y/S_S = 0.30$. IGV wake fluid is characterized by reduced axial velocities, reduced tangential velocities and flow angles, and reduced radial velocities and flow angles. The IGV wake influence is not always visible in the stator exit flow. For example at 50% span, $Y_{O_R}/S_R = 0.00$ and $Y_{O_R}/S_R = 0.69$, the IGV wake effect is obscured by the close proximity

of the much stronger (and opposing) rotor wake influence at the station 4 measurement plane.

At a radial span location of 90%, an overall reduction in the axial velocity level is seen owing to wall boundary layer effects (see Figure 4.5).

4.3. Cross-Section Drawings

Another method of visualizing the data involves viewing the flow in a plane perpendicular to the compressor axis. The wake locations at each cross-section plane were obtained from their corresponding location on cascade drawings. A view of the IGV exit flow (data from Wagner and Okiishi [7]) is shown in Figure 4.7 for a cross-section plane located at measurement station 2 (see Figure 2.5). The data of Wagner and Okiishi [7] suggest that IGV wake locations were not influenced by rotor blade sampling position (i.e., no significant rotor upstream effects on IGV wake location). From this plane view the slightly greater turning near the hub of the IGV design is evident. Figure 4.8 is a similar drawing showing flow at measurement station 3 (first rotor exit flow). Only isolated IGV wake segments were used to obtain the IGV wake avenue position since rotor wakes interacting with the IGV wakes tended to obscure their location. The variation of IGV wake position shown in Figure 4.8 is largely due to the appreciable width of the wake avenue involved. The free vortex design of the rotor blades is evident. The fluid is turned more near the hub than at the tip.

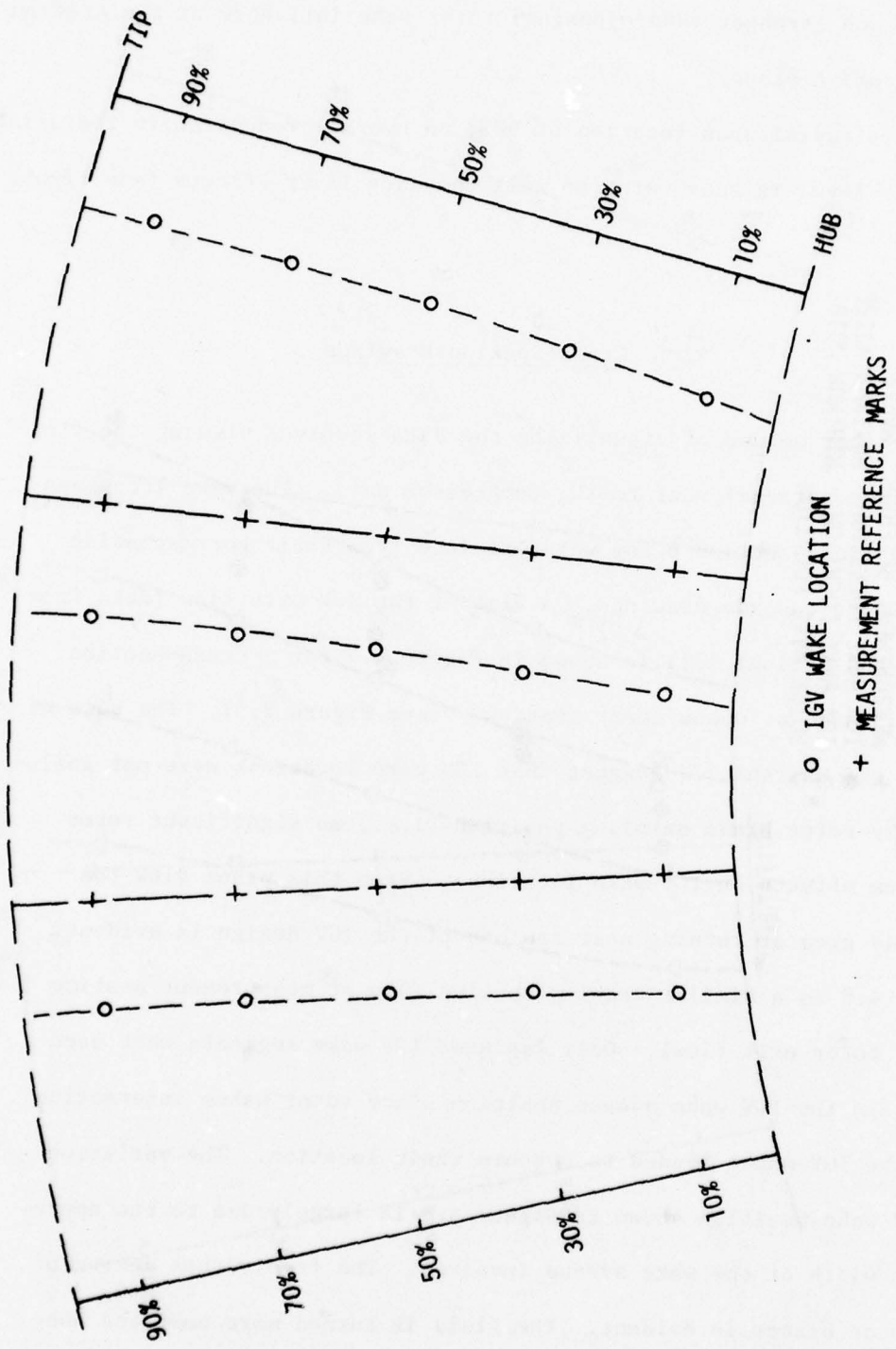


Figure 4.7. Cross section plane view of IGV wake avenue location in IGV row exit plane, measurement station 2.

As observed by Wagner and Okiishi [7] the largest axial velocity defects were found to occur when the IGV wake / rotor wake interaction took place near the measurement plane. In a cross-section drawing like Figure 4.8, this kind of interaction occurs at the measurement plane when the position of the moving rotor wake coincides with the location of the stationary IGV wake avenue, as, for example, at 90% span for a rotor sampling position of $Y_{O_R}/S_R = 0.69$; at 30% span, $Y_{O_R}/S_R = 0.00$; and at 50% span and 70% span for a rotor sampling position between $Y_{O_R}/S_R = 0.69$ and $Y_{O_R}/S_R = 0.00$ (see Figure 4.8). Curiously, at 10% span the rotor exit flow data taken to date (see Wagner and Okiishi [7]) show very large axial velocity defects for all rotor sampling positions. In other words, an interacted rotor wake appears to result for all rotor sampling positions at 10% span (seven different rotor sampling positions in all). An explanation for this behavior may be given in terms of IGV wake orientation. From the cascade drawings it can be seen that the large amounts of turning at 10% causes the IGV wake segments to be substantially inclined toward the measurement plane. Thus, at 10% span an IGV wake segment is most often close enough to the measurement plane to produce what appears to be interacted rotor wake flows.

Figure 4.9 is a hub-to-tip cross-section view of the flow at a plane coinciding with the first stator leading edge. The position of the stator leading edge is sketched in. The stationary IGV wake avenue impinges on the stator blade at one span location only for minimum noise but at two span locations for maximum noise. Also, the slanted rotor wake first intersects the stator leading edge at the

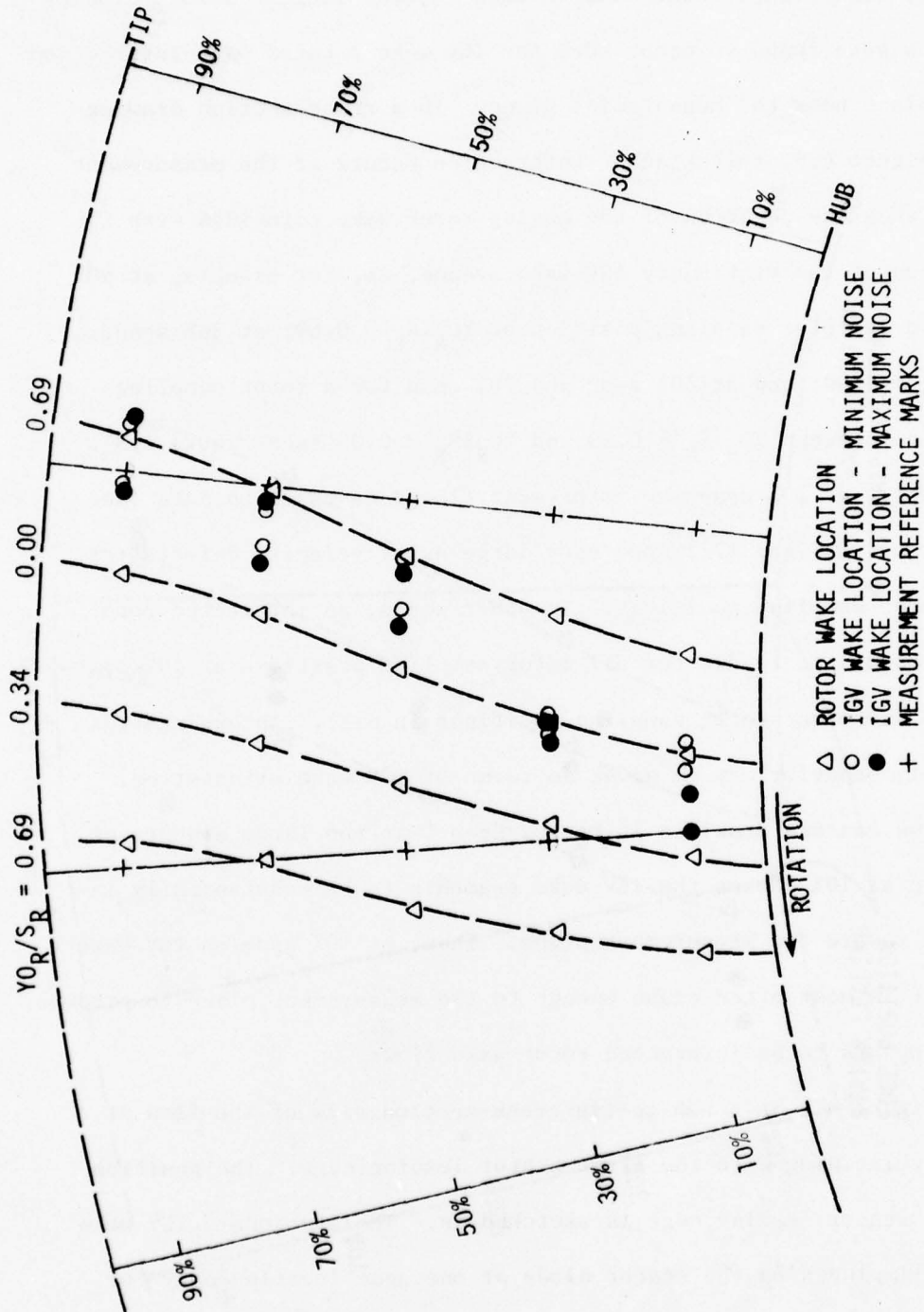
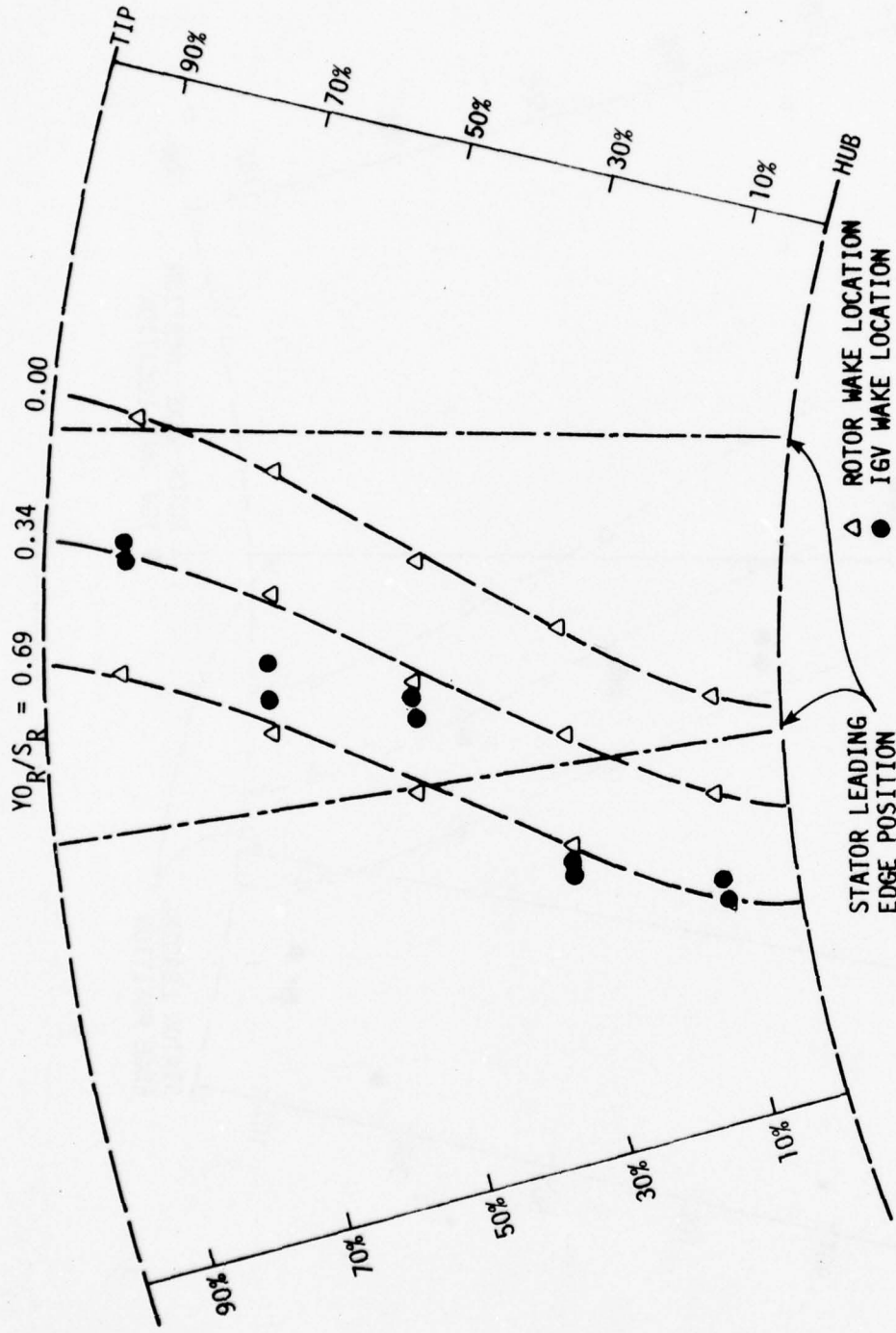
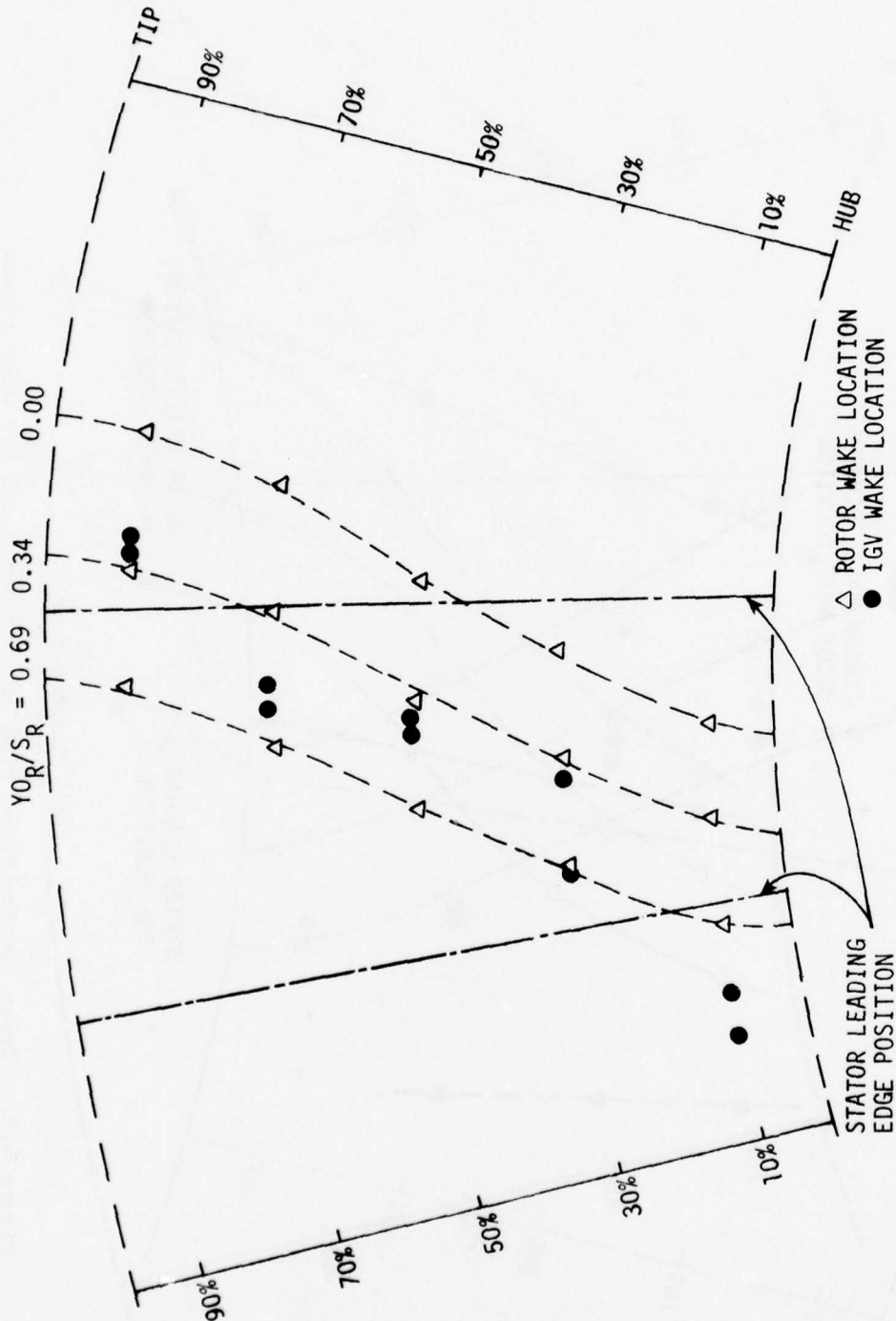


Figure 4.8. Cross section plane view of rotor wake and IGV wake avenue locations in first rotor exit flow, measurement station 3.



(a) Minimum noise.

Figure 4.9. Cross section plane view of rotor wake and IGV wake avenue locations at first stator blade leading edge plane.



(b) Maximum noise.

Figure 4.9. Concluded.

hub with the intersection progressing upward toward the tip as the rotor blade moves. As the rotor wake progressively travels, it encounters that portion or portions of the stator leading edge where the stationary IGV wake avenue is impinging. As noted previously, the IGV wake / rotor wake interaction produces deeper rotor wakes. Related increased periodic incidence angle fluctuations will result in increased discrete frequency pressure fluctuations on the stator blade pressure and suction surfaces. These two span locations of increased stator surface pressure fluctuations for maximum noise are consistent with and help explain the increase in the noise obtained since these surface pressure fluctuations are a primary source of discrete frequency noise.

Analysis of the maximum and minimum noise first stator exit flow data led to another interesting conclusion. In order to detect the influence of different stator leading edge flow conditions on stator exit flow, the maximum and minimum noise configuration data at measurement station 4 were compared selectively. Figure 4.10 illustrates how the relative positions of rotor and stator wakes varied at measurement station 4 with rotor sampling and stator locations and suggests a rational means for comparison. It is desirable to compare stator exit data for maximum and minimum noise at rotor sampling positions resulting in similar rotor wake and stator wake relative positions. For example, the positioning of the rotor wake relative to the stator wake for rotor sampling position $Y_{O_R}/S_R = 0.00$ for minimum noise is very similar to the positioning of those wakes for rotor sampling position $Y_{O_R}/S_R = 0.34$ for maximum noise. Thus, these data were compared (comparison A).

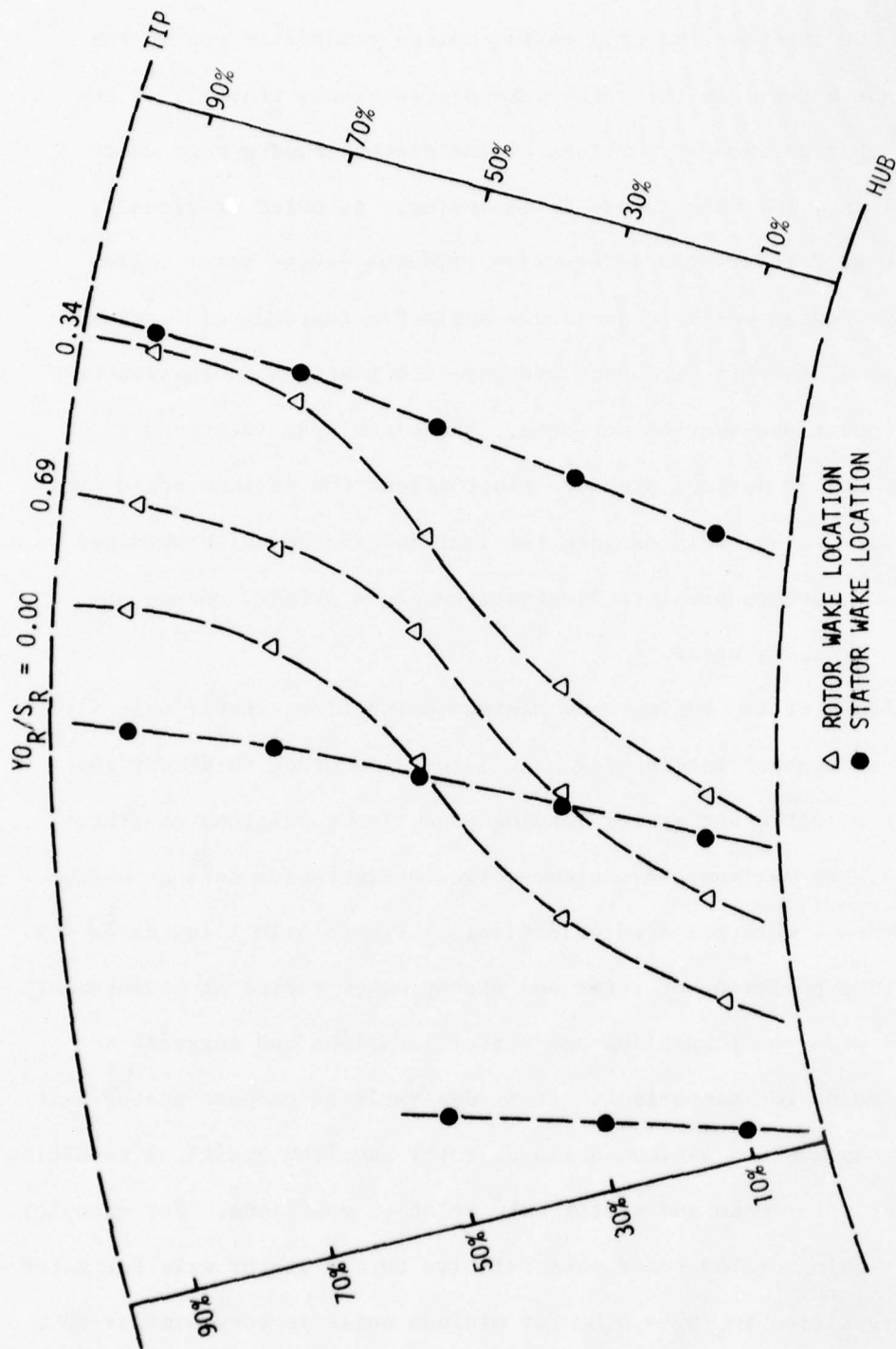
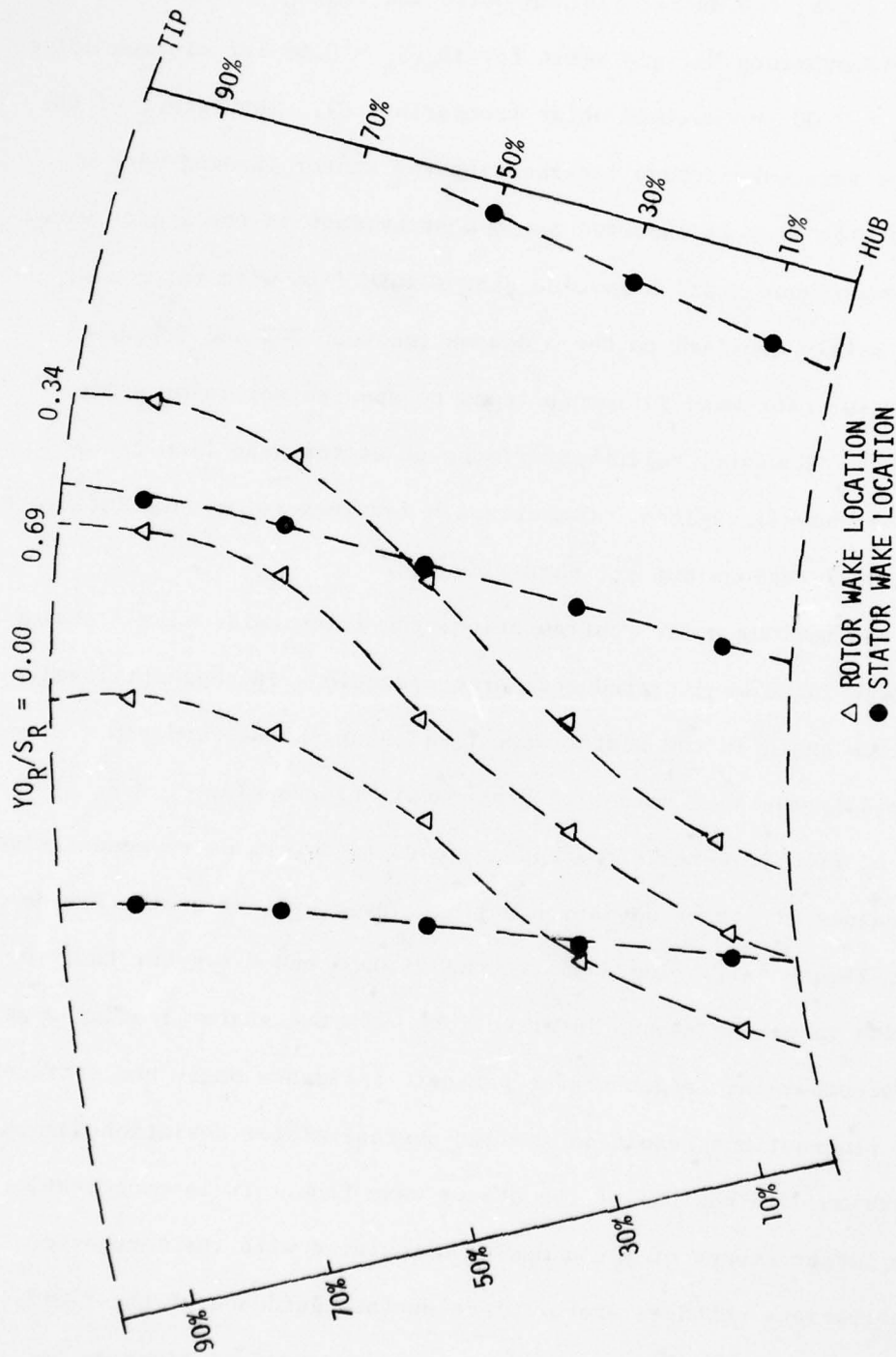


Figure 4.10. Cross section plane view of stator wake and rotor wake locations for first stator exit flow, measurement station 4.

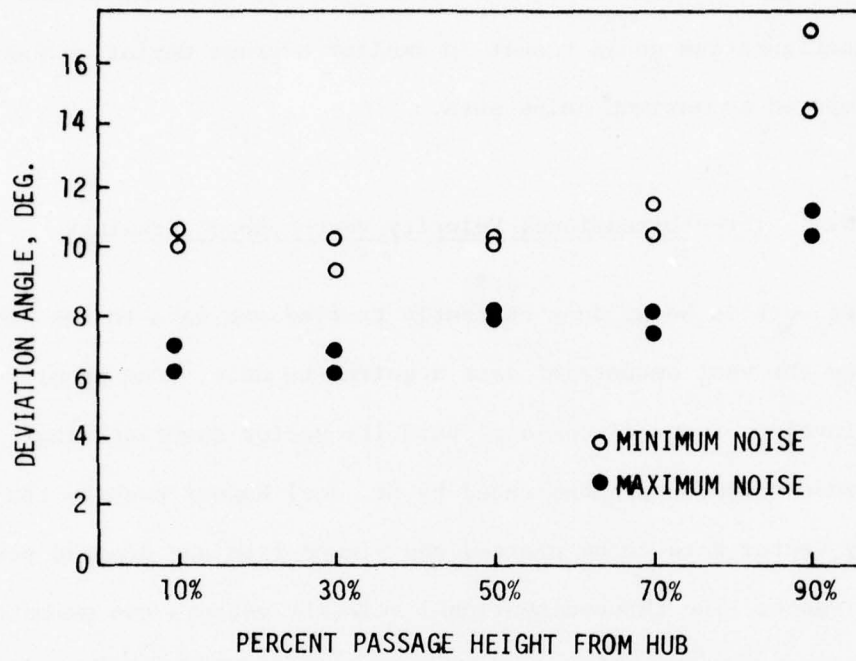


(b) Maximum noise.

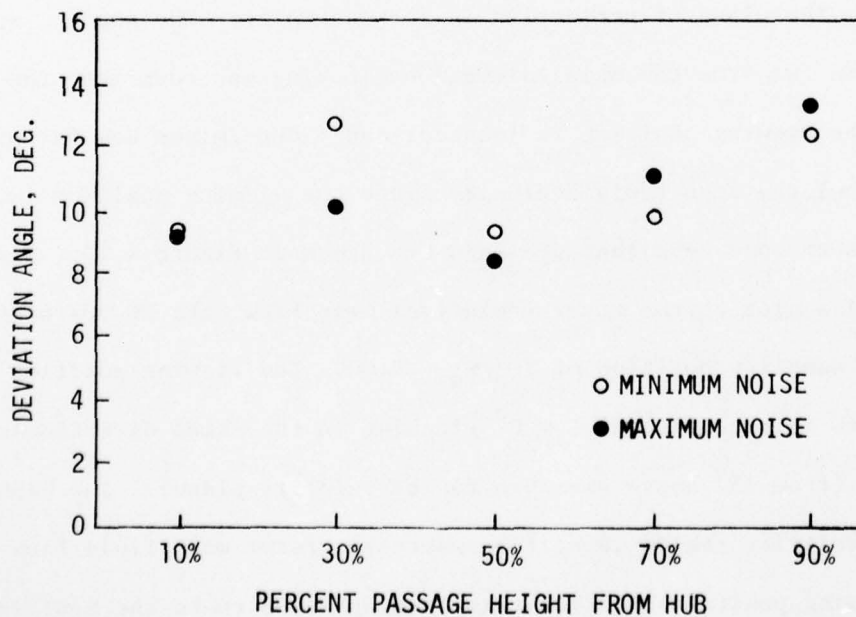
Figure 4.10. Concluded.

Similar relative positioning of the rotor wake and stator wake also occurs for $Y_{O_R}/S_R = 0.34$ for minimum noise and $Y_{O_R}/S_R = 0.69$ for maximum noise (comparison B), and again for $Y_{O_R}/S_R = 0.69$ for minimum noise and $Y_{O_R}/S_R = 0.00$ for maximum noise (comparison C). The effect of the inlet guide vane wake avenue intersecting the stator leading edge on the stator exit flow is expected to be most evident in the stator wake fluid. Comparisons A and C involve stator wake flow with rotor wake influence mainly confined to the mid-span (between 30% and 50% span) region. This rotor wake influence tends to obscure any inlet guide vane effects. However, valid comparisons of stator wake flow can be made in the endwall regions. Comparison B involves rotor wake influence in the endwall regions but not near mid-span.

For the maximum noise configuration, the inlet guide vane / stator leading edge intersection produced large reductions in tangential velocity and flow angle in the stator wake fluid near the hub and tip. Circumferentially averaged values of stator exit flow angle, $\bar{\beta}_\theta$ ($\bar{\beta}_\theta = \frac{1}{S_S} \int_0^{S_S} \beta_\theta(Y) dY$), were calculated and used to determine representative average values of stator deviation angle. The resulting trends are depicted in Figure 4.11. The data of comparison A and C suggest that the inlet guide vane wake avenue intersections with the stator leading edge and the accompanying larger stator periodic incidence angle and surface pressure fluctuations result in smaller average stator deviation angles in the hub and tip regions of the stator wake flow. It is conceivable that the larger amount of fluid mixing associated with the increased flow fluctuations enhances stator blade surface guidance of the fluid. A similar trend in stator wake flow was not discerned at mid-span for



(a) Rotor wake/stator wake interaction near midspan (comparisons A and C).



(b) Rotor wake/stator wake interaction near endwalls (comparison B).

Figure 4.11. Comparison of hub-to-tip variations of first stator deviation angle with stator circumferential placement.

comparison B. The expectation was that near mid-span the minimum noise configuration would result in smaller average deviation angles when compared to maximum noise data.

4.4. Three-Dimensional Velocity Vector Sheet Drawings

More work is being done currently to find new ways to use and visualize the vast amounts of data acquired to date. One promising method involves three-dimensional velocity vector sheet drawings. An in-house computer program coded by Mr. Joel Wagner enables the velocity vector data to be plotted and viewed from any desired position in space. The three-dimensional velocity vectors are geometrically projected onto a plane in space specified in terms of two angles (see Figure 4.12). These two angles, ϵ and η , locate the viewing axis to which the plane of projection is perpendicular. The angle ϵ specifies how far from the axial direction (looking upstream into the flow) the viewing position is located, and η determines how far above (or below) the zero radial velocity plane the viewing position is. Examples of some resultant drawings are shown in Figure 4.13. Figure 4.13a is a plot of the rotor (relative) exit flow data at 50% span for a rotor sampling position of $Y_{O_R}/S_R = 0.00$. The viewing position for this view is specified as $\epsilon = 0^\circ$ (looking in the axial direction), and $\eta = 15^\circ$ (from 15° above the zero radial velocity plane). The high-radial-velocity region identifies where the rotor wake fluid flow is. The viewing position used for this drawing seems to be the most instructive

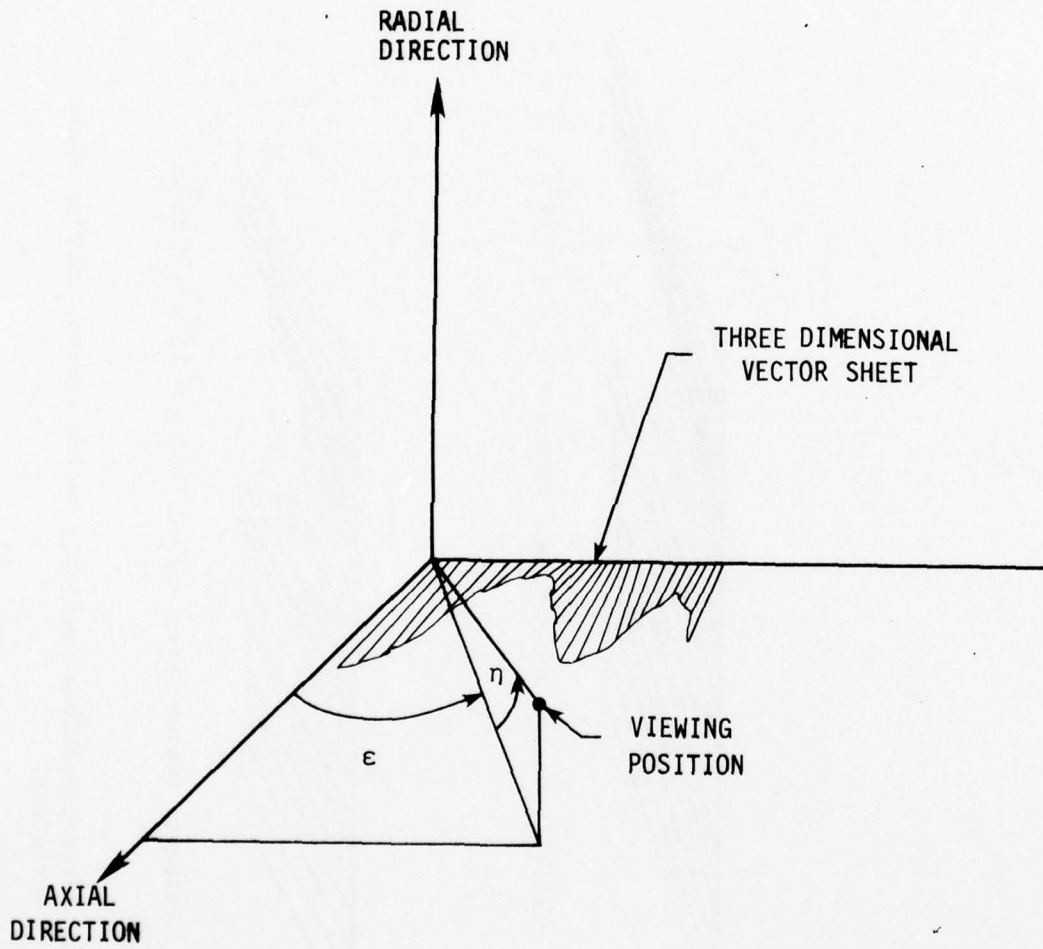


Figure 4.12. Three-dimensional velocity vector viewing angles.

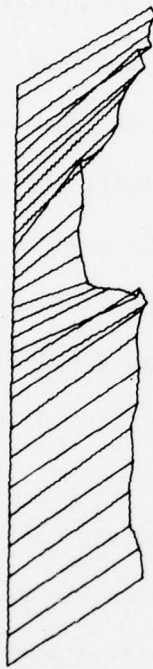


(a) Velocity vector sheet viewed from $\epsilon = 0^\circ$, $\eta = 15^\circ$.



(b) Velocity vector sheet viewed from $\epsilon = 15^\circ$, $\eta = 15^\circ$.

Figure 4.13. Three-dimensional velocity vector sheets, viewing angle variation.



(c) Velocity vector sheet viewed from $\epsilon = 30^\circ$, $\eta = 15^\circ$.



(d) Velocity vector sheet viewed from $\epsilon = 30^\circ$, $\eta = 0^\circ$.

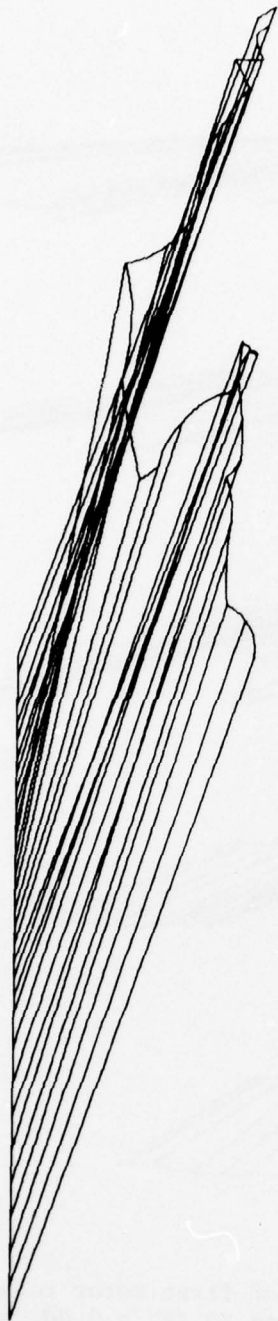
Figure 4.13. Concluded.

and has been used extensively in other drawings. Figures 4.13b - 4.13d show the same data viewed from several different locations.

During development of this technique it was found that there was an interdependence between the physical space scale and the velocity magnitude scale. If a small space scale with relatively long vectors was used, a great deal of crossing over of the vectors occurred. If a large scale was used with relatively short vector lengths, no crossing over of the vectors occurred. There is no "correct" relationship between the physical space scale (meters) and the velocity magnitude scale (meters/second). Examples of two scale ratios are shown in Figure 4.14. The data and viewing position are the same as that used in Figure 4.13a. Only the physical scale / velocity scale ratio has been halved (Figure 4.14a) and doubled (Figure 4.14b). The importance of this ratio on the resultant drawing is evident.

As an extension of this type of flow visualization, hub-to-tip, three-dimensional velocity vector drawings were constructed. Figure 4.15 shows such a drawing for the rotor (relative) exit flow for a rotor position for $Y_{0R}/S_R = 0.00$. The pitch distances and hub-to-tip distances are in proper proportion.

The region of large radial velocity is the rotor wake fluid. The hub-to-tip shape of the rotor wake region can be seen and agrees with the shape sketched in Figure 4.9 for $Y_{0R}/S_R = 0.00$. Some difficulty is encountered in determining the sign of the radial velocity (radially upward or downward) from this kind of presentation of the data alone. A supplementary hub-to-tip radial velocity



(a) Velocity vector sheet at 2 times original scale ratio (length scale/velocity scale).



(b) Velocity vector sheet at 1/2 original scale ratio (length scale/velocity scale).

Figure 4.14. Three-dimensional velocity vector sheets, scale ratio variation.

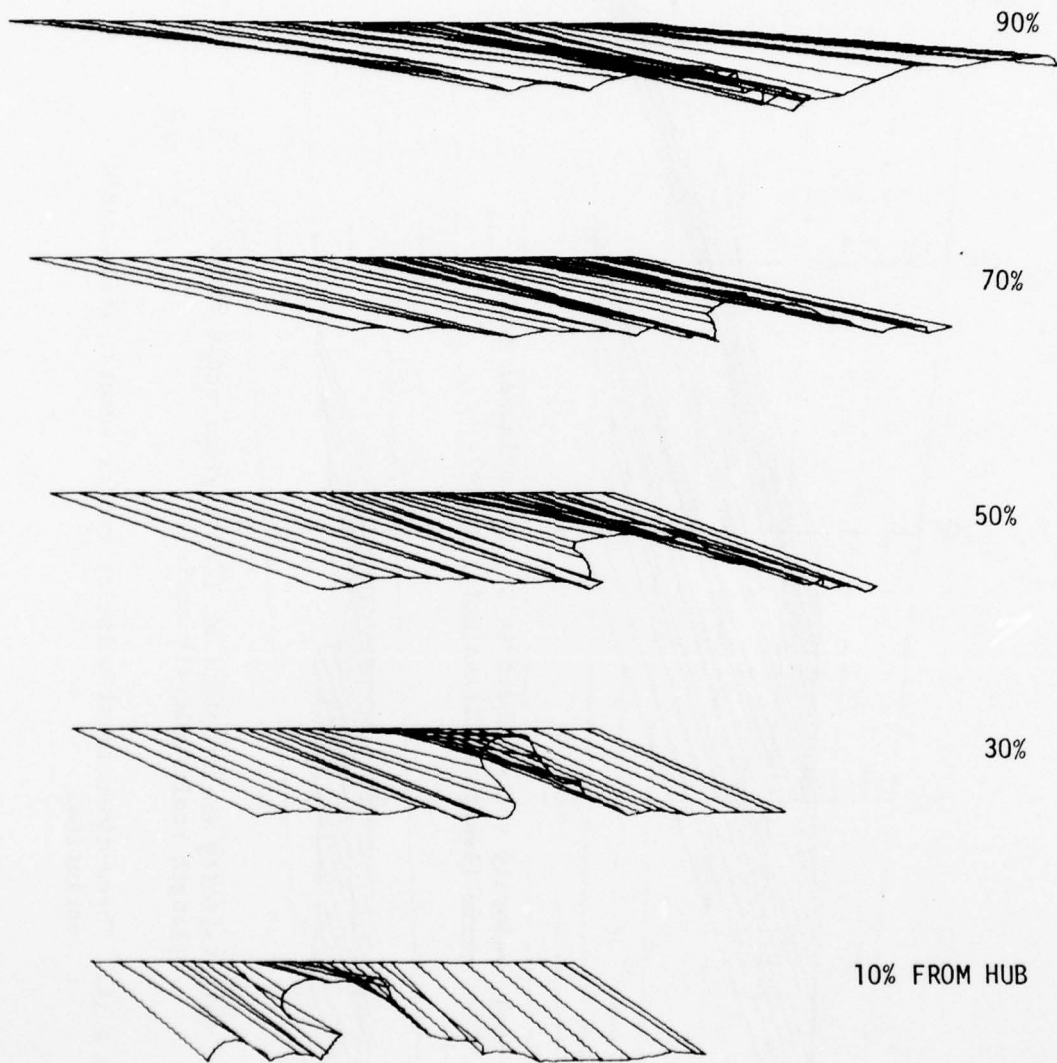


Figure 4.15. Hub-to-tip variation of first rotor relative exit flow.
Rotor sampling position $Y_{O_R}/S_R = 0.00$, minimum noise.

distribution sketch like the one of Figure 4.16 shows clearly the hub-to-tip variation radial velocity profiles for the three-dimensional vector sheet drawing of Figure 4.15.

Similar three-dimensional hub-to-tip velocity vector drawings for the stator exit flow for three different rotor sampling positions are shown in Figure 4.17. The position of the stator wakes can be identified by the downward radial flow as opposed to the strong upward radial flow of the rotor wake fluid.

Work is still continuing in this area and will include an animated-sequence movie film depicting the periodic unsteadiness of the three-dimensional, hub-to-tip, velocity vector sheets. Also, wire models of the velocity vector sheets are being constructed in an effort to optimize the scale relationships and the viewing position.

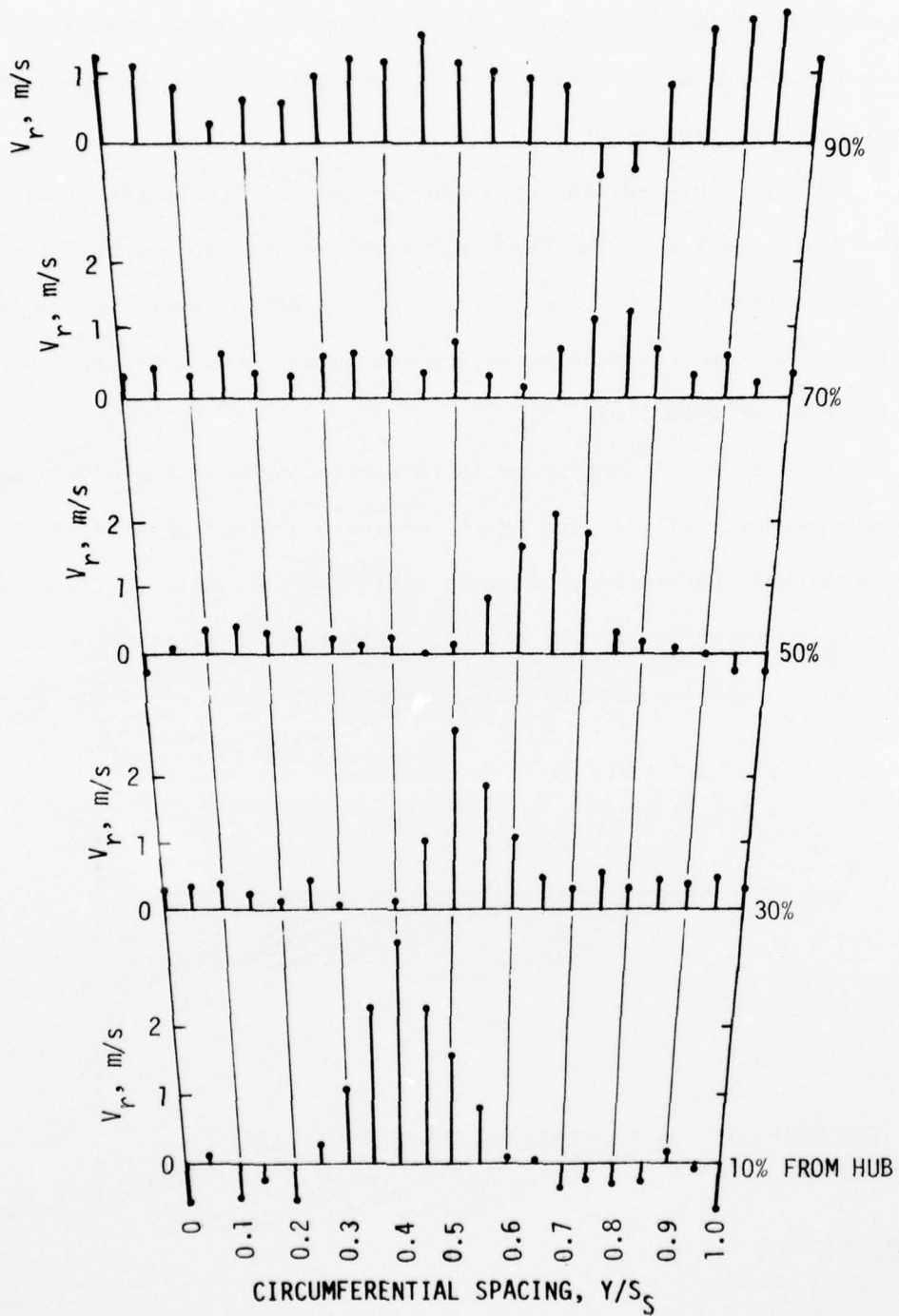
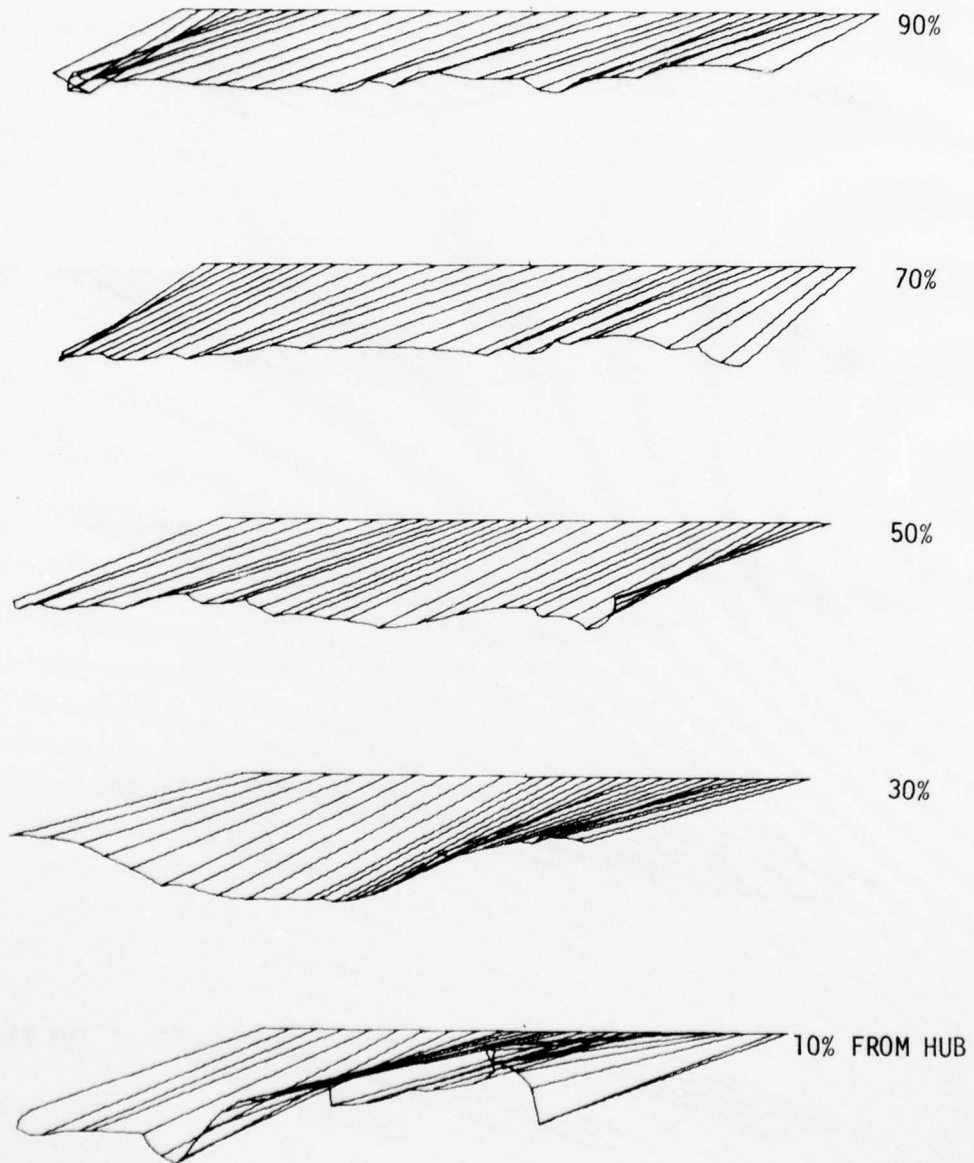
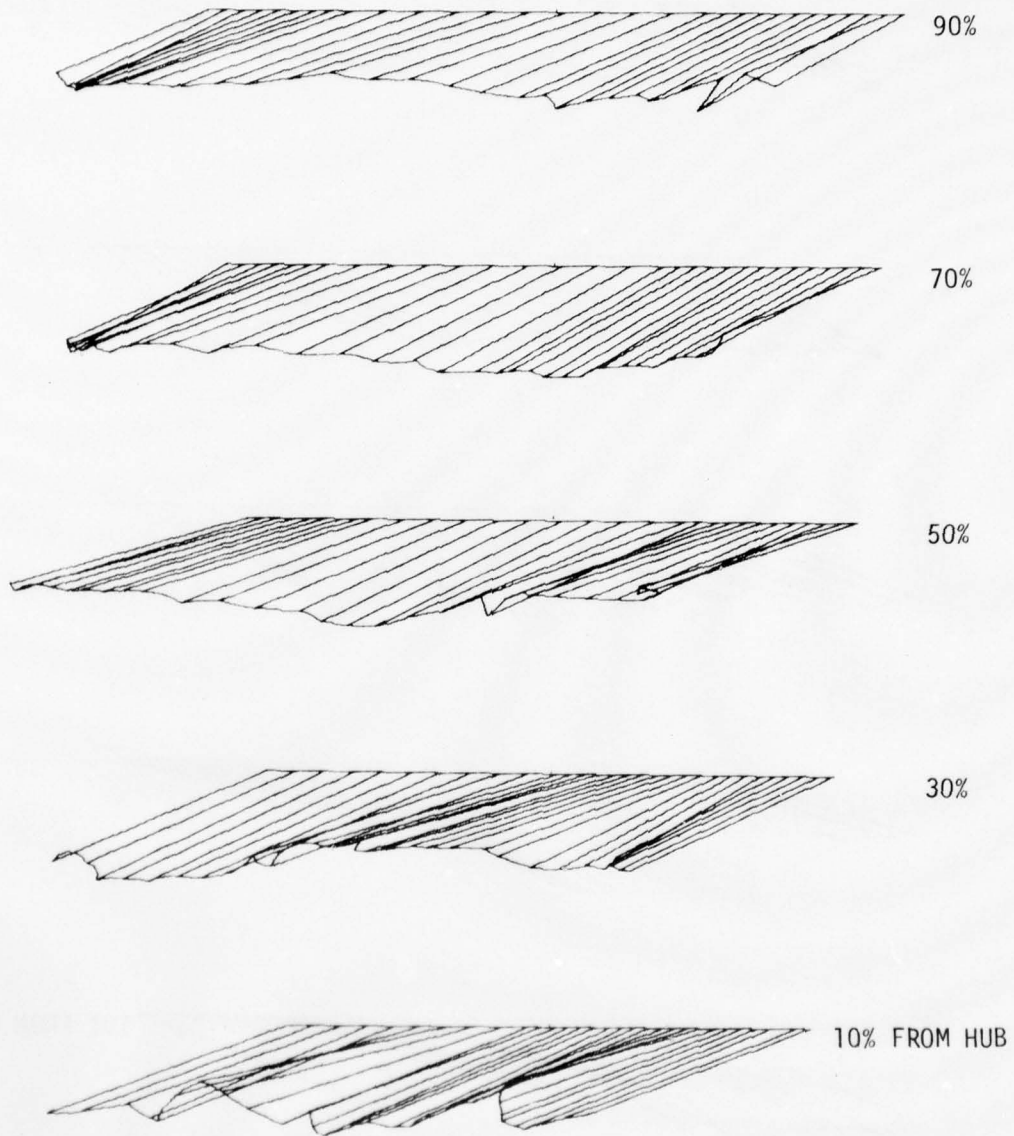


Figure 4.16. Hub-to-tip distribution of radial velocity profiles.



(a) Rotor sampling position $Y_{O_R}/S_R = 0.00$.

Figure 4.17. Hub-to-tip variation of first stator exit flow, maximum noise.



(b) Rotor sampling position $Y_{O_R}/S_R = 0.34$

Figure 4.17. Continued.

AD-A067 969

IOWA STATE UNIV AMES ENGINEERING RESEARCH INST
THE INFLUENCE OF COMPRESSOR INLET GUIDE VANE / STATOR RELATIVE --ETC(U)
SEP 78

F/6 13/7

AFOSR-76-2916

UNCLASSIFIED

ISU-ERI-AMES-79037

AFOSR-TR-79-0509

NL

2 of 2

AD
A067969

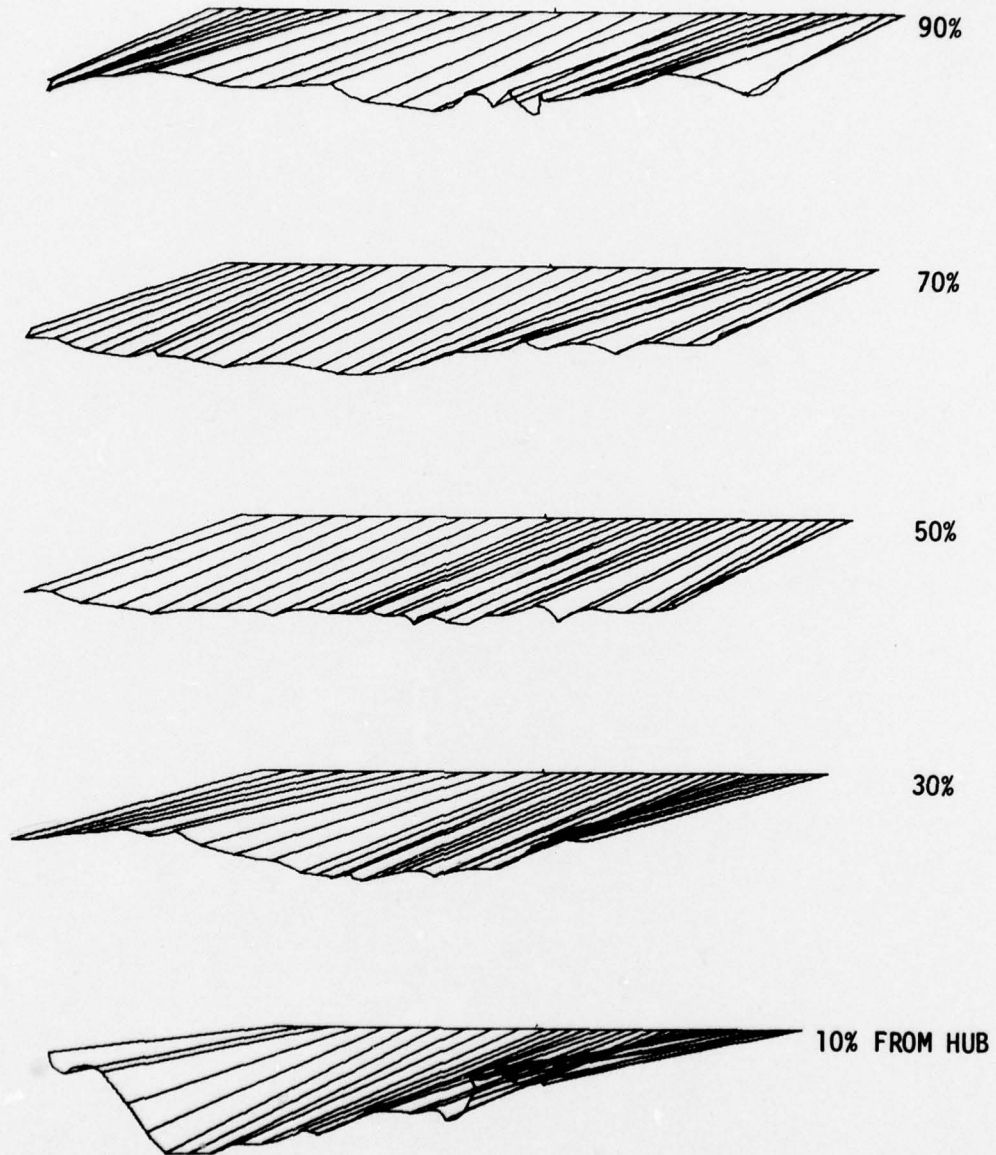


END

DATE
FILMED

6 -79

DDC



(c) Rotor sampling position $Y_{O_R}/S_R = 0.69$.

Figure 4.17. Concluded.

5. CONCLUSIONS

The major conclusions resulting from the present study are summarized below.

Small but discernible and consistent upstream influence of the downstream stator blade row on the first rotor exit flow was observed in regions directly upstream of the stator leading edge. Flow yaw angles and axial velocities were affected most while radial velocities were not significantly changed. The general location of the rotor wake was unaffected.

Blade-to-blade plane and hub-to-tip cross-section drawings were very helpful in organizing and understanding the data. From these drawings, it was evident that the IGV wake avenue intersected the first stator row blades at two span locations for the maximum noise circumferential position of the stator row but at only one span location for the minimum noise placement.

Velocity data indicated that IGV wake / rotor wake interactions generally resulted in deeper rotor wakes and thus larger periodic incidence angle fluctuations. When these larger incidence angle fluctuations occurred near the stator leading edge in the endwall regions, as they did for maximum noise, stator exit flow data showed appreciably smaller stator deviation angles in these regions than for the minimum noise condition (for which these larger incidence angle fluctuations were not present in the endwall regions). This behavior was probably due to the increased mixing of the flow that accompanied the larger stator inlet flow fluctuations in the endwall regions.

Since periodic fluctuations in stator incidence angle that occur with "chopping" of the rotor wakes are a primary source of discrete frequency noise, the observed IGV wake / stator leading edge interaction patterns are consistent with the related inlet noise levels recorded.

6. REFERENCES

1. Mikolajczak, A. A. "The Practical Importance of Unsteady Flow," in "Unsteady Phenomena in Turbomachinery." AGARD-CP-177, April 1976.
2. Schmidt, D. P., and Okiishi, T. H. "Multistage Axial-Flow Turbomachine Wake Production, Transport, and Interaction." ISU-ERI-Ames-77130, TCRL-7, November 1976.
3. Walker, G. J., and Oliver, A. R. "The Effect of Interaction Between Wakes from Blade Rows in an Axial-Flow Compressor on the Noise Generated by Blade Interaction." Transactions of the ASME Journal of Engineering for Power, 94A (1972): 241-248.
4. Smith, L. H., Jr. "Wake Dispersion in Turbomachines." Transactions of the ASME Journal of Basic Engineering, 880 (1966): 688-690.
5. Kerrebrock, J. L., and Mikolajczak, A. A. "Intra-Stator Transport of Rotor Wakes and its Effect on Compressor Performance." Transactions of the ASME Journal of Engineering for Power, 92A (1970): 359-368.
6. Gallus, H. E., Lambertz, J., and Wallmann, T. "Experimentelle Untersuchung der Relativströmung im Laufrad einer Axialverdichterstufe." Westdeutscher Verlag GmbH; Germany, 1978.
7. Wagner, J. H., and Okiishi, T. H. "Analysis of Multistage, Axial-Flow Turbomachine Wake Production, Transport, and Interaction." ISU-ERI-Ames-78173, TCRL-10, December 1977.
8. Gostelow, J. P. "A New Approach to the Experimental Study of Turbomachinery Flow Phenomena." Transactions of the ASME Journal of Engineering for Power, 99A (1977): 97-105.

7. APPENDIX A: PARAMETER EQUATIONS

The equations used in the periodic-average measurement system for the calibration procedures and the acquisition and reduction of data are presented below.

7.1. General Parameters7.1.1. Basic Fluid Properties

Barometric pressure, N/m^2 :

$$P_{\text{atm}} = h_{\text{hg}} @ t_{\text{baro}} [1.0 - 0.0018 (t_{\text{baro}} - 273.15)] \gamma_{\text{hg}} @ 273 \text{ } ^\circ\text{K} \quad (7.1)$$

Density of air, kg/m^3 :

$$\rho = \frac{P_{\text{atm}}}{R t} \quad (7.2)$$

Specific weight of water, N/m^3 :

$$\begin{aligned} \gamma_{\text{H}_2\text{O}} = \frac{g}{g_c} & \left[996.86224 + 0.1768124 \left(\frac{9}{5} t - 459.67 \right) - 2.64966 \right. \\ & \left. \times 10^{-3} \left(\frac{9}{5} t - 459.67 \right)^2 + 5.0063 \times 10^{-6} \left(\frac{9}{5} t - 459.67 \right)^3 \right] \end{aligned} \quad (7.3)$$

7.1.2. Blade-element Quantity

Percent passage height from hub:

$$\text{PHH} = \left(\frac{r - 0.14224}{0.06096} \right) \times 100 \quad (7.4)$$

7.1.3. MiscellaneousVenturi volume flow rate, m^3/s :

$$Q_v = 0.05229 \sqrt{\frac{2g_c \gamma_{H_2O} \Delta P_{vent}}{\rho}} \quad (7.5)$$

Blade velocity, m/s :

$$U = \frac{r \pi \text{RPM}}{30.0} \quad (7.6)$$

Calibration nozzle jet velocity, m/s :

$$V = \sqrt{\frac{2g_c \gamma_{H_2O} \Delta P_n}{\rho}} \quad (7.7)$$

Average Venturi flow coefficient:

$$\bar{\phi}_v = \frac{Q_v}{A U_t} \quad (7.8)$$

Average pressure-rise coefficient:

$$\bar{\psi} = \frac{g \Delta H}{U_t^2} \quad (7.9)$$

7.2. Three-Dimensional Periodic-Average Hot-Wire ParametersEffective cooling velocity, m/s :

$$V_e = K_1 + K_2 E_\ell + K_3 E_\ell^2 \quad (7.10)$$

Sensor yaw angle relationship (see Figure 3.2):

$$\cos \alpha = \cos \theta_0 \cos \theta_p \cos \theta_y + \sin \theta_0 \sin \theta_p \quad (7.11)$$

Effective cooling velocity/actual velocity ratio:

$$\begin{aligned} v_e/v = & b_0 + B_1\alpha + B_2\theta_p + b_3V + b_4\alpha^2 + b_5\theta_p^2 + b_6V^2 + b_7\alpha\theta_p \\ & + b_8\alpha V + b_9\theta_p V \end{aligned} \quad (7.12)$$

Absolute tangential flow angle (see Figures 3.2 and 3.3), degrees:

$$\beta_\theta = \beta_{mv} + \theta_{a,off} + \theta_y \quad (7.13)$$

Radial flow angle (see Figure 3.2), degrees:

$$\beta_r = -\theta_p \quad (7.14)$$

Radial component of fluid velocity, m/s:

$$V_r = V \sin \beta_r \quad (7.15)$$

Axial component of fluid velocity, m/s:

$$V_z = V \cos \beta_r \cos \beta_\theta \quad (7.16)$$

Tangential component of absolute fluid velocity, m/s:

$$V_\theta = V \cos \beta_r \sin \beta_\theta \quad (7.17)$$

Relative fluid velocity, m/s:

$$\dot{V}' = \sqrt{(V_\theta')^2 + (V_z')^2} \quad (7.18)$$

Tangential component of relative fluid velocity, m/s:

$$v_{\theta}' = U - v_{\theta} \quad (7.19)$$

Relative tangential flow angle, degrees:

$$\beta_{\theta}' = \sin^{-1} (v_{\theta}'/v') \quad (7.20)$$

8. APPENDIX B: TABULATION OF PERIODIC-AVERAGE DATA

The periodic-average circumferential survey data are tabulated in this section. The data are for flow downstream of the first rotor row (station 3), and the first stator row (station 4) for the maximum noise configuration.

The column headings are defined as follows:

Y/SS = circumferential spacing, Y/S_S

V = absolute velocity, \vec{V} , m/s

V,AX = axial velocity component, V_Z , m/s

V,TAN = absolute tangential flow component, V_θ , m/s

V,RAD = radial velocity component, V_r , m/s

BETA Y = absolute tangential flow angle, β_θ , degrees

BETA R = radial flow angle, β_r , degrees

V' = relative velocity, \vec{V}' , m/s

V,TAN' = relative tangential flow component, V'_θ , m/s

BETA Y' = relative tangential flow angle, β'_θ , m/s

Table 8.1. Hot-wire circumferential survey data obtained with the periodic-average measurement method for maximum noise.

STATION 3
PHH=10.00
YCR/SR=0.00

Y/SS	V M/S	V,AX M/S	V,TAN M/S	V,RAD M/S	BETA Y DEG	BETA R DEG	V, M/S	V,TAN M/S	BETA Y DEG
-0.000	21.399	14.747	15.507	0.033	46.439	0.089	16.013	-6.241	-22.938
0.052	21.148	14.771	15.135	0.080	45.698	0.210	16.183	-6.612	-24.117
0.102	21.219	14.709	15.292	-0.176	46.114	-0.476	16.062	-6.455	-23.693
0.154	20.351	14.434	15.046	0.147	46.185	0.403	15.914	-6.701	-24.902
0.181	21.359	14.615	15.569	-0.449	46.811	-1.204	15.867	-6.178	-22.914
0.200	21.395	14.813	15.437	-0.151	46.181	-0.405	16.101	-6.310	-23.074
0.251	21.692	14.188	16.659	-0.057	49.580	-1.721	15.073	-5.088	-19.729
0.257	22.074	11.638	18.752	-0.437	58.174	-1.134	12.018	-2.996	-14.434
0.282	21.637	8.565	19.869	0.195	66.680	0.517	8.769	-1.875	-12.371
0.309	21.389	5.891	20.914	1.408	73.978	3.775	6.019	-1.234	-11.828
0.335	20.710	5.291	19.849	2.030	75.075	7.256	5.621	-1.852	-19.734
0.360	20.617	5.566	19.795	3.244	74.294	8.964	5.899	-1.952	-19.326
0.385	21.038	8.752	19.665	3.207	71.049	8.768	7.066	-2.082	-17.137
0.411	21.611	8.110	19.837	2.780	67.763	7.407	8.332	-1.510	-13.255
0.437	21.312	9.957	18.491	3.626	61.697	9.796	10.476	-3.257	-18.110
0.462	21.198	11.182	17.048	3.587	57.642	9.741	11.909	-4.095	-20.132
0.489	21.912	12.257	17.912	3.007	55.616	7.888	12.843	-3.835	-17.373
0.514	22.624	13.333	18.205	1.031	53.780	4.133	13.790	-3.543	-14.879
0.540	22.676	13.711	18.004	1.443	52.709	3.645	14.215	-3.742	-15.271
0.560	22.735	14.115	17.792	1.041	51.573	2.625	14.659	-3.955	-15.653
0.551	22.345	14.796	17.400	0.473	49.825	1.187	15.421	-4.347	-16.373
0.610	22.525	14.529	17.205	0.492	49.820	1.252	15.223	-4.542	-17.359
0.669	22.486	14.635	17.071	0.153	49.394	0.390	15.364	-4.676	-17.720
0.720	22.311	14.691	16.791	-0.120	48.818	-0.390	15.504	-4.956	-18.641
0.771	22.037	14.841	16.290	0.094	47.695	0.244	15.813	-5.457	-20.189
0.822	21.411	14.563	15.090	0.402	47.133	1.076	15.773	-6.057	-22.583
0.874	21.603	15.108	15.528	-0.093	45.593	-0.270	16.242	-5.205	-22.476
0.925	21.752	14.857	15.681	-0.385	46.911	-1.014	15.973	-5.864	-21.540
0.978	20.863	14.468	15.030	-0.192	49.090	-0.527	16.952	-6.717	-24.905
1.000	21.122	14.726	15.140	-0.132	45.790	-0.358	16.142	-6.607	-24.163

Table 8.1. Continued.

STATION 3
PHF=10.00
YCR/SR=0.69

Y/SS	V M/S	V·AX M/S	V·TAN M/S	V·RAD M/S	BETA Y DEG	BETA R DEG	V' M/S	V·TAN' M/S	BETA Y' DEG
0.001	21.103	14.280	15.528	0.526	47.397	1.429	15.070	-6.219	-23.532
0.051	21.407	14.797	15.468	0.265	46.270	0.708	16.074	-6.280	-22.996
0.102	21.601	14.896	15.643	0.017	46.401	0.046	16.098	-6.104	-22.283
0.154	21.141	14.647	15.244	0.206	46.144	0.558	16.025	-6.503	-23.942
0.206	21.023	14.571	15.154	0.157	46.123	0.427	15.953	-6.894	-24.548
0.257	21.081	14.574	15.231	-0.139	46.262	-0.378	15.965	-6.516	-24.090
0.309	21.241	14.550	15.470	0.371	46.755	-1.001	15.647	-6.277	-23.535
0.360	21.267	14.577	15.476	-0.337	46.712	-1.446	15.869	-6.271	-23.278
0.411	21.357	14.674	15.505	-0.615	46.577	-1.649	15.947	-6.242	-23.044
0.462	21.355	14.984	15.187	-0.934	45.385	-2.508	16.357	-6.560	-23.645
0.483	21.467	14.817	15.497	-1.070	46.285	-2.874	16.081	-6.251	-22.270
0.515	21.705	14.427	16.140	-1.510	48.217	-3.989	15.477	-5.602	-21.219
0.540	21.519	12.976	17.119	-1.275	52.839	-3.396	13.778	-4.628	-19.629
0.565	21.624	10.132	19.081	-0.917	62.032	-2.431	10.477	-2.666	-14.741
0.591	21.360	8.054	20.324	0.150	71.871	0.403	8.805	-1.423	-12.073
0.617	20.772	4.918	20.090	1.657	76.249	5.128	9.188	-1.651	-18.561
0.642	20.732	4.999	19.959	2.497	76.229	6.917	9.205	-1.758	-19.730
0.665	20.990	5.349	20.117	2.254	74.579	6.164	9.784	-1.630	-16.568
0.694	21.206	6.800	19.991	1.959	71.215	5.301	7.023	-1.757	-14.485
0.720	21.625	7.846	20.092	1.550	68.668	4.110	8.019	-1.656	-11.914
0.745	21.711	9.048	19.638	1.733	65.280	4.630	9.286	-2.089	-13.002
0.771	21.653	10.175	19.000	2.036	61.842	5.400	10.236	-2.742	-15.083
0.798	21.956	11.290	18.744	1.768	58.924	4.618	11.089	-3.003	-14.668
0.823	22.143	12.010	18.141	1.478	55.190	3.828	13.110	-3.606	-15.558
0.843	22.192	13.359	17.658	1.085	52.940	2.803	13.961	-4.055	-16.302
0.875	22.047	13.662	17.294	0.639	51.676	2.180	14.372	-4.463	-18.093
0.901	22.230	14.373	16.955	0.317	49.712	0.817	15.151	-4.792	-18.438
0.925	21.745	14.374	16.314	0.493	48.618	1.300	15.966	-5.433	-20.704
0.976	22.033	14.002	16.458	-0.260	48.489	-0.675	15.517	-5.249	-19.774
1.000	21.873	14.780	16.127	-0.044	47.495	-0.115	15.813	-5.621	-20.321

Table 8.1. Continued.

STATION 3										
PHH=50.00										
YOR/SR=0.00										
Y/SS	V	V·AX	V·TAN	V·RAD	BETA Y	BETA R	V·	V·TAN·	BETA Y·	LETA Y·
	M/S	M/S	M/S	M/S	DEG	DEG	M/S	M/S	DEG	DEG
0.001	20.108	15.244	13.113	-0.020	40.704	-0.057	19.530	-12.209	-0.057	-28.691
0.052	20.356	15.455	13.308	0.124	40.731	0.516	19.575	-12.014	0.516	-27.860
0.103	20.626	15.470	13.640	0.220	41.402	0.611	19.386	-11.682	0.611	-27.057
0.154	20.716	15.504	13.736	0.284	41.540	0.780	19.355	-11.586	0.780	-26.769
0.200	20.731	15.456	13.813	0.310	41.788	0.974	19.270	-11.509	0.974	-26.673
0.257	20.815	15.476	13.919	0.165	41.967	0.454	19.224	-11.402	0.454	-26.384
0.309	20.900	15.407	14.121	0.221	42.506	0.600	19.048	-11.201	0.600	-26.019
0.355	21.067	15.246	14.538	0.108	43.635	0.255	18.674	-10.784	0.255	-25.272
0.413	20.916	14.858	14.287	0.362	43.378	1.007	18.508	-11.035	1.007	-26.601
0.462	20.763	14.588	14.365	0.316	43.784	0.972	18.566	-10.957	0.972	-26.168
0.487	20.750	14.852	14.491	0.071	44.295	0.157	18.382	-10.831	0.157	-26.103
0.514	21.060	14.849	15.138	0.073	45.941	0.199	17.841	-10.124	0.199	-24.806
0.539	21.139	13.170	16.507	0.962	51.415	2.607	15.848	-8.815	2.607	-25.795
0.565	21.102	12.251	17.097	1.099	51.377	4.615	14.756	-8.225	4.615	-23.675
0.591	21.293	11.861	17.810	1.017	50.035	4.350	14.147	-7.712	4.350	-23.034
0.617	21.307	11.581	17.787	1.867	56.934	5.020	13.810	-7.535	5.020	-23.049
0.642	20.987	11.842	17.210	2.005	55.469	5.481	14.354	-8.112	5.481	-24.410
0.668	20.480	12.358	16.212	1.961	52.685	5.494	15.352	-9.109	5.494	-26.393
0.694	20.212	12.345	15.924	1.591	52.216	4.516	15.515	-9.398	4.516	-27.280
0.719	15.776	12.572	15.234	0.984	50.469	2.852	16.119	-10.088	2.852	-28.745
0.745	19.333	12.428	14.758	0.573	49.976	1.699	16.285	-10.524	1.699	-40.258
0.770	18.723	12.582	13.855	0.527	47.758	1.614	17.023	-11.467	1.614	-42.345
0.798	18.814	13.108	13.495	0.227	45.833	0.691	17.655	-11.828	0.691	-42.061
0.822	16.781	13.095	13.462	0.207	45.792	0.631	17.667	-11.860	0.631	-42.169
0.849	19.010	14.008	12.851	0.040	42.535	0.120	18.755	-12.471	0.120	-41.678
0.874	15.283	14.100	13.154	-0.027	43.012	-0.075	18.660	-12.168	-0.075	-40.794
0.897	15.416	14.346	13.081	0.048	42.357	0.145	18.660	-12.241	0.145	-40.909
0.925	15.932	14.764	13.391	0.017	42.207	0.049	18.933	-11.931	0.049	-38.943
0.976	20.343	15.410	13.280	-0.099	40.755	-0.280	19.537	-12.042	-0.280	-38.005
1.000	20.395	15.443	13.321	0.103	40.781	0.453	19.552	-12.001	0.453	-37.852

Table 8.1. Continued.

STATION 3
PHF=50.00
YCR/SR=0.69

Y/SS	V M/S	V, AX M/S	V, TAN M/S	V, RAD M/S	BETA Y DEG	BETA R DEG	V, M/S	V, TAN M/S	FETA Y, DEG
0.001	17.485	9.817	14.360	1.773	55.643	5.820	14.715	-10.962	-48.155
0.027	18.369	11.176	14.541	1.028	52.455	3.209	15.528	-10.781	-43.568
0.052	19.027	12.963	13.906	0.773	47.010	2.328	17.273	-11.410	-41.368
0.076	20.765	14.832	14.533	0.001	44.417	0.003	18.341	-10.789	-36.034
0.103	22.394	15.629	13.966	0.113	41.579	-0.311	19.378	-11.456	-36.240
0.130	21.078	16.315	14.272	-0.265	41.178	-0.700	19.705	-11.050	-34.110
0.154	21.509	16.123	14.237	0.138	41.445	0.368	19.500	-11.085	-34.511
0.179	21.522	16.157	14.217	0.060	41.345	0.159	19.606	-11.105	-34.500
0.209	21.379	15.879	14.386	0.237	41.987	0.631	19.363	-10.976	-34.388
0.257	21.112	15.840	14.356	0.243	42.186	0.650	19.266	-10.966	-34.695
0.309	21.112	15.590	14.226	0.515	42.381	1.399	19.136	-11.096	-35.439
0.351	21.284	15.524	14.560	0.023	43.165	0.063	18.890	-10.762	-34.730
0.411	21.216	15.394	14.599	0.062	43.482	-0.167	18.760	-10.723	-34.859
0.462	20.660	14.965	14.532	-0.099	44.155	-0.163	18.449	-10.790	-35.792
0.514	20.612	14.751	14.397	-0.076	44.304	-0.210	18.356	-10.925	-36.526
0.565	20.153	14.381	14.118	0.093	44.473	0.265	18.230	-11.204	-37.921
0.617	19.898	14.330	13.762	-0.025	43.843	-0.073	18.411	-11.560	-38.893
0.668	19.632	14.194	13.563	0.108	43.698	0.310	18.432	-11.759	-39.642
0.715	19.473	14.370	13.140	0.178	42.440	0.525	18.639	-12.182	-40.289
0.745	19.567	14.555	13.076	0.172	41.937	0.503	19.021	-12.246	-40.075
0.771	19.649	14.770	12.951	-0.123	41.235	-0.359	19.271	-12.371	-39.937
0.797	19.435	14.804	12.590	0.185	40.379	0.555	19.526	-12.732	-40.696
0.822	19.664	14.286	13.510	-0.202	43.401	-0.764	18.557	-11.812	-39.585
0.848	19.276	13.117	14.118	0.435	47.103	1.294	17.251	-11.204	-40.503
0.874	19.116	11.656	15.148	0.314	52.423	0.942	15.472	-10.174	-41.117
0.899	18.382	9.482	15.722	0.906	58.906	2.825	13.493	-9.600	-45.356
0.925	17.729	8.556	15.486	1.529	61.050	4.301	13.051	-9.556	-49.039
0.950	17.365	8.135	15.459	1.874	62.247	6.122	13.785	-9.863	-50.485
0.976	17.185	8.745	14.715	1.574	59.278	5.255	13.747	-10.608	-50.499
1.000	17.471	9.257	14.748	1.139	57.774	3.737	14.080	-10.574	-48.677

Table 8.1. Continued.

STATION 4
PHH=10.00
YCR/SR=0.00

Y/SS	V M/S	V,AX M/S	V,TAN M/S	V,RAD M/S	BETA Y DEG	BETA R DEG	V, M/S	V,TAN M/S	BETA Y DEG
-0.000	17.757	15.438	8.734	0.835	29.498	2.695	20.191	-13.013	-40.129
0.052	18.488	15.925	9.391	-0.052	30.528	-0.160	20.156	-12.356	-37.807
0.103	17.909	15.498	8.975	0.027	30.074	0.085	20.083	-12.772	-39.493
0.154	17.665	14.880	9.519	-0.158	32.609	-0.511	19.260	-12.228	-39.412
0.206	17.088	14.754	8.617	-0.256	30.288	-0.859	19.750	-13.130	-41.667
0.258	17.653	15.199	8.920	-1.032	30.409	-3.351	19.888	-12.827	-40.163
0.308	18.004	15.337	9.343	-1.276	31.349	-4.065	19.725	-12.404	-38.965
0.359	18.091	14.971	10.096	-1.103	33.993	-3.495	18.971	-11.651	-37.892
0.411	17.621	14.259	10.351	-0.234	35.977	-0.762	18.253	-11.396	-38.634
0.462	17.463	13.806	10.685	0.407	37.738	1.334	17.691	-11.062	-38.702
0.488	17.204	13.490	10.655	0.686	38.305	2.285	17.464	-11.092	-39.429
0.513	17.112	13.321	10.714	0.766	38.809	2.566	17.297	-11.032	-39.634
0.540	16.626	12.956	10.394	0.729	38.739	2.512	17.226	-11.353	-41.228
0.565	15.866	12.468	9.755	1.055	38.041	3.814	17.299	-11.992	-43.885
0.591	15.229	12.085	9.197	1.143	37.272	4.303	17.423	-12.550	-46.083
0.617	15.335	11.929	9.635	0.169	38.928	0.630	17.000	-12.112	-45.437
0.642	14.459	11.492	8.772	0.207	37.354	0.820	17.333	-12.975	-48.468
0.668	13.691	11.266	7.753	0.642	34.536	2.687	17.965	-13.994	-51.164
0.694	13.555	11.444	7.223	0.772	32.259	3.263	18.491	-14.524	-51.764
0.721	13.406	11.813	6.237	1.132	27.835	4.842	19.496	-15.510	-52.707
0.745	13.704	12.196	6.009	1.718	26.232	7.203	19.910	-15.738	-52.227
0.771	14.468	12.685	6.630	2.113	27.596	8.396	19.734	-15.117	-50.000
0.796	14.886	12.852	7.028	2.651	28.672	10.258	19.540	-14.719	-48.874
0.823	15.339	12.801	7.953	2.860	31.851	10.745	18.819	-13.795	-47.140
0.848	15.635	12.905	8.358	2.838	32.927	10.459	18.597	-13.390	-46.055
0.874	16.167	13.451	8.659	2.336	32.771	8.307	18.768	-13.088	-44.216
0.900	16.459	14.080	8.249	1.146	30.363	7.492	19.505	-13.499	-43.792
0.925	16.932	14.740	8.158	1.699	28.962	5.759	20.048	-13.590	-42.675
0.977	17.980	15.612	8.902	0.538	29.692	1.715	20.217	-12.845	-39.446
1.000	17.856	15.510	8.818	0.717	29.621	2.302	20.192	-12.929	-39.814

Table 8.1. Continued.

STATION 4										
PHH=10.00										
YOR/SR=0.34										
Y/SS	V M/S	V·AX M/S	V·TAN M/S	V·RAD M/S	BETA Y DEG	BETA R DEG	V· M/S	V·TAN· M/S	BETA Y· DEG	
-0.000	17.111	14.540	9.014	0.317	31.797	1.060	19.327	-12.733	-41.208	
0.051	16.252	13.711	8.723	0.222	32.464	0.782	18.911	-13.024	-43.529	
0.103	15.347	13.036	8.092	0.358	31.829	1.335	18.879	-13.656	-46.330	
0.155	15.481	13.108	8.234	-0.220	32.135	-0.815	18.826	-13.513	-45.873	
0.205	15.959	13.198	8.966	-0.332	34.188	-1.191	18.373	-12.782	-44.081	
0.257	16.214	13.243	9.327	0.730	35.158	2.581	18.156	-12.420	-43.164	
0.308	16.456	13.425	9.423	1.330	35.064	4.637	18.224	-12.324	-42.552	
0.360	16.881	13.833	9.617	1.062	34.808	3.606	18.398	-12.130	-41.247	
0.411	17.106	14.130	9.630	0.482	34.276	1.616	18.614	-12.117	-40.616	
0.462	17.060	14.268	9.353	-0.078	33.246	-0.263	18.899	-12.394	-40.981	
0.489	16.456	13.886	8.825	0.306	32.438	1.065	18.968	-12.922	-42.940	
0.515	16.729	13.956	9.220	-0.289	33.450	-0.591	18.754	-12.527	-41.912	
0.539	16.831	14.012	9.306	-0.592	33.589	-2.016	18.738	-12.441	-41.602	
0.565	16.242	13.701	8.719	-0.271	32.471	-0.957	18.906	-13.028	-43.559	
0.591	15.986	13.429	8.670	-0.198	32.848	-0.708	18.744	-13.077	-44.239	
0.617	15.701	13.446	8.098	-0.380	31.059	-1.388	19.160	-13.649	-45.429	
0.643	15.332	13.015	8.090	-0.493	31.864	-1.842	18.866	-13.658	-46.380	
0.668	14.228	12.346	7.070	0.194	29.799	0.780	19.179	-14.677	-49.931	
0.654	13.885	12.149	6.717	0.284	28.940	1.174	19.326	-15.030	-51.051	
0.720	13.548	12.075	6.085	0.844	26.745	3.572	19.776	-15.662	-52.369	
0.746	13.862	12.364	6.156	1.181	26.467	4.886	19.899	-15.592	-51.586	
0.771	14.637	13.111	6.363	1.357	25.888	5.320	20.213	-15.384	-49.560	
0.796	15.591	13.775	7.142	1.519	27.406	5.590	20.076	-14.605	-46.674	
0.822	17.039	14.851	8.291	1.012	29.173	3.406	20.041	-13.456	-42.178	
0.848	17.642	15.359	8.655	0.657	29.402	2.133	20.182	-13.092	-40.445	
0.874	18.028	15.522	9.160	0.415	30.547	1.319	19.984	-12.587	-39.039	
0.899	18.141	15.649	9.173	0.247	30.377	0.781	20.075	-12.574	-38.783	
0.925	18.074	15.466	9.352	0.100	31.159	0.317	19.821	-12.396	-38.711	
0.977	17.092	14.665	8.771	0.363	30.884	1.218	19.582	-12.976	-41.503	
1.000	16.643	14.370	8.387	0.394	30.270	1.357	19.621	-13.360	-42.915	

Table 8.1. Continued.

STATION 4										
PHH=10.00										
YCR/SR=0.69										
Y/SS	V M/S	V·AX M/S	V·TAN M/S	V·RAD M/S	BETA Y DEG	BETA R DEG	V· M/S	V·TAN· M/S	BETA Y· DEG	BETA Y· DEG
0.001	13.953	10.780	8.682	1.764	38.848	7.262	16.938	-13.065	-50.475	-50.475
0.052	14.701	11.503	9.085	1.125	38.302	4.389	17.107	-12.662	-47.747	-47.747
0.102	14.949	12.107	8.667	1.336	35.596	5.128	17.823	-13.080	-47.214	-47.214
0.154	15.880	13.246	8.749	0.408	33.443	1.473	18.559	-12.998	-44.459	-44.459
0.205	16.556	13.885	9.002	-0.520	32.957	-1.799	18.847	-12.745	-42.549	-42.549
0.257	16.794	13.925	9.298	-1.302	33.731	-4.448	18.685	-12.450	-41.799	-41.799
0.308	16.907	14.006	9.378	-1.318	33.807	-4.471	18.685	-12.369	-41.449	-41.449
0.360	17.106	14.106	9.591	-1.286	34.214	-4.311	18.621	-12.156	-40.754	-40.754
0.412	17.152	14.180	9.613	-0.835	34.135	-2.790	18.663	-12.134	-40.553	-40.553
0.463	17.285	14.309	9.666	-0.773	34.041	-2.564	18.727	-12.081	-40.175	-40.175
0.514	16.803	13.975	9.323	-0.362	33.708	-1.236	18.699	-12.424	-41.639	-41.639
0.539	16.802	13.886	9.451	-0.406	34.240	-1.384	18.548	-12.296	-41.525	-41.525
0.565	16.526	13.373	9.685	-0.673	35.913	-2.334	18.009	-12.062	-42.048	-42.048
0.591	15.851	12.907	9.194	-0.359	35.463	-1.297	18.005	-12.553	-44.203	-44.203
0.617	14.891	11.985	8.837	-0.121	36.401	-0.467	17.616	-12.911	-47.129	-47.129
0.643	14.499	11.577	8.727	-0.187	37.008	-0.738	17.423	-13.021	-48.358	-48.358
0.668	14.009	11.347	8.207	-0.370	35.879	-1.512	17.666	-13.540	-50.035	-50.035
0.694	13.623	11.036	7.983	-0.253	35.878	-1.065	17.643	-13.765	-51.278	-51.278
0.720	13.920	11.475	7.862	-0.526	34.414	-2.167	18.014	-13.886	-50.429	-50.429
0.746	14.211	11.948	7.694	-0.045	32.779	-0.180	18.446	-14.053	-49.629	-49.629
0.771	14.769	12.412	7.989	0.500	32.769	1.940	18.529	-13.758	-47.945	-47.945
0.796	15.281	12.852	8.200	1.054	32.539	3.955	18.673	-13.547	-46.510	-46.510
0.823	15.824	12.919	9.009	1.530	34.692	5.549	18.142	-12.738	-44.596	-44.596
0.848	15.898	12.851	9.243	1.465	35.726	5.287	17.930	-12.504	-44.214	-44.214
0.873	15.258	12.256	8.993	1.713	36.270	6.431	17.688	-12.754	-46.140	-46.140
0.895	15.099	11.965	9.123	1.261	37.326	4.790	17.393	-12.624	-46.535	-46.535
0.926	14.472	11.762	8.354	1.142	35.383	4.524	17.825	-13.393	-48.710	-48.710
0.952	14.543	11.534	8.811	0.913	37.377	3.599	17.331	-12.936	-48.280	-48.280
0.976	14.161	10.935	8.882	1.435	39.086	5.817	16.884	-12.865	-49.635	-49.635
1.000	14.308	11.085	9.982	1.084	39.018	4.345	16.906	-12.765	-49.031	-49.031

Table 8.1. Continued.

STATION 4										
PHH=30.00										
YOR/SR=0.00										
Y/SS	V M/S	V.AX M/S	V.TAN M/S	V.RAD M/S	BETA Y DEG	BETA R DEG	V ^o M/S	V.TAN ^o M/S	BETA Y ^o DEG	
0.000	16.230	13.624	8.759	1.037	32.737	3.663	20.098	-14.776	-47.322	
0.051	16.302	13.881	8.482	1.062	31.426	3.734	20.476	-15.053	-47.319	
0.102	16.547	14.268	8.328	0.936	30.270	3.243	20.853	-15.207	-46.825	
0.154	16.950	14.653	8.500	0.588	30.119	1.985	20.994	-15.034	-45.736	
0.206	17.295	14.999	8.608	0.218	29.852	0.722	21.161	-14.927	-44.861	
0.258	17.762	15.580	8.525	-0.296	28.687	-0.955	21.634	-15.010	-43.932	
0.308	17.892	15.750	8.484	-0.288	28.511	-0.923	21.785	-15.050	-43.699	
0.360	18.098	15.916	8.595	-0.594	28.371	-1.882	21.829	-14.939	-43.188	
0.411	18.091	15.912	8.579	-0.699	28.333	-2.214	21.837	-14.955	-43.225	
0.463	17.929	15.811	8.425	-0.700	28.051	-2.239	21.870	-15.110	-43.701	
0.514	17.826	15.649	8.501	-0.781	28.512	-2.512	21.700	-15.034	-43.851	
0.539	17.707	15.493	8.541	-0.746	28.868	-2.413	21.560	-14.993	-44.061	
0.566	17.730	15.468	8.625	-0.846	29.143	-2.735	21.484	-14.910	-43.548	
0.591	17.622	15.301	8.701	-0.837	29.626	-2.723	21.311	-14.833	-44.111	
0.617	17.466	15.036	8.850	-0.806	30.481	-2.645	21.017	-14.684	-44.322	
0.642	17.045	14.598	8.774	-0.762	31.008	-2.561	20.760	-14.760	-45.317	
0.668	16.585	13.970	8.907	-0.763	32.521	-2.638	20.227	-14.628	-46.319	
0.694	15.607	12.996	8.630	-0.467	33.587	-1.713	19.775	-14.905	-48.914	
0.719	14.354	11.958	7.939	0.133	33.583	0.530	19.652	-15.595	-52.521	
0.746	13.792	11.161	8.101	-0.152	35.972	0.632	19.047	-15.434	-54.127	
0.771	13.016	10.754	7.332	0.054	34.287	0.236	19.446	-16.202	-56.426	
0.797	12.879	10.759	7.074	0.254	33.324	1.130	19.665	-16.461	-56.830	
0.823	13.371	11.285	7.156	0.478	32.378	2.049	19.890	-16.379	-55.433	
0.848	14.159	12.180	7.190	0.652	30.553	2.638	20.384	-16.345	-53.306	
0.874	14.886	12.864	7.413	1.075	29.954	4.141	20.625	-16.121	-51.412	
0.900	15.393	13.174	7.855	1.302	30.805	4.852	20.479	-15.680	-49.964	
0.925	15.768	13.456	8.123	1.257	31.120	4.574	20.459	-15.411	-48.875	
0.950	15.978	13.502	8.458	1.206	32.065	4.328	20.239	-15.076	-48.154	
0.976	15.967	13.598	8.286	1.177	31.355	4.227	20.431	-15.249	-48.275	
1.000	16.029	13.587	8.439	1.058	31.844	3.765	20.310	-15.096	-48.012	

Table 8.1. Continued.

STATION 4										
PHH=30.00										
YOR/SR=0.34										
Y/SS	V M/S	V·AX M/S	V·TAN M/S	V·RAD M/S	BETA Y DEG	BETA R DEG	V· M/S	V·TAN' M/S	BETA Y· DEG	
-0.000	16.606	14.509	8.074	0.220	29.094	0.758	21.203	-15.461	-46.818	
0.051	16.726	14.766	7.853	0.240	28.007	0.822	21.539	-15.681	-46.722	
0.103	17.446	15.176	8.599	-0.330	29.537	-1.083	21.293	-14.936	-44.543	
0.154	17.618	15.338	8.665	-0.202	29.464	-0.656	21.363	-14.869	-44.110	
0.205	17.820	15.462	8.855	-0.286	29.800	-0.918	21.320	-14.680	-43.514	
0.257	17.697	15.342	8.821	-0.056	29.897	-0.181	21.257	-14.714	-43.803	
0.308	17.868	15.397	9.065	-0.137	30.489	-0.439	21.129	-14.469	-43.221	
0.359	17.756	15.177	9.216	-0.012	31.267	-0.039	20.866	-14.319	-43.333	
0.411	17.464	14.759	9.316	0.615	32.260	2.019	20.494	-14.219	-43.932	
0.462	17.933	15.056	9.738	0.259	32.895	0.827	20.421	-13.796	-42.499	
0.514	17.276	14.584	9.201	1.058	32.248	3.510	20.448	-14.334	-44.505	
0.540	17.465	14.789	9.241	0.962	32.000	3.159	20.567	-14.294	-44.025	
0.567	17.358	14.686	9.193	1.046	32.045	3.455	20.527	-14.341	-44.319	
0.551	17.234	14.593	9.088	1.214	31.912	4.038	20.535	-14.447	-44.712	
0.617	17.399	14.604	9.428	0.746	32.844	2.458	20.305	-14.107	-44.007	
0.643	17.020	14.189	9.368	0.762	33.434	2.566	20.051	-14.166	-44.954	
0.668	16.635	14.109	8.770	0.870	31.864	2.998	20.422	-14.765	-46.302	
0.654	16.291	13.715	8.765	0.688	32.582	2.421	20.155	-14.770	-47.121	
0.720	15.853	13.464	8.418	0.679	32.015	2.448	20.243	-15.117	-48.311	
0.745	15.114	13.002	7.691	0.473	30.606	1.792	20.495	-15.843	-50.626	
0.771	14.759	12.557	7.754	0.105	31.695	0.407	20.167	-15.780	-51.489	
0.757	14.507	12.660	7.076	-0.318	29.203	-1.255	20.764	-16.458	-52.432	
0.822	14.082	12.487	6.498	-0.396	27.491	-1.611	21.123	-17.037	-53.761	
0.848	14.074	12.700	6.061	-0.188	25.513	-0.765	21.601	-17.473	-53.988	
0.874	14.334	13.034	5.960	-0.255	24.574	-1.018	21.880	-17.574	-53.439	
0.899	14.673	13.386	6.001	0.300	25.148	1.173	22.059	-17.533	-52.639	
0.925	15.423	13.945	6.579	0.359	25.259	1.332	21.953	-16.955	-50.565	
0.951	15.964	14.176	7.337	0.210	27.364	0.752	21.525	-16.198	-48.807	
0.976	16.182	14.310	7.554	0.072	27.828	0.255	21.452	-15.981	-48.156	
1.000	16.451	14.551	7.674	0.082	27.806	0.284	21.524	-15.861	-47.465	

Table 8.1. Continued.

STATION 4										
PHI=30.00										
YOR/SR=0.69										
Y/SS	V M/S	V·AX M/S	V·TAN M/S	V·RAD M/S	BETA Y DEG	BETA R DEG	V· M/S	V·TAN' M/S	BETA Y' DEG	
0.000	16.599	13.666	9.386	0.829	34.482	2.862	19.671	-14.149	-45.995	
0.053	16.650	13.532	9.665	0.836	35.534	2.879	19.378	-13.870	-45.707	
0.102	16.521	13.476	9.498	1.063	35.175	3.690	19.459	-14.037	-46.168	
0.154	16.765	13.547	9.811	1.139	35.913	3.894	19.284	-13.724	-45.372	
0.207	16.755	13.609	9.761	1.268	35.650	4.329	19.363	-13.774	-45.346	
0.257	17.074	13.800	9.991	1.114	35.904	3.741	19.336	-13.543	-44.461	
0.308	17.125	13.955	9.833	1.351	35.170	4.526	19.557	-13.701	-44.474	
0.360	17.636	14.490	10.012	0.918	34.642	2.984	19.820	-13.523	-43.023	
0.411	17.810	14.834	9.836	0.631	33.546	2.030	20.192	-13.699	-42.721	
0.464	17.820	15.053	9.526	0.468	32.328	1.506	20.563	-14.008	-42.942	
0.515	17.951	15.215	9.526	0.057	32.052	0.183	20.681	-14.008	-42.636	
0.540	17.965	15.285	9.439	-0.000	31.696	-0.001	20.793	-14.096	-42.681	
0.565	17.978	15.331	9.389	-0.096	31.483	-0.305	20.860	-14.146	-42.697	
0.591	17.797	15.135	9.363	0.027	31.744	0.088	20.734	-14.171	-43.117	
0.616	17.869	15.228	9.347	-0.227	31.542	-0.728	20.813	-14.188	-42.975	
0.643	17.687	15.144	9.137	-0.038	31.104	-0.122	20.896	-14.398	-43.553	
0.668	17.414	14.985	8.871	0.117	30.626	0.384	20.966	-14.664	-44.380	
0.694	17.304	14.814	8.942	0.092	31.115	0.306	20.795	-14.593	-44.568	
0.719	17.022	14.524	8.874	-0.234	31.425	-0.786	20.637	-14.660	-45.268	
0.745	16.272	13.573	8.970	-0.301	33.461	-1.061	19.908	-14.564	-47.018	
0.771	15.263	12.649	8.533	-0.377	34.004	-1.417	19.622	-15.001	-49.863	
0.797	14.444	11.783	8.330	-0.632	35.257	-2.509	19.236	-15.205	-52.226	
0.822	13.536	10.994	7.684	-0.434	35.644	-1.837	19.126	-15.651	-54.912	
0.848	13.491	10.904	7.945	-0.009	36.078	-0.040	19.025	-15.590	-55.031	
0.874	14.032	11.552	7.960	0.287	34.570	1.173	19.391	-15.574	-53.435	
0.900	14.707	12.148	8.253	0.792	34.191	3.086	19.522	-15.282	-51.519	
0.925	15.444	12.726	8.707	0.870	34.381	3.229	19.540	-14.827	-49.362	
0.950	15.810	13.029	8.912	0.880	34.374	3.191	19.585	-14.622	-48.298	
0.976	16.158	13.253	9.200	0.899	34.767	3.188	19.523	-14.335	-47.246	
1.000	16.270	13.489	9.051	0.925	33.861	3.260	19.792	-14.484	-47.038	

Table 8.1. Continued.

STATION 4
PHH=50.00
YOR/SR=0.00

Y/SS	V M/S	V.AX M/S	V.TAN M/S	V.RAD M/S	BETA Y DEG	BETA R DEG	V' M/S	V.TAN' M/S	BETA Y' DEG
-0.000	17.517	15.658	7.809	0.825	26.506	2.700	23.492	-17.513	-48.200
0.051	18.359	16.101	8.796	0.652	28.648	2.036	23.073	-16.526	-45.745
0.103	18.262	15.759	9.191	0.813	30.252	2.553	22.551	-16.131	-45.667
0.154	18.211	15.517	9.518	0.528	31.524	1.660	22.148	-15.804	-45.526
0.206	17.820	14.975	9.645	0.524	32.784	1.685	21.680	-15.677	-46.312
0.257	17.449	14.543	9.637	0.297	33.529	0.975	21.390	-15.685	-47.163
0.308	16.619	13.902	9.075	0.702	33.149	2.421	21.379	-16.243	-49.440
0.334	16.339	13.633	8.981	0.375	33.375	2.339	21.281	-16.341	-50.162
0.359	16.501	13.838	8.980	0.367	32.981	1.275	21.414	-16.342	-49.742
0.366	16.369	13.741	8.888	0.348	32.897	1.218	21.421	-16.434	-50.099
0.410	16.135	13.671	8.555	0.498	32.038	1.769	21.634	-16.767	-50.807
0.437	16.323	13.866	8.630	0.178	31.899	0.623	21.700	-16.692	-50.284
0.462	16.443	13.986	8.646	-0.047	31.725	-0.165	21.764	-16.676	-50.013
0.483	16.413	14.083	8.429	0.039	30.901	0.137	21.993	-16.893	-50.183
0.513	16.418	14.027	8.532	-0.027	31.311	-0.093	21.878	-16.790	-50.123
0.540	16.550	14.194	8.511	-0.118	30.947	-0.408	22.002	-16.811	-49.826
0.565	16.560	14.324	8.309	-0.119	30.118	-0.413	22.240	-17.013	-49.904
0.616	16.752	14.594	8.216	-0.353	29.379	-1.207	22.485	-17.106	-49.529
0.668	16.797	14.803	7.938	-0.105	28.201	-0.357	22.833	-17.384	-49.586
0.720	16.643	14.798	7.611	0.298	27.220	1.027	23.079	-17.711	-50.121
0.771	16.544	14.890	7.188	0.577	25.770	1.998	23.463	-18.134	-50.611
0.796	16.356	14.746	7.053	0.562	25.562	1.969	23.478	-18.269	-51.090
0.823	15.993	14.308	7.135	0.395	26.503	1.416	23.141	-18.187	-51.808
0.848	15.420	13.540	7.378	-0.414	28.587	-0.559	22.479	-17.944	-52.964
0.874	14.538	12.759	6.956	-0.414	28.597	-1.631	22.363	-18.366	-55.212
0.899	14.015	12.152	6.915	-0.968	29.640	-3.959	22.057	-18.407	-56.568
0.925	13.890	12.205	6.615	-0.474	28.458	-1.957	22.336	-18.707	-56.880
0.950	14.717	12.955	6.981	0.168	28.318	0.656	22.455	-18.341	-54.765
0.977	16.056	14.127	7.594	0.756	28.260	2.699	22.668	-17.728	-51.451
1.000	17.074	15.001	8.096	0.964	28.356	3.235	22.842	-17.226	-48.948

Table 8.1. Continued.

STATION 4											
PHH=50.00											
YDR/SR=0.34											
Y/SS	V M/S	V·AX M/S	V·TAN M/S	V·RAD M/S	BETA Y DEG	BETA R DEG	V° M/S	V·TAN° M/S	BETA Y° DEG		
0.000	17.558	15.099	8.937	1.353	30.620	4.410	22.281	-16.385	-47.339		
0.026	17.807	15.171	9.257	1.115	31.390	3.590	22.096	-16.065	-46.640		
0.053	17.609	15.018	9.098	1.335	31.207	4.347	22.108	-16.225	-47.212		
0.077	17.662	15.035	9.191	1.197	31.437	3.886	22.051	-16.131	-47.015		
0.103	17.536	14.921	9.153	1.049	31.526	3.431	22.002	-16.169	-47.299		
0.128	17.441	14.808	9.155	1.055	31.727	3.468	21.923	-16.167	-47.513		
0.154	17.215	14.670	8.956	0.962	31.405	3.202	21.578	-16.366	-48.127		
0.181	16.968	14.520	8.721	1.015	30.991	3.428	22.055	-16.601	-48.826		
0.207	16.755	14.367	8.649	0.923	31.049	3.151	22.009	-16.673	-49.248		
0.257	16.502	14.206	8.384	0.464	30.548	1.611	22.107	-16.538	-50.013		
0.308	16.313	14.135	8.128	0.499	29.901	1.752	22.258	-17.194	-50.577		
0.360	16.317	14.216	8.006	0.263	29.387	0.925	22.404	-17.316	-50.616		
0.412	16.085	14.221	7.514	0.177	27.851	0.630	22.789	-17.808	-51.390		
0.462	16.388	14.395	7.829	-0.201	28.541	-0.703	22.654	-17.493	-50.548		
0.514	16.536	14.445	8.043	-0.331	29.109	-1.148	22.522	-17.279	-50.106		
0.566	16.712	14.543	8.219	-0.330	29.464	-1.133	22.454	-17.103	-49.616		
0.617	16.664	14.547	8.128	0.070	29.195	0.239	22.522	-17.194	-49.767		
0.668	16.744	14.717	7.976	0.393	28.455	1.344	22.748	-17.346	-49.688		
0.719	16.667	14.727	7.744	0.963	27.738	3.314	22.932	-17.578	-50.043		
0.746	16.920	14.857	8.094	0.207	28.582	0.701	22.749	-17.228	-49.226		
0.772	16.488	14.391	8.010	0.778	29.100	2.703	22.512	-17.312	-50.265		
0.757	15.920	13.759	7.963	0.255	30.060	3.078	22.151	-17.359	-51.600		
0.822	15.261	12.839	8.236	0.484	32.678	1.819	21.373	-17.087	-53.078		
0.847	14.286	11.918	7.873	0.240	33.450	0.963	21.130	-17.449	-55.665		
0.874	13.654	11.529	7.315	0.043	32.396	0.181	21.381	-18.007	-57.370		
0.900	13.669	11.895	6.733	0.113	29.512	0.474	22.069	-18.589	-57.385		
0.925	14.364	12.895	6.305	0.333	26.271	1.327	22.927	-18.957	-55.776		
0.950	15.260	13.891	6.235	1.001	24.186	3.761	23.603	-19.083	-53.950		
0.977	16.472	14.526	7.650	1.340	27.773	4.666	22.876	-17.672	-50.580		
1.001	17.159	14.985	8.278	1.161	28.915	3.880	22.695	-17.044	-48.678		

Table 8.1. Continued.

STATION 4										
PHH=50.00										
YOR/SR=0.69										
V/SS	V M/S	V·AX M/S	V·TAN M/S	V·RAD M/S	BETA Y DEG	BETA R DEG	V° M/S	V·TAN° M/S	BETA Y° DEG	
0.000	16.509	14.329	8.165	0.741	29.675	2.573	22.354	-17.157	-50.132	
0.053	16.798	14.537	8.378	0.820	29.956	2.797	22.325	-16.944	-49.373	
0.102	17.026	14.798	8.409	0.451	29.608	1.518	22.473	-16.913	-48.817	
0.154	16.836	14.713	8.183	0.273	29.082	0.929	22.588	-17.139	-49.355	
0.205	16.754	14.648	8.133	0.048	29.040	0.164	22.584	-17.189	-49.565	
0.258	16.422	14.411	7.873	0.137	28.650	0.478	22.630	-17.449	-50.447	
0.308	16.222	14.160	7.914	0.042	29.200	0.150	22.440	-17.408	-50.874	
0.361	15.960	13.839	7.949	-0.026	29.873	-0.093	22.211	-17.373	-51.459	
0.411	15.929	13.624	8.250	-0.271	31.197	-0.974	21.842	-17.072	-51.410	
0.463	15.627	13.343	8.134	-0.073	31.368	-0.267	21.759	-17.188	-52.178	
0.514	15.789	13.310	8.489	-0.229	32.530	-0.632	21.459	-16.833	-51.665	
0.539	15.859	13.346	8.564	-0.224	32.690	-0.808	21.422	-16.758	-51.466	
0.565	16.013	13.405	8.756	-0.239	33.152	-0.854	21.310	-16.566	-51.021	
0.551	16.050	13.454	8.751	-0.084	33.040	-0.300	21.345	-16.571	-50.927	
0.619	16.262	13.669	8.806	-0.236	32.791	-0.831	21.439	-16.516	-50.387	
0.642	16.277	13.671	8.832	-0.173	32.863	-0.610	21.420	-16.490	-50.339	
0.668	16.593	14.024	8.857	-0.459	32.274	-1.584	21.628	-16.465	-49.578	
0.694	16.471	13.864	8.892	-0.137	32.677	-0.476	21.497	-16.430	-49.842	
0.720	16.539	13.957	8.866	-0.350	32.425	-1.211	21.578	-16.456	-49.696	
0.745	16.553	14.135	8.605	-0.411	31.333	-1.423	21.892	-16.717	-49.785	
0.772	16.114	13.655	8.553	-0.167	32.062	-0.593	21.625	-16.769	-50.842	
0.796	15.930	13.439	8.551	-0.194	32.469	-0.699	21.491	-16.771	-51.294	
0.823	15.219	13.029	7.865	0.040	31.116	0.152	21.783	-17.457	-53.264	
0.848	15.178	13.134	7.588	-0.531	30.016	-2.004	22.068	-17.734	-53.475	
0.874	14.071	12.269	6.886	-0.230	29.304	-0.937	22.145	-18.436	-56.357	
0.899	13.604	12.112	6.175	-0.429	27.030	-1.808	22.653	-19.143	-57.678	
0.925	13.465	12.129	5.837	-0.335	25.700	-1.426	22.951	-19.485	-58.098	
0.952	13.987	12.607	6.054	-0.194	25.652	-0.795	23.026	-19.268	-56.802	
0.976	14.560	13.246	6.043	0.101	24.524	0.399	23.391	-19.279	-55.508	
1.000	15.406	13.834	6.767	0.432	26.066	1.608	23.144	-18.555	-53.294	

Table 8.1. Continued.

STATION 4										
PMH=70.00										
YOR/SR=0.00										
Y/SS	V M/S	V.AX M/S	V.TAN M/S	V.RAD M/S	BETA Y DEG	BETA R DEG	V _i M/S	V.TAN ^o M/S	BETA Y ^o DEG	
0.001	13.960	13.006	5.066	-0.215	21.282	-0.883	25.594	-22.043	-59.458	
0.026	15.212	13.983	5.990	-0.091	23.191	-0.344	25.328	-21.119	-56.492	
0.052	15.770	14.365	6.498	0.350	24.338	1.272	25.124	-20.612	-55.126	
0.077	16.353	14.691	7.180	0.227	26.048	0.797	24.758	-19.929	-53.605	
0.103	16.495	14.949	6.962	0.387	24.972	1.346	25.088	-20.148	-53.426	
0.129	16.694	15.136	7.023	0.515	24.891	1.768	25.151	-20.086	-53.000	
0.154	16.977	15.294	7.360	0.380	25.697	1.283	24.979	-19.750	-52.246	
0.180	17.206	15.401	7.665	0.301	26.459	1.002	24.805	-19.444	-51.618	
0.205	17.212	15.517	7.437	0.395	25.607	1.314	25.056	-19.672	-51.734	
0.257	17.212	15.435	7.592	0.602	26.192	2.006	24.883	-19.517	-51.661	
0.309	17.407	15.335	8.229	0.356	28.219	1.173	24.323	-18.880	-50.916	
0.359	17.320	14.963	8.712	0.429	30.208	1.419	23.715	-18.398	-50.878	
0.411	17.133	14.584	8.983	0.394	31.632	1.317	23.265	-18.126	-51.181	
0.462	16.748	14.261	8.755	0.692	31.545	2.369	23.244	-18.355	-52.154	
0.514	16.667	14.066	8.928	0.469	32.404	1.612	22.987	-18.181	-52.272	
0.565	16.456	14.042	8.565	0.513	31.383	1.788	23.261	-18.544	-52.867	
0.616	16.160	13.938	8.163	0.477	30.356	1.691	23.521	-18.946	-53.659	
0.668	16.013	13.940	7.869	0.417	29.445	1.493	23.759	-19.240	-54.076	
0.719	15.861	13.938	7.565	0.272	28.490	0.984	24.006	-19.545	-54.506	
0.746	15.874	13.914	7.639	0.154	28.769	0.555	23.931	-19.470	-54.449	
0.771	15.517	13.555	7.544	0.357	29.100	1.317	23.802	-19.565	-55.286	
0.757	15.454	13.567	7.398	0.163	28.603	0.603	23.929	-19.711	-55.461	
0.822	14.654	12.917	6.986	0.504	28.405	1.967	23.913	-20.124	-57.304	
0.848	14.328	12.473	7.046	0.255	29.463	1.018	23.624	-20.063	-58.131	
0.874	13.372	11.552	6.728	0.295	30.217	1.265	23.428	-20.381	-60.455	
0.859	12.522	10.987	6.004	0.189	28.656	0.863	23.794	-21.105	-62.499	
0.926	12.095	10.844	5.346	-0.334	26.240	-1.581	24.316	-21.764	-63.514	
0.950	11.723	10.712	4.757	-0.238	23.945	-1.164	24.787	-22.353	-64.395	
0.976	12.233	11.362	4.471	-0.777	21.480	-3.643	25.330	-22.638	-63.348	
1.000	12.637	11.871	4.268	-0.745	19.777	-3.382	25.742	-22.841	-62.538	

Table 8.1. Continued.

STATION 4											
PHM=70.00											
YCR/SR=0.34											
Y/SS	V	V·AX	V·TAN	V·RAD	BETA Y	BETA R	V·	V·TAN°	BETA Y°	V·TAN°	BETA Y°
	M/S	M/S	M/S	M/S	DEG	DEG	M/S	M/S	DEG	M/S	DEG
-0.000	13.719	12.375	5.919	-0.199	25.563	-0.832	24.539	-21.190	-59.716	-21.190	-59.716
0.026	14.935	13.354	6.665	0.549	26.522	2.105	24.420	-20.445	-56.848	-20.445	-56.848
0.052	15.971	14.206	7.285	0.441	27.148	1.583	24.389	-19.825	-54.375	-19.825	-54.375
0.077	16.319	14.304	7.829	0.641	28.694	2.251	24.007	-19.047	-53.429	-19.047	-53.429
0.103	16.633	14.541	8.063	0.459	29.007	1.581	23.963	-18.805	-53.033	-18.805	-53.033
0.129	16.423	14.154	8.304	0.657	30.401	2.291	23.536	-18.821	-52.770	-18.821	-52.770
0.155	16.533	14.302	8.289	0.322	30.095	1.116	23.638	-18.885	-53.439	-18.885	-53.439
0.205	16.253	14.005	8.225	0.613	30.425	2.161	23.511	-18.572	-52.799	-18.572	-52.799
0.257	16.491	14.097	8.538	0.577	31.201	2.005	23.316	-18.748	-53.123	-18.748	-53.123
0.308	16.621	14.361	8.362	0.317	30.211	1.094	23.616	-19.304	-52.547	-19.304	-52.547
0.359	16.466	14.481	7.806	0.699	28.326	2.434	24.132	-19.585	-53.326	-19.585	-53.326
0.411	16.698	14.899	7.525	0.461	26.795	1.581	24.608	-19.543	-53.061	-19.543	-53.061
0.462	16.457	14.851	7.167	0.497	25.762	1.725	24.865	-20.193	-52.676	-20.193	-52.676
0.514	16.621	14.996	7.165	0.210	25.539	0.725	24.953	-20.015	-53.329	-20.015	-53.329
0.566	16.452	14.969	6.917	0.289	24.801	1.005	25.136	-20.035	-53.398	-20.035	-53.398
0.618	16.787	15.136	7.259	-0.166	25.621	-0.567	24.963	-20.186	-53.653	-20.186	-53.653
0.669	16.652	15.064	7.094	-0.145	25.217	-0.500	25.051	-20.045	-53.575	-20.045	-53.575
0.720	16.477	14.996	6.969	-0.200	24.926	-0.693	25.110	-20.115	-53.834	-20.115	-53.834
0.771	16.389	14.881	7.074	-0.141	25.426	-0.490	24.957	-20.256	-54.478	-20.256	-54.478
0.745	16.496	14.854	6.923	-0.178	24.989	-0.623	24.577	-20.486	-55.790	-20.486	-55.790
0.757	16.413	14.844	6.994	-0.355	25.230	-1.239	24.999	-20.359	-62.979	-20.359	-62.979
0.822	16.303	14.752	6.928	-0.397	25.155	-1.394	24.999	-20.400	-61.497	-20.400	-61.497
0.848	16.003	14.462	6.851	-0.117	25.350	-0.419	24.890	-20.486		-20.486	
0.874	15.425	13.927	6.624	-0.163	25.436	-0.604	24.771	-20.359		-20.359	
0.899	14.527	12.877	6.710	-0.433	27.521	-3.460	24.124	-20.857		-20.857	
0.925	13.653	11.839	6.751	-0.624	29.694	-3.127	23.550	-20.717		-20.717	
0.951	12.357	10.637	6.253	-0.874	30.449	-2.926	23.472	-21.095		-21.095	
0.976	12.592	10.830	6.392	-0.643	30.550	-1.764	23.377				
1.001	12.944	11.455	6.015	0.398	27.704		24.004				

Table 8.1. Continued.

STATION 4											
PHM=70.00											
YOR/SR=0.69											
Y/SS	V M/S	V·AX M/S	V·TAN M/S	V·RAD M/S	BEIA Y DEG	BETA R DEG	V· M/S	V·TAN· M/S	BETA Y· DEG		
-0.000	13.786	11.730	7.226	0.492	31.634	2.044	23.086	-19.883	-59.462		
0.026	14.555	12.091	8.099	0.235	33.817	0.926	22.529	-19.010	-57.542		
0.051	14.551	12.376	7.647	0.306	31.710	1.206	23.064	-19.463	-57.549		
0.077	14.802	12.533	7.874	0.129	32.138	0.358	22.959	-19.236	-56.913		
0.102	14.896	12.679	7.818	-0.093	31.658	-0.542	23.085	-19.291	-56.685		
0.128	15.178	12.983	7.862	-0.144	31.197	-0.508	23.217	-19.248	-56.001		
0.154	15.289	13.344	7.462	-0.136	29.213	0.797	23.751	-19.648	-55.818		
0.181	15.230	13.465	7.114	0.212	27.848	0.234	24.107	-19.996	-56.044		
0.205	15.780	13.861	7.542	0.064	28.552	0.319	23.979	-19.567	-54.688		
0.231	15.987	14.191	7.361	0.089	27.416	0.256	24.318	-19.748	-54.299		
0.257	16.412	14.619	7.459	0.073	27.033	-0.270	24.492	-19.650	-53.353		
0.310	16.867	15.052	7.612	-0.079	26.826	0.565	24.632	-19.498	-52.333		
0.359	16.929	15.127	7.599	0.167	26.674	0.392	24.687	-19.510	-52.213		
0.412	16.981	15.047	7.869	0.116	27.606	-0.268	24.426	-19.241	-51.973		
0.464	17.067	15.078	7.996	-0.080	27.938	-0.967	24.345	-19.113	-51.732		
0.513	17.136	14.920	8.423	-0.289	29.447	-1.209	23.912	-18.686	-51.394		
0.565	17.031	14.644	8.687	-0.359	30.678	-1.077	23.533	-18.422	-51.518		
0.616	16.925	14.316	9.022	-0.318	32.220	-0.483	23.067	-18.087	-52.253		
0.668	16.652	13.955	9.085	-0.140	33.065	0.970	22.795	-18.025	-52.253		
0.719	16.229	13.489	9.019	0.275	33.768	0.791	22.566	-18.090	-53.290		
0.770	16.175	13.221	9.316	0.223	35.171	0.783	22.167	-17.793	-53.387		
0.796	15.875	12.983	9.133	0.217	35.123	1.569	22.175	-17.977	-54.163		
0.822	15.164	12.185	9.016	0.415	36.498	-0.840	21.814	-18.093	-56.041		
0.848	14.453	11.409	8.870	-0.212	37.863	-1.216	21.514	-18.240	-57.973		
0.873	13.070	10.180	8.193	-0.277	38.828	-2.665	21.482	-18.917	-61.714		
0.899	12.298	9.753	7.450	-0.786	37.374	-3.553	21.946	-19.660	-63.614		
0.925	11.107	8.955	6.553	-0.495	36.195	-2.675	22.423	-20.557	-66.462		
0.951	11.129	9.365	5.990	-0.519	32.605	-1.008	23.102	-21.119	-66.086		
0.976	11.775	10.316	5.673	-0.207	28.805	1.560	23.790	-21.437	-64.301		
1.000	12.700	11.206	5.966	0.346	28.029	1.560	23.930	-21.144	-62.076		

Table 8.1. Continued.

STATION 4										
PHH=90.00										
YOR/SR=0.00										
Y/SS	V M/S	V.AX M/S	V.TAN M/S	V.RAD M/S	BETA Y DEG	BETA R DEG	V' M/S	V.TAN' M/S	BETA Y' DEG	
-0.000	10.946	9.808	4.858	0.114	26.348	0.596	25.963	-24.035	-67.804	
0.026	11.549	10.552	4.686	-0.276	23.945	-1.367	26.411	-24.211	-66.451	
0.051	12.780	11.815	4.870	-0.128	22.403	-0.575	26.774	-24.026	-63.815	
0.077	14.318	12.839	6.333	0.262	26.254	1.050	25.961	-22.564	-60.361	
0.103	14.780	12.991	7.009	0.745	28.348	2.891	25.453	-21.888	-59.310	
0.128	14.776	12.786	7.345	0.949	29.876	3.684	25.059	-21.552	-59.321	
0.154	14.941	12.786	7.706	0.609	31.079	2.337	24.749	-21.190	-58.895	
0.180	14.922	12.704	7.797	0.697	31.539	2.677	24.629	-21.100	-58.949	
0.206	15.051	12.780	7.929	0.573	31.815	2.181	24.556	-20.968	-58.637	
0.257	15.095	12.909	7.790	0.727	31.111	2.761	24.741	-21.106	-58.550	
0.308	15.299	13.143	7.807	0.600	30.710	2.248	24.850	-21.090	-58.068	
0.359	15.364	13.043	8.102	0.529	31.849	1.975	24.546	-20.794	-57.902	
0.411	15.418	13.029	8.233	0.407	32.288	1.514	24.429	-20.664	-57.767	
0.463	15.106	12.883	7.872	0.512	31.427	1.941	24.658	-21.025	-58.503	
0.514	15.044	12.806	7.890	0.247	31.639	0.940	24.602	-21.006	-58.632	
0.565	14.969	12.682	7.925	0.655	32.003	2.506	24.508	-20.971	-58.838	
0.618	15.534	13.112	8.313	0.522	32.374	1.924	24.406	-20.584	-57.503	
0.668	15.305	12.989	8.013	1.151	31.673	4.312	24.593	-20.883	-58.120	
0.719	15.576	13.420	7.852	0.935	30.332	3.442	24.960	-21.045	-57.476	
0.745	15.577	13.578	7.569	0.994	29.138	3.660	25.283	-21.328	-57.518	
0.772	15.220	13.182	7.551	0.937	29.805	3.530	25.088	-21.346	-58.304	
0.797	15.739	13.798	7.540	0.689	28.654	2.510	25.427	-21.357	-57.135	
0.823	15.699	13.882	7.306	0.598	27.757	2.183	25.669	-21.591	-57.260	
0.849	15.369	13.499	7.285	0.961	28.354	3.585	25.481	-21.612	-58.012	
0.874	14.849	13.195	6.735	1.012	27.042	3.907	25.792	-22.162	-59.231	
0.899	14.221	12.669	6.404	0.849	26.818	3.421	25.815	-22.492	-60.610	
0.925	13.138	11.483	6.303	1.008	28.764	4.401	25.344	-22.594	-63.059	
0.950	12.017	10.656	5.495	0.817	27.277	3.900	25.714	-23.402	-65.518	
0.976	10.978	9.770	4.978	0.533	26.998	2.785	25.838	-23.919	-67.782	
1.000	10.245	9.406	4.055	0.193	23.323	1.081	26.563	-24.841	-69.261	

Table 8.1. Continued.

STATION 4

PHH=90.00
YOR/SR=0.34

Y/SS	V M/S	V*AX M/S	V*TAN M/S	V*RAD M/S	BETA Y DEG	BETA R DEG	V' M/S	V*TAN' M/S	BETA Y' DEG
0.001	11.507	9.974	5.738	0.127	29.911	0.630	25.216	-23.159	-66.701
0.026	11.782	10.128	6.009	-0.359	30.681	-1.746	25.029	-22.888	-66.130
0.051	12.593	10.896	6.307	-0.273	30.065	-1.242	25.080	-22.590	-64.250
0.077	13.724	11.842	6.934	0.178	30.352	0.745	24.952	-21.563	-61.667
0.103	14.512	12.322	7.662	0.228	31.875	0.900	24.551	-21.235	-59.874
0.128	14.641	12.352	7.854	0.306	32.451	1.199	24.400	-21.043	-59.587
0.154	14.734	12.458	7.858	0.369	32.244	1.436	24.450	-21.038	-59.368
0.180	14.651	12.252	8.023	0.412	33.217	1.610	24.204	-20.874	-59.589
0.206	14.691	12.434	7.814	0.395	32.145	1.541	24.477	-21.083	-59.469
0.257	14.890	12.504	8.079	0.304	32.865	1.171	24.285	-20.818	-59.010
0.308	14.750	12.508	7.803	0.473	31.956	1.838	24.524	-21.094	-59.333
0.359	14.783	12.413	8.016	0.435	32.853	1.686	24.292	-20.881	-59.269
0.411	14.520	12.262	7.750	0.629	32.295	2.481	24.445	-21.146	-59.892
0.463	14.454	12.341	7.551	0.870	31.463	3.443	24.656	-21.345	-59.966
0.514	14.722	12.683	7.441	0.716	30.398	2.788	24.925	-21.456	-59.412
0.565	14.902	12.995	7.245	0.841	29.141	3.235	25.252	-21.652	-59.029
0.617	15.307	13.531	7.122	0.708	27.762	2.651	25.636	-21.775	-58.144
0.668	15.912	14.129	7.293	0.617	27.301	2.224	25.814	-21.604	-56.816
0.719	16.351	14.680	7.177	0.583	26.054	2.044	26.216	-21.720	-55.946
0.745	16.476	14.907	6.980	0.727	25.090	2.528	26.506	-21.917	-55.779
0.770	16.753	15.164	7.114	0.307	25.133	1.050	26.541	-21.783	-55.156
0.757	16.279	14.853	6.643	0.506	24.095	1.782	26.756	-22.254	-56.279
0.823	15.957	14.618	6.472	0.588	23.881	2.105	26.769	-22.425	-56.502
0.848	15.728	14.481	6.104	0.641	22.857	2.335	27.004	-22.793	-57.571
0.874	15.504	14.147	6.335	0.310	24.123	1.144	26.630	-22.562	-57.910
0.899	14.654	13.475	5.730	0.579	23.039	2.265	26.800	-23.166	-59.816
0.925	13.456	12.489	4.939	0.832	21.575	3.543	27.018	-23.958	-62.467
0.950	13.886	12.270	6.473	-0.605	27.813	-2.497	25.562	-22.424	-61.313
0.976	11.869	10.527	5.468	0.399	27.448	1.925	25.685	-23.425	-65.805
1.000	10.961	9.808	4.887	-0.235	26.484	-1.228	25.936	-24.010	-67.779

Table 8.1. Concluded.

STATION 4
PHH=90.00
YOR/SR=0.69

Y/SS	V M/S	V·AX M/S	V·TAN M/S	V·RAD M/S	BETA Y DEG	BETA R DEG	V· M/S	V·TAN° M/S	BETA Y° DEG
-0.000	10.632	8.718	6.064	-0.519	34.822	-2.800	24.441	-22.833	-69.103
0.026	11.608	9.614	6.501	-0.252	34.066	-1.242	24.372	-22.396	-66.768
0.053	13.358	11.127	7.458	-0.272	33.831	-1.162	24.155	-21.439	-62.570
0.078	14.355	12.056	7.790	0.221	32.868	0.884	24.308	-21.107	-60.267
0.102	14.604	12.117	8.146	0.294	33.913	1.154	24.029	-20.751	-59.717
0.128	14.129	11.813	7.734	0.516	33.213	2.093	24.237	-21.163	-60.830
0.154	13.962	11.718	7.632	0.480	33.076	1.967	24.280	-21.265	-61.144
0.180	13.962	11.759	7.501	0.624	32.535	2.560	24.414	-21.395	-61.207
0.205	13.881	11.593	7.603	0.665	33.254	2.746	24.246	-21.294	-61.432
0.227	14.167	11.933	7.653	0.555	32.673	2.241	24.366	-21.244	-60.677
0.309	14.655	12.383	7.831	0.316	32.308	1.236	24.436	-21.066	-59.552
0.359	14.774	12.640	7.643	0.306	31.162	1.188	24.728	-21.254	-59.260
0.411	14.654	12.530	7.587	0.414	31.196	1.617	24.720	-21.310	-59.545
0.463	14.521	12.377	7.580	0.445	31.484	1.757	24.650	-21.317	-59.859
0.513	14.809	12.676	7.655	-0.158	31.126	-0.613	24.737	-21.242	-59.174
0.565	15.134	13.020	7.711	-0.239	30.634	-0.904	24.867	-21.186	-58.427
0.616	15.453	13.357	7.763	-0.345	30.163	-1.280	25.002	-21.134	-57.706
0.668	15.783	13.672	7.872	0.454	29.932	1.649	25.079	-21.025	-56.965
0.719	16.221	14.011	8.173	0.035	30.256	0.123	25.016	-20.724	-55.937
0.745	15.742	13.393	8.260	0.463	31.662	1.687	24.602	-20.637	-57.018
0.770	16.079	13.598	8.581	0.087	32.254	0.309	24.447	-20.316	-56.206
0.757	15.554	13.058	8.445	0.330	32.893	1.216	24.265	-20.452	-57.444
0.823	15.330	13.084	8.911	0.029	34.256	0.106	23.888	-19.986	-56.790
0.848	15.314	12.908	8.238	0.212	32.546	0.795	24.360	-20.659	-58.003
0.873	15.160	12.684	8.297	0.298	33.189	1.126	24.192	-20.600	-58.377
0.899	14.295	12.088	7.620	0.419	32.226	1.681	24.471	-21.277	-60.399
0.925	13.202	10.977	7.309	0.618	33.657	2.681	24.219	-21.588	-63.048
0.951	11.771	9.693	6.678	0.076	34.562	0.371	24.242	-22.219	-66.431
0.976	10.467	8.889	5.470	-0.789	31.606	-4.324	25.057	-23.427	-69.222
1.000	5.418	8.155	4.709	-0.136	30.001	-0.828	25.526	-24.188	-71.368

REPORT DOCUMENTATION PAGE		READ INSTRUCTIONS BEFORE COMPLETING FORM
1. REPORT NUMBER AFOSR-TR. 79-0509	2. GOVT ACCESSION NO.	3. RECIPIENT'S CATALOG NUMBER
4. TITLE (and Subtitle) THE INFLUENCE OF COMPRESSOR INLET GUIDE VANE / STATOR RELATIVE CIRCUMFERENTIAL POSITIONING ON BLADE WAKE TRANSPORT AND INTERACTION	5. TYPE OF REPORT & PERIOD COVERED INTERIM 30 Sep 77 - 31 Aug 78	
	6. PERFORMING ORG. REPORT NUMBER TCRL-13	
7. AUTHOR(s) G J HOLBROOK T H OKIISHI	8. CONTRACT OR GRANT NUMBER(s) AFOSR 76-2916	
	9. PERFORMING ORGANIZATION NAME AND ADDRESS IOWA STATE UNIVERSITY ENGINEERING RESEARCH INSTITUTE AMES, IOWA 50010	
11. CONTROLLING OFFICE NAME AND ADDRESS AIR FORCE OFFICE OF SCIENTIFIC RESEARCH/NA BLDG 410 BOLLING AIR FORCE BASE, D C 20332	10. PROGRAM ELEMENT, PROJECT, TASK AREA & WORK UNIT NUMBERS 2307A4 61102F	
	12. REPORT DATE Sep 78	
14. MONITORING AGENCY NAME & ADDRESS (if different from Controlling Office)	13. NUMBER OF PAGES 23	
	15. SECURITY CLASS. (of this report) UNCLASSIFIED	
15a. DECLASSIFICATION/DOWNGRADING SCHEDULE		
16. DISTRIBUTION STATEMENT (of this Report) Approved for public release; distribution unlimited.		
17. DISTRIBUTION STATEMENT (of the abstract entered in Block 20, if different from Report)		
18. SUPPLEMENTARY NOTES		
19. KEY WORDS (Continue on reverse side if necessary and identify by block number) AXIAL-FLOW COMPRESSOR TURBOMACHINE WAKE INTERACTION AXIAL-FLOW TURBOMACHINE TURBOMACHINE FLUID FLOW AXIAL-FLOW FAN MULTISTAGE AXIAL-FLOW TURBOMACHINE AXIAL-FLOW BLOWER AXIAL-FLOW PUMP		
20. ABSTRACT (Continue on reverse side if necessary and identify by block number) <p>A periodically sampling hot-wire measurement system was used to obtain numerous periodic-average (electronically and arithmetically averaged values of periodically sampled data) three-dimensional velocity vector data for flow through the first stage (inlet guide vane, rotor, and stator rows) of a low-speed, multistage, axial-flow research compressor. New data are presented for the maximum noise circumferential position of the first stator blade row. Comparisons are made between these data and similar data previously acquired and reported for the minimum noise configuration of the compressor. The inlet guide</p>		

20. (Continued)

vane (IGV) wake avenue was found to intersect first stator row blades at two span locations, one near the hub and the other near the tip, for maximum noise, and at only one span location, near mid-span, for minimum noise. This difference in IGV wake / stator leading edge intersection patterns resulted in variations of the first stator exit flow deviation angle near the hub and tip portions of the compressor annulus. These variations were explained in terms of the larger fluctuations of stator inlet flow associated with the inlet guide vane wake avenues. The difference in IGV wake / stator leading edge interaction patterns was also judged to be consistent with the related level of compressor inlet noise. Blade-to-blade plane and hub-to-tip cross-section drawings showing blade wake locations and interaction patterns are included to aid data interpretation and comparison. In addition, examples of three-dimensional hub-to-tip velocity vector sheet drawings of blade row exit flow are shown.